JOURNAL OF CAVE AND KARST STUDIES

June 2022
Volume 84, Number 2
ISSN 1090-6924
A Publication of the National Speleological Society



DEDICATED TO THE ADVANCEMENT OF SCIENCE, EDUCATION, EXPLORATION, AND CONSERVATION

Published By
The National Speleological Society

http://caves.org/pub/journal

Office
6001 Pulaski Pike NW
Huntsville, AL 35810 USA
Tel:256-852-1300
nss@caves.org

Editor-in-Chief
Malcolm S. Field
Washington, DC
703-347-8601
field.malcolm1@gmail.com

Production Editor
Scott A. Engel
Knoxville, TN
225-281-3914
saecaver@gmail.com

The *Journal of Cave and Karst Studies* , ISSN 1090-6924, CPM Number #40065056, is a multi-disciplinary, refereed journal published four times a year by the National Speleological Society. The *Journal* is available by open access on its website, or check the website for current print subscription rates. Back issues are available from the NSS office.

POSTMASTER: send address changes to the National Speleological Society Office listed above.

The Journal of Cave and Karst Studies is covered by the following ISI Thomson Services Science Citation Index Expanded, ISI Alerting Services, and Current Contents/Physical, Chemical, and Earth Sciences.

Copyright © 2022
by the National Speleological Society, Inc.

BOARD OF EDITORS

Anthropology
George Crothers
University of Kentucky
Lexington, KY
george.crothers@utk.edu

Conservation-Life Sciences
Julian J. Lewis & Salisa L. Lewis
Lewis & Associates, LLC.
Borden, IN
lewisbioconsult@aol.com

Earth Sciences
Benjamin Schwartz
Texas State University
San Marcos, TX
bs37@txstate.edu

Yongli Gao
University of Texas at San Antonio
yongli.gao@utsa.edu

Mario Parise
University Aldo Moro
Bari, Italy
mario.parise@uniba.it

Carol Wicks
Louisiana State University
Baton Rouge, LA
cwicks@lsu.edu

Exploration
Paul Burger
National Park Service
Eagle River, Alaska
paul_burger@nps.gov

Microbiology
Kathleen H. Lavoie
State University of New York
Plattsburgh, NY
lavoiekh@plattsburgh.edu

Paleontology
Greg McDonald
National Park Service
Fort Collins, CO
greg_mcdonald@nps.gov

Social Sciences
Joseph C. Douglas
Volunteer State Community College
Gallatin, TN
615-230-3241
joe.douglas@volstate.edu

Book Reviews
Arthur N. Palmer & Margaret V Palmer
State University of New York
Oneonta, NY
palmeran@oneonta.edu

Front cover: Select Mt. Rainier Caves, see Stenner et. al. in this issue.

Miloš Briestenský, Fabrizio Ambrosino, Iveta Smetanová, Lenka Thinová, Stanka Šebela, Josef Stemberk, Lucia Pristašová, Concepción Pla, and David Benavente. Radon in dead-end caves in Europe. *Journal of Cave and Karst Studies*, v. 84, no. 2, p. 41-50. DOI:10.4311/2021ES0101

RADON IN DEAD-END CAVES IN EUROPE

Miloš Briestenský[1,C], Fabrizio Ambrosino[2], Iveta Smetanová[3], Lenka Thinová[4], Stanka Šebela[5], Josef Stemberk[1], Lucia Pristašová[6], Concepción Pla[7], and David Benavente[8]

Abstract

We report the results of 3-years of Radon-222 monitoring in six show caves across Europe, selected with the feature of having only one, or no natural entrance, defined as dead-end caves. The caves are located in Spain, Slovakia, Slovenia, and Czechia. The consecutive monitoring was performed between January 2017 and January 2020. Continuous measurements of the radon activity concentration using spectrometry detection and analysis of the α-particles of ^{222}Rn progeny were performed. Meteorological parameters influencing gas flow were recorded inside and outside of the caves. Although the radon activity concentrations differed from one cave to another, all six of the studied caves revealed very similar trends, showing evident seasonal variability with higher values in summer and lower values in winter. The measured values of radon activity concentrations ranged between 633 and 26,785 Bq/m^3. The temperature differences between the inside and outside of the caves is the main radon movements driving force. The results of this study have significant practical implications, making it possible to provide cave administrators with recommendations regarding employee or visitor time-limited access to the investigated caves. Ours is the first comparative study encompassing the most interesting dead-end caves in Europe.

INTRODUCTION

Radon-222 is a naturally-occurring inert radioactive gas with a half-life of 3.824 d, originating from the radioactive decay of ^{226}Ra in the ^{238}U radioactive decay chain in the Earth's crust (Stein, 1987). Only a fraction of the radon atoms created in a mineral grain emanates into the void space between grains, where they are dissolved in water or mixed in soil gases, and are thus transported by convection toward the ground surface and the atmosphere (Nero, 1988; Sabbarese et al., 2020a). This transport is influenced by a number of geophysical and geochemical parameters (Etiope and Martinelli, 2001; Ambrosino et al., 2020a). Radon represents the most significant source of ionizing radiation exposure: up to 70 % of natural background radiation or 50 % of all irradiation sources (UNSCEAR, 2000; Ambrosino et al., 2020g). Radon poses a substantial threat to human health when a buildup occurs in confined spaces, such as dwellings and workplaces, where people spend long periods of time (Field, 2007; Pantelić et al., 2019; Ambrosino et al., 2020b). Decades of epidemiological studies concerning the effects of radon on human health show a statistically significant increase in lung cancer risk from prolonged indoor exposure (Darby et al., 2001). Underground working and living spaces with little or no ventilation are the most significant in terms of potential human exposure to radon (Sabbarese et al., 2020a). In particular, caves are recognized as special indoor occupational environments where extremely elevated concentrations of ^{222}Rn may occur (Cigna, 2005; Sainz et al., 2007; Ambrosino et al., 2019a). Therefore, radon releases represent a significant phenomenon that may affect the utilization of caves. This aspect poses a threat to human health for persons working in such localities (cavers, tour guides, maintenance personnel, employees working in shops built over cave entrances, etc.) and visitors (Field, 2007). Many recommendations concerning indoor radon concentrations have been made and a reference level of 300 Bq/m^3 in workplaces is strictly recommended by the Council Directive of the European Union (2013/59/Euratom) (Euratom, 2014). A large body of world literature investigating the distribution of radon in caves focuses on two main areas: radiation protection (Lario et al., 2005; Thinová et al., 2005b; Field, 2007; Bahtijari et al., 2008), and tracing the underground airflow (Šebela et al., 2010; Ambrosino et al., 2020c; Pla et al., 2020; Sabbarese et al., 2020b).

European caves, known for centuries, are of great interest to cavers and scientists alike. Generally, publicly accessible caves are usually monitored, but there are many caves under exploration without any monitoring. Radon activity concentrations are mainly influenced by air circulation due to the geomorphological situation of each cave (Cigna, 2005; Field 2007). Some caves have more than one entrance at different elevations with convective circulation of air. The main force controlling this type of circulation are differences in air density (Wigley, 1967; Badino, 2010). The second

[1]Institute of Rock Structure and Mechanics, Czech Academy of Sciences, V Holešovičkách 41, 18209 Prague, Czechia
[2]Department of Physics „Ettore Pancini", University of Naples „Federico II", Italy
[3]Earth Science Institute, Slovak Academy of Sciences, Dúbravská cesta 9, 840 05 Bratislava, Slovakia
[4]Faculty of Nuclear Sciences and Physical Engineering, Czech Technical University in Prague, Břehová 7, 11519 Prague, Czechia
[5]Karst Research Institute ZRC SAZU, Titov trg 2, SI-6230 Postojna, Slovenia
[6]State Nature Conservancy of the Slovak Republic, Slovak Caves Administration, Hodžova 11, 031 01 Liptovský Mikuláš, Slovakia
[7]Department of Civil Engineering, University of Alicante, Carretera San Vicente del Raspeig s/n, 03690 Alicante, Spain
[8]Department of Earth and Environmental Sciences, University of Alicante, Carretera San Vicente del Raspeig s/n, 03690 Alicante, Spain
[C]Corresponding author: briestensky@irsm.cas.cz

type of air circulation is barometric circulation, which responds to differences between the inner and outer barometric pressure (Richon et al., 2005; Badino, 2010; Gregorič et al., 2013). This type of circulation usually occurs in caves with one entrance (dead-end caves) or in caves with small entrances. Dead-end caves are distinctive due to their limited ventilation and stable regime of CO_2 concentrations (Czuppon et al., 2018; Prelovšek et al., 2018). The radon may often reach very high concentrations within passages in vast underground karst systems, defined as dead-end passages (e.g., Pisani rov, Postojna Cave in Slovenia) (Gregorič et al., 2013).

The present research provides a comprehensive survey of the distribution of radon levels in representative dead-end caves with different geological and structural settings located across Europe. Six caves were selected in Spain, Czechia, Slovakia, and Slovenia (Fig. 1). The monitoring period was between January 2017 and January 2020, during which time the meteorological parameters inside and outside of the caves were also recorded. Ours is the first such comparative study concerning dead-end caves. The marginal aim of our work was to show the seasonal radon trends and the influence of meteorological factors in order to understand the common characteristic features of these types of caves. Moreover, this study represents one step further in addressing public health issues relating to radon gas exposure in caves, and in creating greater awareness of the necessity for the implementation of thorough indoor air quality monitoring protocols (Sabbarese et al., 2021).

DESCRIPTION OF THE SELECTED CAVES

Here we describe the main features of the six investigated dead-end caves across Europe. The main meteorological data, i.e. temperature, air pressure, and relative humidity, monitored inside the caves, by means of the appropriate sensors connected to a data-logger, are also reported.

Rull Cave (Spain)

Rull Cave (38° 48' 40″ N; 00° 10' 38″ W, Fig. 1) is located in Vall d'Ebo, in the south-east of Spain (Alicante province). Rull Cave developed in massive Miocene conglomerates that were deposited on Cretaceous limestones (Pla et al., 2016). These materials conform to the host rock of the cave, which has a thickness varying from 9 m to 23 m. Above the cave, the soil has a discontinuous thickness of approximately 1 m, with a coarse to fine texture mainly composed of quartz (Pla et al., 2017). Rull Cave is located in an area with a Mediterranean or warm climate (Csa climate type, Koppen–Geiger Classification) and with hot and dry summers (Garcia-Anton et al., 2017). The cave is defined as having an individual central chamber (20 m high) described as being almost round in shape with a surface of 1,535 m^2. It has a single entrance located at the top of the cave (Pla et al., 2017) (Fig. 2a). Temperatures in Rull Cave range between 15 and 17 °C, the mean relative humidity reaches about 98 % and the pressure ranges between 933 and 985 hPa. ^{222}Rn measurements have been taken continually since 2016 by a RADIM 5WP monitor (Pla et al., 2020).

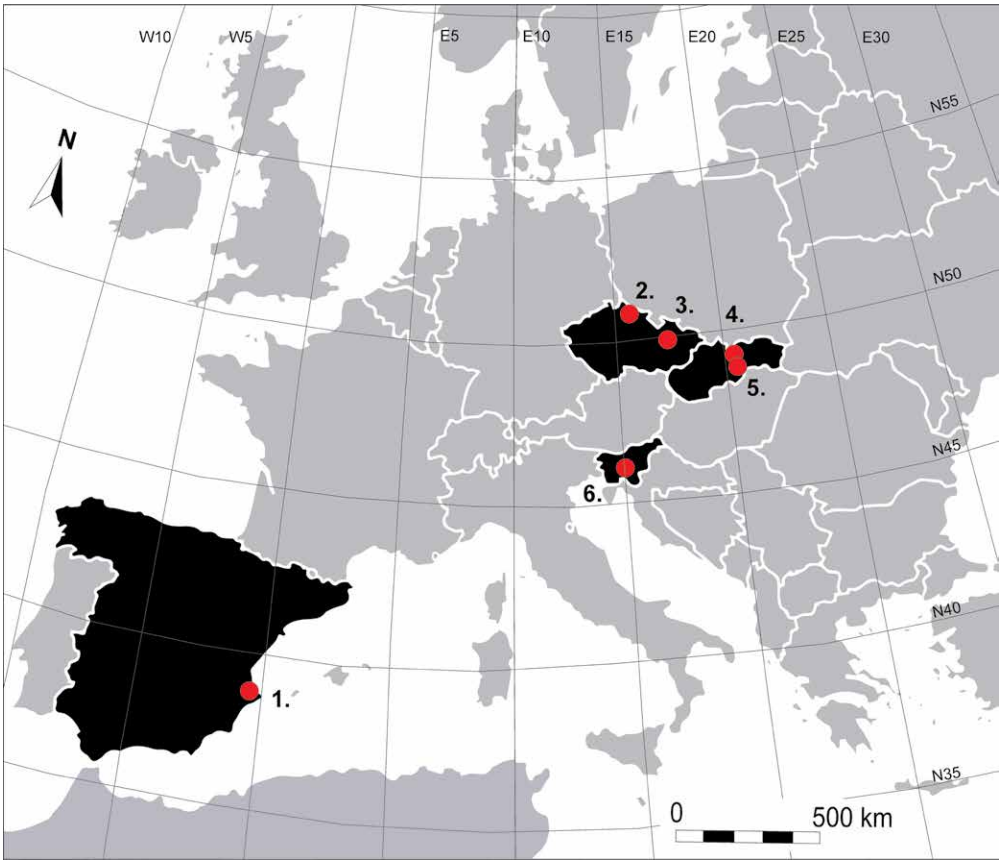


Figure 1. Location of the studied dead-end caves: 1. Rull Cave (Spain), 2. Bozkov Dolomite Caves (Czechia), 3. Mladeč Caves (Czechia), 4. Važecká Cave (Slovakia), 5. Ochtinská Aragonite Cave (Slovakia), 6. Županova Cave (Slovenia). (Source: modified from Google Earth).

Bozkov Dolomite Caves (Czechia)

Bozkov Dolomite Caves (50° 38' 51″ N; 15° 20' 18″ E, Fig. 1) are located in the region of Lugian, in the north-west of Czechia (North Bohemia

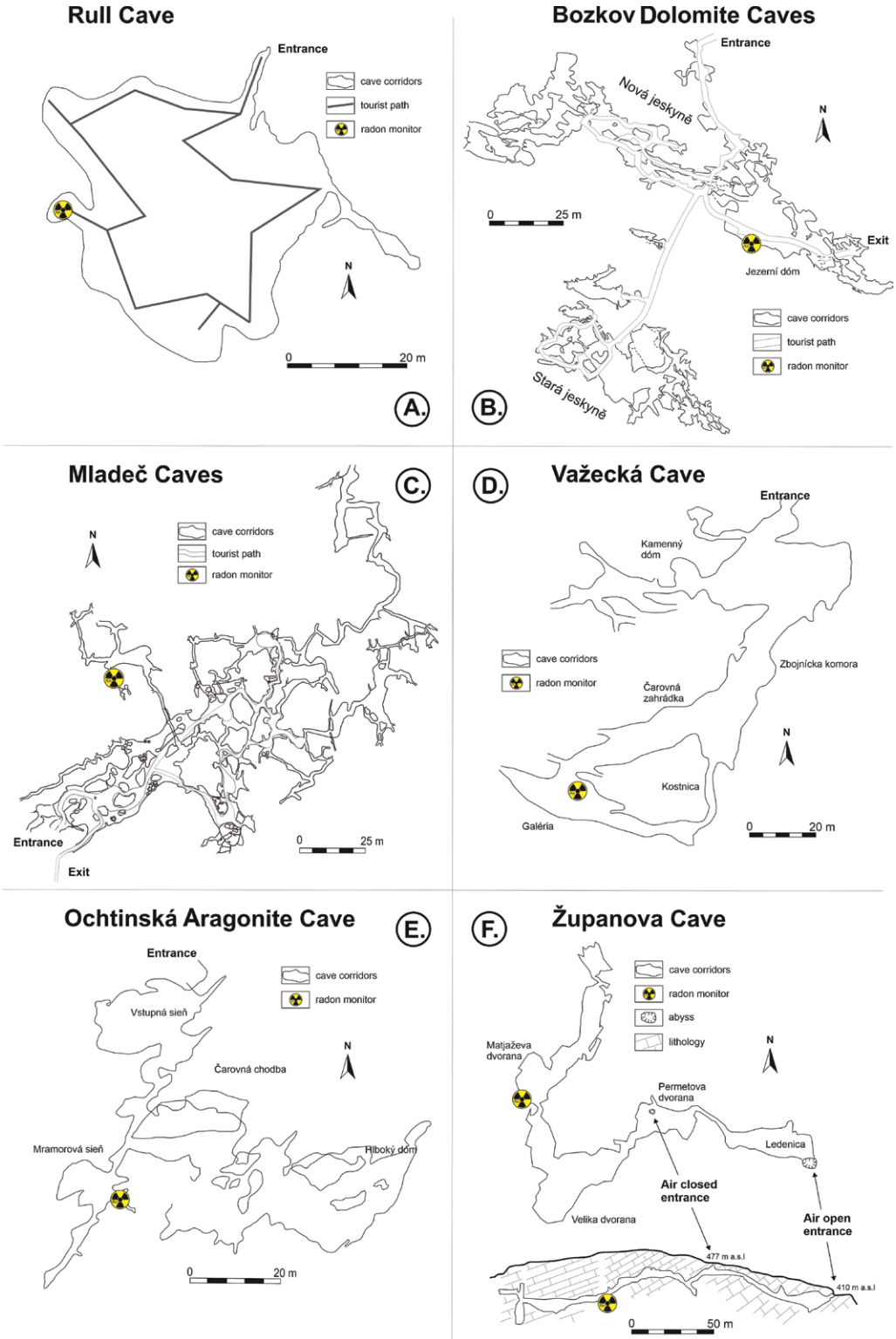


Figure 2. Plan view of the six studied dead-end caves with the locations of the radon monitors.

region, Liberec province). The significant Lugian-Jílovice-Kyšperk Fault intersects the cave system and the lentil of calcareous metamorphosed dolomites that are corroded by groundwater (Rovenská et al., 2008). The caves originated in the karstic mass in the Železný Brod crystalline region, which originated in the Silurian period (Rovenská and Thinová, 2010). The caves consist of two independent systems with two entrances (one used as an exit for visitors), which are connected by an artificial tunnel (Fig. 2b). The entrance to the underground space was discovered by dolomite miners in the 1940s. Lower parts of the caves are flooded, and some lakes are visible from the tourist path. The average temperature in the cave is between 7.5 °C and 9 °C, relative humidity is near to 100 %, and the pressure ranges between 935 hPa and 990 hPa. The cave tour is 350 m long (Rovenská and Thinová, 2010). Continuous radon monitoring began in the caves in 2001, using a RADIM 3A monitor and passive solid-state nuclear track detectors to obtain average seasonal concentrations (Rovenská et al., 2008; Thinová and Burian, 2008).

Mladeč Caves (Czechia)

Mladeč Caves (49° 42' 23″ N; 17° 00' 57″ E, Fig. 1) are situated on the edge of the eastern Třesín ridge in the eastern part of Czechia, within the Bohemian Massif (Olomouc province). The caves are formed in Devonian calcite limestones (Stránský and Thinová, 2017). The Třesín Threshold represents a significant borderline between the NW situated Mohelnice Basin and the Uničov-Litovel Depression (northern Upper Morava Graben part). Moreover, this line creates a borderline between two geomorphological provinces: the Western Carpathians and the Czech Highlands (Ambrosino et al., 2020d). The Graben is a part of the Nisa-Morava fault zone, which is defined by slow, brittle, active deformations, low-magnitude seismicity, and daily CO_2 fluxes (Špaček et al., 2015). The total length of the

Mladeč Cave corridors is 1,250 m (Hromas, 2009). The cave corridors were formed by groundwater from Hradečka Stream on three levels and they are defined as phreatic or deep phreatic caves (Hromas, 2009). The corridors generally follow the N-S and NW-SE oriented faults and the steep layers. The NW-SE striking lineaments are associated with the Haná Fault Zone here. The caves have two openings, one is used as an entrance and the other as an exit (Fig. 2c). The temperature in the caves is between 9 °C and 12.5 °C, mean relative humidity is 80 %, and the pressure ranges between 952 hPa and 1020 hPa. Continuous radon monitoring began in 2011 using a RADIM 3A monitor (Ambrosino et al., 2020d; Stránský and Thinová, 2017).

Važecká Cave (Slovakia)

Važecká Cave (49° 03' 23″ N; 19° 58' 19″ E, Fig. 1) is situated in the northern part of the Low Tatra Mts. on the north edge of the Važec Karst area, in the north of Slovakia (Žilina province). It developed at the contact of the Kozie chrbty Mts. and the Podtatranská Basin, in the Middle Triassic dark-grey limestones of the Gutenstein Formation of the Hronic Unit (Droppa, 1962). Tectonic activity of the WNW-ESE faults and flood-water injections from the Biely Váh River into exposed and faulted carbonates led to the modeling of the underground cave spaces (Bella et al., 2016). Moreover, previous morphological features were remodeled by slab and block breakdown, forced by frost weathering during the last-glacial stages (Bella et al., 2016). The cave is located almost at the bottom of the Biely Váh river valley, just 8 m above the river bed. It is 530 m long and consists of subhorizontal halls, without any significant vertical segmentation (Smetanová et al., 2020). The cave has only one entrance (Fig. 2d). A large part of the cave is filled by fluvial sediments. The temperature in the cave is between 6 °C and 8.5 °C, mean relative humidity is 93 %, and the pressure ranges between 900 hPa and 950 hPa. Continuous radon monitoring began in 2012 using a BARASOL BMC2 probe (Smetanová et al., 2020).

Ochtinská Aragonite Cave (Slovakia)

Ochtinská Aragonite Cave (48° 39' 49″ N; 20° 18' 20″ E, Fig. 1) is located in the south-east of Slovakia (Košice province). It was discovered during the excavation of an adit in 1954 (Bosák et al., 2002). It developed in Lower Devonian crystalline marble and Fe-ochre of the Drnava Formation (Gelnica Group) in the Slovenské rudohorie Mts., belonging to the Inner Western Carpathians (Gaál, 2004). The rock massif here was affected by Hercynian, Alpine orogenesis, as well as by the rejuvenation of Tertiary and Quaternary faults. The general direction of the faults is NE-SW and is often also followed by ankerite accumulations (Gaál, 2004). The cave may be divided into wet parts, like the Marble Hall with an air temperature of 7.8 °C to 8.5 °C, and dry parts, like the Deep Dome with an air temperature of 8.6 °C to 10 °C (Zelinka, 2004). The cave has no known natural entrance and a 145 m long artificial tunnel (Fig. 2e). The cave does not have any particular connection with the outside climate (Zelinka, 2004). Mean relative humidity is approximately 40 %, and the pressure ranges between 915 hPa and 968 hPa. Continuous radon monitoring began in 2016 by RADIM 3A monitor (Ambrosino et al., 2019a).

Županova Cave (Slovenia)

Županova Cave (45° 55' 10″ N; 14° 38' 31″ E, Fig. 1) is situated in the center of Slovenia (Grosuplje province). The cave was created in lower Jurassic limestones (J1, lower and middle Lias), belonging to the External Dinarides (Placer, 2008). Approximately 500 m to the west of Županova Cave principal entrance is Dobrepolje Fault (NW–SE), which separates the uplifted Triassic SW block from the subsided NE block of Županova Cave (Ravbar and Košutnik, 2014). There is also evidence of dextral horizontal movement along the Dobrepolje Fault. The fault is one of the so-called Dinaric oriented (NW–SE) faults in Southern Slovenia, which are still tectonically active. Measurements of air temperature show relative stability in Županova Cave, and it is normally not affected by the external atmosphere (Ravbar and Košutnik, 2014). The monitored values range between 9.4 °C and 9.9 °C. The cave has two entrances, but the second one is closed (Fig. 2f). The first entrance is open throughout the year. Mean relative humidity is approximately 45 %, and the pressure ranges between 933 hPa and 990 hPa. The first short-term monitoring of ^{222}Rn in Županova Cave took place in 1985 (Kobal et al., 1986, with continuous monitoring using a RADIM 3A from 2017 (Ambrosino et al., 2020e).

RADON MONITORING METHODOLOGY

The Radon-222 activity concentration in the Ochtinská Aragonite Cave, Mladeč Caves, Bozkov Dolomite Caves, and Županova Cave is continuously passively monitored using a RADIM 3A monitor. The monitor uses spectrometric detection of alpha particles, with an energy of 6.002 MeV, emitted by radon progeny ^{218}Po decay having a half-live of approximately 3.1 min (Sabbarese et al., 2017a; Stránský and Thinová, 2017). Detection of alpha particles is based on electrostatic collection on a silicon detector, using a hemispherical metallic chamber with a volume of 8.3×10^{-4} m^3 (the detection efficiency is 0.8 count m^3/ Bqh). The background elimination is provided once per year, by deleting alpha particles at 5.30 MeV from radon progeny ^{210}Po (half-life of 138.4 d) that contribute to a long-lasting background on the silicon detector surface (Ambrosino, 2020), In very damp environments, the radon gauge is placed in a plastic box containing a bowl with a desiccant ($CaCl_2$) inert toward radon, to avoid the extreme influence of relative humidity

on the radon measurements (Ambrosino et al., 2020d). Measurement intervals are set to 30 minutes, and for statistical analysis, the daily averages are considered.

A "cave" version of the RADIM 3A monitor, the RADIM 5WP (desiccant inside the monitor, lower sensitivity), has been used for continuous measurements of ^{222}Rn activity concentrations by diffusion in the Rull Cave (Legarda et al., 2010; Pla et al., 2020). The working principle of the device is similar to the newest model described above: the radon activity concentration is determined by measuring the gross α-activity of the radon decay products ^{218}Po and ^{214}Po, which are collected electrostatically (after decay of the radon in a diffusion chamber) on the surface of a Si-semiconductor detector (Ambrosino et al., 2018a). The detection efficiency is 0.4 imp Bq/(h m^3). Measurement intervals are set to 30 minutes, and the daily averages are used.

In Važecká Cave, radon activity concentrations are continuously monitored using BARASOL BMC2 multi sensors. The radon diffuses inside a detection volume (1.48 × 10^{-3} m^3) through three cellulose filters, which trap all of the solid daughter products (Smetanová et al., 2020). The sensor is an implanted silicon detector with a depleted depth of 100 µm and sensitive area of 400 mm^2. It enables spectrometric detection of decay of ^{222}Rn and its daughter products in the detection volume (window set at between 1.5 MeV and 6 MeV) (Kumar et al., 2009). The sensitivity is 50 imp Bq/(h m^3), measurement intervals are 10 minutes, and the daily averages are taken.

In all of the dead-end caves (except Bozkov Dolomite Cave and Važecká Cave), the radon monitors are located in relatively deep areas with no public access (Fig. 2), where parameters such as ventilation and aerosol spectrum are not influenced by the movement of visitors (Thinová et al., 2005b; Ambrosino et al., 2020d).

RESULTS AND DISCUSSION

The time series of ^{222}Rn activity concentration measurements in the six investigated dead-end caves, and meteorological air parameters inside and outside of the caves, are for the period between January 2017 and January 2020. Such a long period is appropriate and accurate for defining the annual regime in the caves and for estimating the radon activity concentrations, and enables seasonal/periodic trends to be highlighted. In fact, neither 1- to 3-month long measurements nor a half-year to one-year long intervals may be used to correctly estimate radon activity concentrations (Somlai et al., 2011). The daily ^{222}Rn time series recorded in the monitored European dead-end caves between 2017 and 2020 are shown in Figure 3. Short data drop-outs occurred in the recorded radon time series in some of the caves due to failure of the data logging network. These were filled-in using the well-proven SSA spectral method (Ambrosino et al., 2019b), which *eigendecomposes* the time series and subsequently reconstructs them, recursively imputing the missing values using additive component regressions (Ambrosino et al., 2020a; Golyandina and Osipov, 2007). The measured radon value ranges are 633−4,321 Bq/m^3 for Rull Cave (Spain), 1,336−8,456 Bq/m^3 for Bozkov Dolomite Caves (Czechia), 2,865−11,483 Bq/m^3 for Mladeč Caves (Czechia), 3,560−26,785 Bq/m^3 for Važecká Cave (Slovakia), 3,571−11,913 Bq/m^3 for Ochtinská Aragonite Cave (Slovakia), and 743−6,769 Bq/m^3 for Županova Cave (Slovenia).

There are major differences in the radon activity concentrations among the dead-end caves (Fig. 3). The radon concentrations in Važecká Cave (Slovakia) are nearly double the general levels of the other five caves, highlighted in Fig. 3 by the secondary y-axes. The speleological characteristics of the investigated dead-end caves, i.e. the karst rocks and bedrock types, their origin, composition and ^{226}Ra content, influence the radon concentration levels (Sabbarese et al., 2017b; UNSCEAR, 2000). Discontinuities, such as cracks, faults, and fractures, permit the efficient transport of soil gases containing radon and CO_2 (Gregorič et al., 2013; Smetanová et al., 2020). Such transport occurs only if these discontinuities are not completely filled by water-carried silt or clay particles unless they are loosened by rock movements. Then, the nature of the dead-end cave characterized by limited ventilation and relative few entries, contributes to the accumulation of an increase in gas levels inside the caves. The caves appear not to be affected by proximity to nearby caves, and they do not show similar radon activity concentration values. On the other hand, the six dead-end caves exhibit very similar behavior, having an annual periodic trend. More precisely, radon levels in all of the caves reflect seasonal changes, with an increase during the start of the warm period, from around March, and a decrease during the start of the cold period, from around September. Therefore, during the cold or warm season, the radon values tend to stabilize for about three months. This periodicity, more pronounced in some of the caves but always clearly notable, suggests that natural ventilation largely controls the underground accumulation of radon.

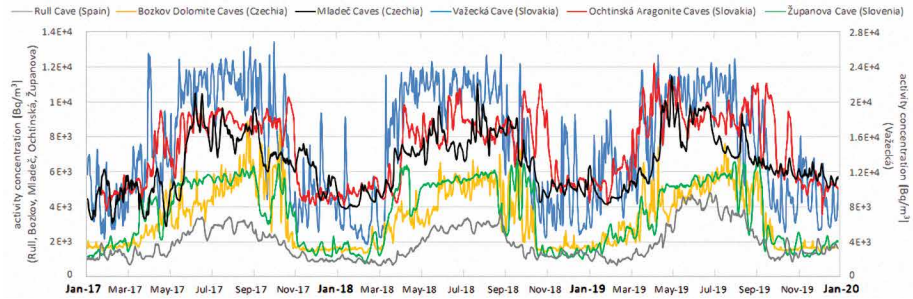


Figure 3. Daily ^{222}Rn time series of the six studied European dead-end caves for January 2017–January 2020.

To investigate this aspect, the recorded meteorological parameters were taken into account during the data processing. These parameters are monitored inside the caves alongside radon, while outside they are measured using a Weather Station data-logger located nearby. The meteorological trends of the six caves have been shown separately in several studies with different scopes during the last decade (Rovenská and Thinová, 2010; Ambrosino et al., 2020f; Pla et al., 2020; Smetanová et al., 2020). The current 2017−2020 meteorological monitoring values show a similar trend to those mentioned in the previous publications. The meteorological data are not reported in the present work so to not burden this paper with many figures. Instead, a cross-correlation study using the Matlab tool between the meteorological parameters and the ^{222}Rn activity concentrations in all of the caves was performed to find the dominant factor driving the radon variability (Ambrosino et al., 2019b). The results (not shown) conclude that the difference between the outer and inner air temperatures almost exclusively controls the ^{222}Rn changes, with an average value equal to 0.82 °C and a mean lag time impact on ^{222}Rn being one week at most. The high values of outer-inner temperature differences correspond to the high radon activity concentration levels, and vice versa. This strong dependence is also clearly visible in Fig. 4, where the two independent signals are compared for all of the caves. In the winter, significantly lower radon levels are observed compared to the summer (Sainz et al., 2018) because during the winter and early spring, cold and dense outside air enters the caves along the floor, and the soil gas with radon remains in the deeper areas of the rock massive (Kamra, 2015). This natural convective circulation, as a result of internal-external buoyancy temperature differences, causes the air flow outside to carry the radon continuously emanated from the bedrocks with it, resulting in a decrease in the radon concentrations in the caves (Rowberry et al., 2016). The ventilation mechanism is stronger in the summer when the difference between the outer-inner and concurrently noon-midnight temperature is higher, and the soil gas is drawn from the bedrock area into the cave. Therefore, due to the outdoor temperatures in the summer being higher than the constant temperatures in the caves, more radon is pulled out of the subsoil, because the inner cooler denser air keeps the radon emitted from the rocks in the caves, resulting in significantly high radon concentrations (Rovenská and Thinová, 2010).

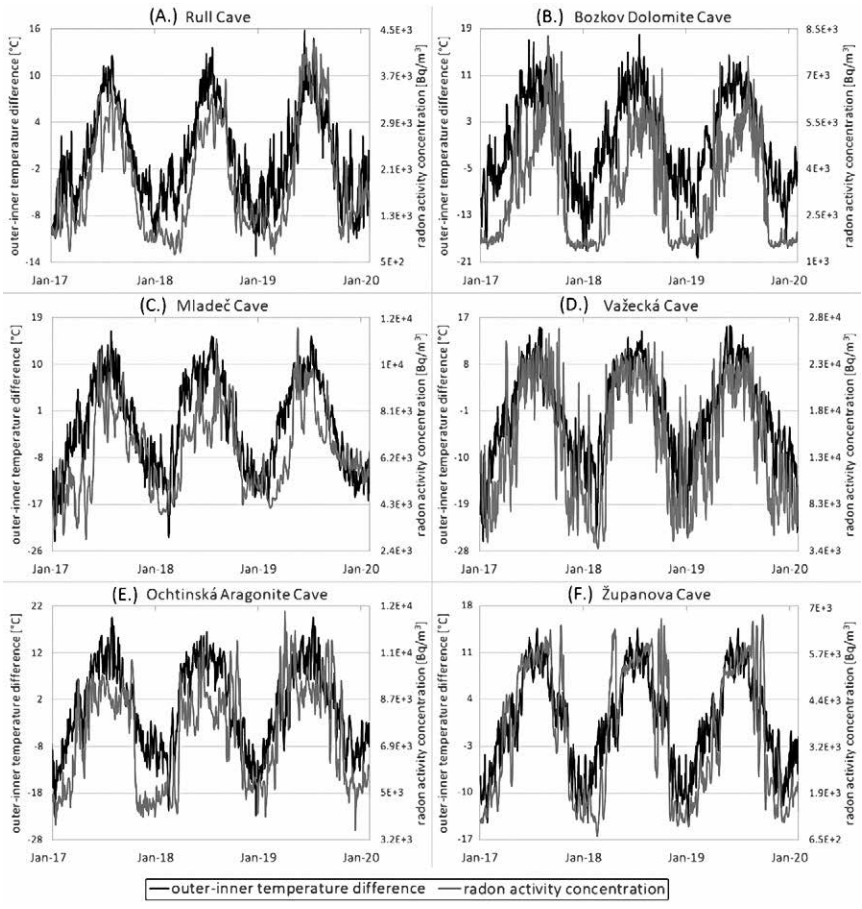


Figure 4. ^{222}Rn activity concentrations vs. the difference between outer and inner air temperatures in the six studied dead-end caves across Europe from January 2017–January2020 (the letters indicating the caves reflect those used in Figure 2). The much higher radon concentrations in Važecká Cave (Slovakia) are shown on the secondary y-axes.

To isolate the seasonal cycles, a 24-hour running continuous Pearson's (linear) correlation with a half hour step (i.e., a sort of daily correlation over time, was run using the Matlab tool) (Press et al., 2007). Similar to the seasonal variations, the diurnal variations in all of the caves are mainly influenced by the temperature difference, with a mean correlation coefficient *R* of 0.77. Therefore, diurnal and seasonal air exchange due to the convective circulation effect results in diurnal and seasonal fluctuations in natural gas and aerosol concentrations (Bezek et al., 2012; Sainz et al., 2018). Sifting through the literature dedicated to the issues of ^{222}Rn monitoring in caves, it is worthy to note how such a seasonal-periodic modulation found in the present work is characteristic only in dead-end caves (Zelinka 2004; Richon et al., 2005; Perrer et al., 2007; Oh and Kim, 2011; Turek et al., 2015; Ambrosino et al., 2018b; Czuppon et al., 2018; Sainz et al., 2018; Pla et al., 2020; Smetanová et al., 2020). In fact, it emerges that the show caves with more than one entry or large entries exhibit entirely different behavior with variable radon patterns not implicit for any dominant meteorological factor other than a combination of them, as is the case of Driny Cave in Slovakia (Rowberry et al., 2016), Olibano Cave in Italy (Ambrosino et al., 2019c), Zbrašov Ara-

Table 1. Pearson's (linear) correlation coefficients of ^{222}Rn time series for the six studied dead-end caves.

Location	Correlation Coef., *R*
Ochtinská - Županova	0.82
Ochtinská - Važecká	0.72
Ochtinská - Bozkov	0.75
Ochtinská - Mladeč	0.60
Županova - Važecká	0.83
Županova - Bozkov	0.82
Županova - Mladeč	0.72
Važecká - Bozkov	0.76
Važecká - Mladeč	0.68
Bozkov - Mladeč	0.68
Rull - Ochtinská	0.62
Rull - Mladeč	0.76
Rull - Bozkov	0.76
Rull - Važecká	0.70
Rull - Županova	0.73

gonite Caves in Czechia (Briestenský et al., 2014), Jenolan Caves in Australia (Zahorowski et al., 1998), Tapolca Cave in Hungary (Somlai et al., 2009), Maomaotou Big Cave in China (Tang et al., 2020), and others all over the world.

Two additional analyses were performed to determine the degree of similarity among the six studied caves qualitatively visible in Figure 3, and also to highlight the seasonal variations of the ^{222}Rn time series: a Pearson's (linear) correlation analysis (Press et al., 2007) of ^{222}Rn signals among the caves (Table 1), and the monthly average of ^{222}Rn activity concentration levels per mean year (Fig. 5). The results of the correlation analysis in Table 1 show how the six dead-end caves have similar radon levels, with *R* values greater than or equal to 0.6, and with a maximum *R* of 0.83 and mean values of *R* 0.73 ± 0.06. These high correlation coefficient values, together with Figure 5, confirm and summarize what has been constantly stated in our paper (i.e., the periodic annual seasonality of the ^{222}Rn signals in the dead-end caves with overall levels increasing from the cold to the warm season (Perrer et al., 2007; Dueñas et al., 2011; Oh and Kim, 2011; Sainz et al., 2018).

Figures 3 and 5 validate the high radon activity concentrations, ranging from 633 Bq/m^3 to 26,785 Bq/m^3, recorded inside all of the dead-end caves. The latest European Union Directive on ionizing radiation protection (2013/59/Euratom) establishes a reference level for the annual average of indoor radon activity concentrations in air of 300 Bq/m^3 (Euratom, 2014), which also extends to all show caves and agencies granting permission for activities in non-tourist caves (Field, 2007; Dumitru et al., 2015). All of the investigated dead-end caves are well above the European Union reference level for indoor radon gas of 300 Bq/m^3, whereby posing a potential radiological health hazard to cave guides, cavers, and also occasional visitors and employees (Lario et al., 2005; Thinová et al., 2005a; Somlai et al., 2009; Ambrosino et al., 2020f). Our survey on dead-end caves may be a further contribution to the radon concentration monitoring effort in caves worldwide, also aiming to put in evidence on the risk level due to radon inhalation and its human health impact on people in dead-end caves. Therefore, we expect these results to be of great interest to the administrative staff of the investigated show caves and, at the same time, agencies involved in granting permits to access these caves, to inform employees and the public about the high levels of radon in the caves, especially during the summer, and to recommend adequate local regulations.

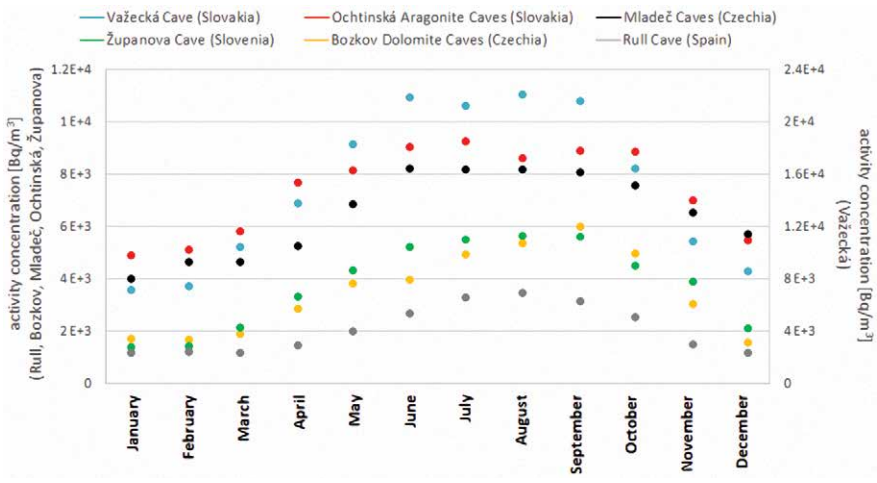


Figure 5. Average monthly variations per mean year of ^{222}Rn activity concentrations in the six studied dead-end caves, for the monitoring period January 2017–January 2020. The much higher radon concentrations in Važecká Cave (Slovakia) are shown on the secondary y-axes.

CONCLUSIONS

Dead-end show caves are underground environments with no significant ventilation, a relatively stable climate, and only one or two small entry points. In this study, six dead-end caves across Europe were continuously monitored with the aim of investigating the ^{222}Rn levels in relation to meteorological parameters. Different elevated radon activity concentrations, ranging from 633 Bq/m^3 to 26,785 Bq/m^3, were recorded during January 2017 to January 2020. The environments of the caves show a very similar behavior (calculated mean linear correlation factor *R* of 0.73 ± 0.06), with stable ^{222}Rn activity concentrations and particular periodic trends indicating strong seasonal changes, higher in the summer rather than in the winter. Air density differences between cave air and the outside atmosphere may create density-driven flows, resulting in air exchange between the cave and the atmosphere outside. Because air density is

influenced by temperature, the temperature gradient between the outer and inner atmospheres of the dead-end caves is the dominant meteorological parameter (mean cross-correlation factor *R* of 0.82) determining the variation in radon levels. All of the investigated dead-end caves exceed the European reference level of indoor annual average radon concentration of 300 Bq/m^3. The results obtained in this work may help to improve the characterization of special dead-end cave environments, and underline the importance of radon monitoring to assess the radiation risk for people entering and remaining for a certain time. The presented paper is a first comprehensive radon survey focused on dead-end show caves in Europe.

ACKNOWLEDGEMENTS

The authors would like to express thanks to the involved caves Administrations for the support provided during the investigation. Our work was also supported by: the Centre of Advanced Applied Sciences [CZ.02.1.01/0.0/0.0/16–019/0000778], the CzechGeo-EPOS project 'Distributed system of permanent observatory measurements and temporary monitoring of geophysical fields in the Czech Republic' [CZ.02.1.01/0.0/0.0/16_013/0001800], the Long-term Conceptual Development Research Organization [RVO: 67985891], the Spanish Ministry of Science, Innovation, and Universities [grant number RTI2018-099052-B-I00], the Regional Government of Comunidad Valenciana (Spain) [grant number AICO/2020/175], the Scientific Grant Agency of the Ministry of Education, Science, Research and Sport of the Slovak Republic (VEGA project no. 2/0083/18 and 2/0015/21).

REFERENCES

Ambrosino, F., 2020, Study on a peak shape fitting model for the analysis of alpha-particle spectra: Applied Radiation and Isotopes, v. 159, p. 109090. https://doi.org/10.1016/j.apradiso.2020.109090.

Ambrosino, F., Buompane, R., Pugliese, M., Roca, V., and Sabbarese, C., 2018a, RaMonA system for radon and thoron measurement: Nuovo Cimento C, v. 41, no. 6, p. 222. https://doi.org/10.1393/ncc/i2018-18222-5.

Ambrosino, F., De Cesare, W., Roca, V., and Sabbarese, C., 2019c, Mathematical and geophysical methods for searching anomalies of the Radon signal related to earthquakes: Journal of Physics: Conference Series, v. 1226, p. 012025. https://doi.org/10.1088/1742-6596/1226/1/012025.

Ambrosino, F., Pugliese, M.,Roca, V., and Sabbarese, C., 2018b, Innovative methodologies for the analysis of radon time series: Nuovo Cimento C, v. 41, no. 6, p. 223. https://doi.org/10.1393/ncc/i2018-18223-4.

Ambrosino, F., Roca, V., Buompane, R., and Sabbarese, C., 2020b, Development and calibration of a method for direct measurement of ^{220}Rn (Thoron) activity concentration: Applied Radiation and Isotopes, v. 166, p. 109310. https://doi.org/10.1016/j.apradiso.2020.109310.

Ambrosino, F., Sabbarese, C., Roca, V., Giudicepietro, F., and De Cesare,W., 2020a, Connection between ^{222}Rn emission and geophysical-geochemical parameters recorded during the volcanic unrest at Campi Flegrei caldera (2011-2017): Applied Radiation and Isotopes, v. 166, p. 109385. https://doi.org/10.1016/j.apradiso.2020.109385.

Ambrosino, F., Sabbarese, C., Roca, V., Giudicepietro, F., and Chiodini, G., 2020c, Analysis of 7-years Radon time series at Campi Flegrei area (Naples, Italy) using artificial neural network method: Applied Radiation and Isotopes, v. 163, p. 109239. https://doi.org/10.1016/j.apradiso.2020.109239.

Ambrosino, F., Thinová, L., Briestenský, M., and Sabbarese, C., 2019a, Analysis of Radon time series recorded in Slovak and Czech caves for the detection of anomalies due to seismic phenomena: Radiation Protection Dosimetry, v. 186, no. 2-3, p. 428–432. https://doi.org/10.1093/rpd/ncz245.

Ambrosino, F., Thinová, L., Briestenský, M., and Sabbarese, C., 2019b, Anomalies identification of Earth's rotation rate time series (2012–2017) for possible correlation with strong earthquakes occurrence: Geodesy and Geodynamics, v. 10, no. 6, p. 455–459. https://doi.org/10.1016/j.geog.2019.06.002.

Ambrosino, F., Thinová, L., Briestenský, M., Giudicepietro, F., Roca, V., and Sabbarese, C., 2020d, Analysis of geophysical and meteorological parameters influencing ^{222}Rn activity concentration in Mladeč caves (Czech Republic) and in soils of Phlegrean Fields caldera (Italy): Applied Radiation and Isotopes, v. 160, p. 109140. https://doi.org/10.1016/j.apradiso.2020.109140.

Ambrosino, F., Thinová, L., Briestenský, M., Šebela, S., and Sabbarese, C., 2020e, Detecting time series anomalies using hybrid methods applied to Radon signals recorded in caves for possible correlation with earthquakes: Acta Geodaetica et Geophysica, v. 55, p. 405–420. https://doi.org/10.1007/s40328-020-00298-1.

Ambrosino, F., Thinová, L., Briestenský, M., and Sabbarese, C., 2020f, Study of ^{222}Rn continuous monitoring time series and dose assessment in six European caves: Radiation Protection Dosimetry, v. 191, no. 2, p. 233–237. https://doi.org/10.1093/rpd/ncaa159.

Ambrosino, F., Thinová, L., Hýža, M., and Sabbarese, C., 2020g, ^{214}Bi/^{214}Pb radioactivity ratio three-year monitoring in rainwater in Prague: Nukleonika, v. 65, no. 2, p. 115–119. https://doi.org/10.2478/nuka-2020-0018.

Badino, G., 2010, Underground meteorology - "What's the weather underground?": Acta Carsologica, v. 39, no. 3, p. 427–448. https://doi.org/10.3986/ac.v39i3.74.

Bahtijari,M., Vaupotič, J., Gregorič, A., Stegnar, P., and Kobal, I., 2008. Exposure to radon in the Gadime Cave, Kosovo: Journal of Environmental Radioactivity, v. 99, p. 343–348. https://doi.org/10.1016/j.jenvrad.2007.08.003.

Bella, P., Littva, J., Pruner, P., Bosák, P., Šlechta, S., Hercman, H., and Čížiková, K., 2016, Geological setting, morphology and evolution of the Važecká Cave, Slovakia: Acta Carsologica Slovaca, v. 54, no. 1, p. 5–31.

Bezek, M., Gregorič, A., Kávási, N., and Vaupotič, J., 2012, Diurnal and seasonal variations of concentration and size distribution of nano aerosols (10–1100 nm) enclosing radon decay products in the Postojna Cave, Slovenia: Radiation Protection Dosimetry, v. 152, no. 1-3, p. 174–178. https://doi.org/10.1093/rpd/ncs218.

Bosák, P., Bella, P., Cílek, V., Ford, D.C., Hercman, H., Kadlec, J., Osborne, A., and Pruner, P., 2002, Ochtiná Aragonite Cave (Western Carpathians, Slovakia): Morphology, mineralogy of the fill and genesis: Geologica Carpathica, v. 53, no. 6, p. 399-410.

Briestenský, M., Thinová, L., Praksová, R., Stemberk, J., Rowberry, M.D., and Knejflová, Z., 2014, Radon, carbon dioxide and fault displacements in central Europe related to the Tōhoku earthquake: Radiation Protection Dosimetry, v. 160, no. 1-3, p. 78–82. https://doi.org/10.1093/rpd/ncu090.

Cigna, A.A., 2005, Radon in caves: International Journal of Speleology, v. 34, no. 1–2, p. 1–18. https://doi.org/10.5038/1827-806X.34.1.1.

Czuppon, G., Demény, A., Leél-Ossy, S., Ótvari, M., Molnár, M., Stieber, J., Kiss, K., Kármár, K., Surányi, G., and Harzpra, L., 2018, Cave monitoring in the Béke and Baradla caves (Northeastern Hungary): implications for the conditions for the formation cave carbonates: International Journal of Speleology, v. 47, no. 1, p. 13–28. https://doi.org/10.5038/1827-806X.47.1.2110.

Darby, S., Hill, D., and Doll, R., 2001, Radon: A likely carcinogen at all exposures: Annals of Oncology, v. 12, no. 10, p. 1341–1351. https://doi.org/10.1023/A:1012518223463.

Droppa, A., 1962, Speleologický výskum Važeckého krasu (Speleological research of Važec karst area): Geografical Journal, v. 14, no. 4, p. 264–293. https://doi.org/10.1016/j.radmeas.2011.06.039.

Dueñas, C., Fernández, M.C., Cañete, S., Pérez, M., and Gordo, E., 2011, Seasonal variations of radon and the radiation exposure levels in Nerja cave, Spain: Radiation Measurements, v. 46, no. 10, p. 1181–1186. https://doi.org/10.1016/j.radmeas.2011.06.039.

Dumitru, O.A., Onac, B.P., Fornós, J.J., Cosma, C., Ginés, A., Ginés, J., and Merino, A., 2015, Radon survey in caves from Mallorca Island, Spain: Science of The Total Environment, v. 526, p. 196–203. https://doi.org/10.1016/j.scitotenv.2015.04.076.

Etiope, G., and Martinelli, G., 2001, Migration of carrier and trace gases in the geosphere: An overview: Physics of Earth Planet Interiors, v. 129, p. 185–204. https://doi.org/10.1016/S0031-9201(01)00292-8.

Euratom, 2014, Council Directive 2013/59/Euratom of 5 December 2013 laying down basic safety standards for protection against the dangers arising from exposure to ionising radiation, and repealing Directives 89/618/Euratom, 90/641/Euratom, 96/29/Euratom, 97/43/Euratom and 2003/122/Euratom: Official Journal of the European Union, v. 57, p. 1–73.

Field, M.S., 2007, Risks to cavers and cave workers from exposures to low-level ionizinga radiation from ^{222}Rn decay in caves: Journal of Cave and Karst Studies, v. 69, no. 1, p. 207–228.

Gaál, Ľ., 2004, Geológia Ochtinskej aragonitovej jaskyne: Slovenský kras, v. 42, p. 37–56.

Garcia-Anton, E., Cuezva, S., Fernandez-Cortes, A., Alvarez-Gallego, M., Pla, C., Benavente, D., Cañaveras, J.C., and Sanchez-Moral, S., 2017, Abiotic and seasonal control of soil-produced CO2 efflux in karstic ecosystems located in oceanic and Mediterranean climates: Atmospheric Environment, v. 164, p. 31–49. https://doi.org/10.1016/j.atmosenv.2017.05.036.

Golyandina, N., and Osipov, E., 2007, The "Caterpillar"-SSA method for analysis of time series with missing values: Journal of Statistical Planning and Inference, v. 137, p. 2642–2653. https://doi.org/10.1016/j.jspi.2006.05.014.

Gregorič, A., Vaupotič, J., and Gabrovšek, F., 2013, Reasons for large fluctuation of radon and CO_2 levels in a dead-end passage of a karst cave (Postojna Cave, Slovenia): Natural Hazards and Earth System Sciences, v. 13, p. 287–297. https://doi.org/10.5194/nhess-13-287-2013.

Hromas, J., 2009, Caves, *in* Mackovčin, P., and Sedláček, M., eds., Protected Natural Areas of the Czech Republic, Bundle XIV, p. 382–385.

Kamra, L., 2015, Seasonal emanation of radon at Ghuttu, northwest Himalaya: Differentiation of atmospheric temperature and pressure influences: Applied Radiation and Isotopes, v. 105, p. 170–175. https://doi.org/10.1016/j.apradiso.2015.08.031.

Kobal, I., Burger, J., Smodiš, B., and Škofljanec, M., 1986, Radon concentrations in Slovene tourist Caves: Naše jame, v. 28, p. 11–17.

Kumar, A., Singh, S., Mahajan, S., Bajwa Singh, B., Kalia, R., and Dhar, S., 2009, Earthquake precursory studies in Kangra valley of North West Himalayas, India, with special emphasis on radon emission: Applied Radiation and Isotopes, v. 67, no. 10, p. 1904–1911. https://doi.org/10.1016/j.apradiso.2009.05.016.

Lario, J., Sánchez-Moral, S., Cañaveras, J.C., Cuezva, S., and Soler, V., 2005, Radon continuous monitoring in Altamira Cave (northern Spain) to assess user's annual effective dose: Journal of Environmental Radioactivity, v. 80, no. 2, p. 161–174. https://doi.org/10.1016/j.jenvrad.2004.06.007

Legarda, F., Idoeta, R., Alegría, N., and Herranz, M., 2010, An active radon sampling device for high humidity places: Radiation Measurements, v. 45, no. 1, p. 122–128. https://doi.org/10.1016/j.radmeas.2010.01.003.

Nero, A.V., 1988, Radon and its decay products in indoor air: an overview, *in* Nazaroff, W.W., and Nero, Jr., A.V., eds., Radon and its Decay Products in Indoor Air, New York, John Wiley & Sons, p. 1–53.

Oh, Y.H., and Kim, G., 2011, Factors controlling the air ventilation of a limestone cave revealed by ^{222}Rn: Geosciences Journal, v. 15, no. 1, p. 115–119. https://doi.org/10.1007/s12303-011-0010-3.

Pantelić, G., Čeliković, I., Živanović, M., Vukanac, I., Nikolić, J.K., Cinelli, G., and Gruberc, V., 2019, Qualitative overview of indoor radon surveys in Europe: Journal of Environmental Radioactivity, v. 204, p. 163–174. https://doi.org/10.1016/j.jenvrad.2019.04.010.

Perrier, F., Richon, P., Gautam, U., Tiwari, D.R., Shrestha, P., and Sapkota, S.N., 2007, Seasonal variations of natural ventilation and radon-222 exhalation in a slightly rising dead-end tunnel: Journal of Environmental Radioactivity, v. 97, no. 2-3, p. 220–235. https://doi.org/10.1016/j.jenvrad.2007.06.003.

Pla, C., Cuezva, S., Garcia-Anton, E., Fernandez-Cortes, A., Cañaveras, J.C., Sanchez-Moral, S., and Benavente, D., 2016, Changes in the CO_2 dynamics in near-surface cavities under a future warming scenario: factors and evidence from the field and experimental findings: Science of the Total Environment, v. 565, p. 1151–1164. https://doi.org/10.1016/j.scitotenv.2016.05.160

Pla, C., Cuezva, S., Martinez-Martinez, J., Fernandez-Cortes, A., Garcia-Anton, E., Fusi, N., Crosta, G.B., Cuevas-Gonzalez, J., Cañaveras, J.C., Sanchez-Moral, S., and Benavente, D., 2017, Role of soil pore structure in water infiltration and CO2 exchange between the atmosphere and underground air in the vadose zone: A combined laboratory and field approach: Catena, v. 149, p. 402-416. https://doi.org/10.1016/j.catena.2016.10.018.

Pla, C., Fernandez-Cortes, A., Cuezva, S., Galiana-Merino, J.J., Cañaveras, J.C., Sanchez-Moral, S., and Benavente, D., 2020, Insights on climate-driven fluctuations of cave ^{222}Rn and CO_2 concentrations using statistical and wavelet analyses: Geofluids, v. 2020. https://doi.org/10.1155/2020/8858295.

Placer, L., 2008, Principles of the tectonic subdivision of Slovenia: Geologija, v. 51, no. 2, p. 205–217. https://doi.org/10.5474/geologija.2008.021.

Prelovšek, M., Šebela, S., and Turk J., 2018, Carbon dioxide in Postojna Cave (Slovenia): spatial distribution, seasonal dynamics and evaluation of plausible sources and sinks: Environmental Earth Sciences, v. 77, p. 289. https://doi.org/10.1007/s12665-018-7459-6.

Press, W.H., Teukolsky, S.A., Vetterling, W.T., and Flannery, B.P., 2007, Numerical Recipes: The Art of Scientific Computing, Third Edition: New York, Cambridge University Press, 745 p.

Ravbar, N., and Košutnik, J., 2014, Variations of karst underground air temperature induced by various factors (Cave of Županova jama, Central Slovenia): Theoretical and Applied Climatology, v. 116, p. 327–341. https://doi.org/10.1007/s00704-013-0955-4.

Richon, P., Perrier, F., Sabroux, J-C., Trique, M., Ferry, C., Voisin, V., and Pili, E., 2005. Spatial and time variations of radon-222 concentration in the atmosphere of a dead-end horizontal tunnel: Journal of Environmental Radioactivity, v. 78, p. 179–198. https://doi.org/10.1016/j.jenvrad.2004.05.001.

Rovenská, K., and Thinová, L., 2010, Seasonal variation of radon in the Bozkov cave: Nukleonika, v. 55, no. 4, p. 483–489.

Rovenská, K., Thinová, L., and Ždímal, V., 2008, Assessment of the dose from radon and its decay products in the Bozkov dolomite cave: Radiation Protection Dosimetry, v. 130, no. 1, p. 34–37. https://doi.org/10.1093/rpd/ncn114.

Rowberry, M.D., Martí, X., Frontera, C., Van De Wiel, M.J., and Briestenský, M., 2016, Calculating flux to predict future cave radon concentrations: Journal of Environmental Radioactivity, v. 157, p. 16–26. https://doi.org/10.1016/j.jenvrad.2016.02.023.

Sabbarese, C., Ambrosino, F., Buompane, R., Pugliese, M., and Roca, V., 2017a, analysis of alpha particles spectra of the radon and thoron progenies generated by an electrostatic collection detector using new software: Applied Radiation and Isotopes, v. 122, p. 180–185. https://doi.org/10.1016/j.apradiso.2017.01.042.

Sabbarese, C., Ambrosino, F., De Cicco, F., Pugliese, M., Quarto, M., and Roca, V., 2017b, Signal decomposition and analysis for the identification of periodic and anomalous phenomena in radon time-series: Radiation Protection Dosimetry, v. 177, no, 1-2, p. 202–206. https://doi.org/10.1093/rpd/ncx159.

Sabbarese, C., Ambrosino, F., D'Onofrio, A., and Roca, V., 2020a, Radiological characterization of natural building materials from the Campania region (Southern Italy): Construction and Building Materials, v. 268. https://doi.org/10.1016/j.conbuildmat.2020.121087.

Sabbarese, C., Ambrosino, F., Chiodini, G., Giudicepietro, F., Macedonio, G., Caliro, S., De Cesare, W., Bianco, F., Pugliese, M., and Roca, V., 2020b, Continuous Radon monitoring during seven years of volcanic unrest at Campi Flegrei caldera (Italy): Scientific Reports, v. 10, p. 9551. https://doi.org/10.1038/s41598-020-66590-w.

Sabbarese, C., Ambrosino, F., and D'Onofrio, A., 2021, Development of radon transport model in different types of dwellings to assess indoor activity concentration: Journal of Environmental Radioactivity, v. 227, p. 106501. https://doi.org/10.1016/j.jenvrad.2020.106501.

Sainz, C., Quindós, L.S., Fuente, I., Nicolas, J., and Quindós, L., 2007, Analysis of themain factors affecting the evaluation of the radon dose in workplaces: the case of tourist caves: Journal of Hazardous Materials, v. 145, p. 368–371. https://doi.org/10.1016/j.jhazmat.2006.11.033.

Sainz, C., Rábago, D., Celaya, S., Fernández, E., Quindós, G., Quindós, L., Fernández, A., Fuente, I., Arteche, J.L., and Quindós, L.S., 2018, Continuous monitoring of radon gas as a tool to understand air dynamics in the cave of Altamira (Cantabria, Spain): Science of the Total Environment, v. 624, p. 416–423. https://doi.org/10.1016/j.scitotenv.2017.12.146.

Šebela, S., Vaupotič, J., Košťák, B., and Stemberk, J. 2010, Direct measurement of present-day tectonic movement and associated radon flux in Postojna Cave, Slovenia: Journal of Cave and Karst Studies, v. 72, no. 1, p. 21-34. https://doi.org/10.4311/jcks2009es0077.

Smetanová, I., Holý, K., Luhová, L., Csicsay, K., Haviarová, D., and Kunáková, L., 2020, Seasonal variation of radon and CO_2 in the Važecká Cave, Slovakia: Nukleonika, v. 65, no. 2, p. 153–157. https://doi.org/10.2478/nuka-2020-0025.

Somlai, J., Hakl., J., Kávási, N., Szeiler, G., Szabó, P., and Kovács, T., 2011, Annual average radon concentration in the show caves of Hungary: Journal of Radioanalytical and Nuclear Chemistry, v. 287, p. 427–433. https://doi.org/10.1007/s10967-010-0841-9.

Somlai, J., Szeiler, G., Szabó, P., Várhegyi, A., Tokonami, S., Ishikawa, T., Sorimachi, A., Yoshinaga, S., and Kovács, T., 2009, Radiation dose of workers originating from radon in the show Cave of Tapolca, Hungary: Journal of Radioanalytical and Nuclear Chemistry, v. 279, no.1, p. 219–225. https://doi.org/10.1007/s10967-007-7307-3.

Špaček, P., Bábek, O., Štepancíková, P., Švancara, J., Pazdírková, J., and Sedláček, J., 2015, The Nysa Morava zone: an active tectonic domain with Late Cenozoic sedimentary grabens in the Western Carpathians' foreland (NE Bohemian Massif): International Journal of Earth Sciences, v. 104, no. 4, p. 963–990. http://dx.doi.org/10.1007/s00531-014-1121-7.

Stein, L., 1987, Chemical properties of radon, in Hopke, P.K., ed., Radon and Its Decay Products: occurrence, properties, and health effects: Washington, D.C., American Chemical Society, p. 241–251.

Stránský, V., and Thinová, L., 2017. Radon concentration time series modeling and application discussion: Radiation Protection Dosimetry, v. 177, no. 1-2, p. 155–159. https://doi.org/10.1093/rpd/ncx207.

Tang, W., Lan, G., Yang, H., Yin, J.-J., and Pu, J., 2020, Variations and influence factors of ^{210}Pb-specific radioactivity in modern calcite depositions in a subtropical cave, South China: Applied Geochemistry, v. 113, p. 104468. https://doi.org/10.1016/j.apgeochem.2019.104468.

Thinová, L., Berka, Z., Brandejsova, E., Ždímal, V., and Milka, D., 2005a, Effective dose calculation using radon daughters and aerosol particles measurement in Bozkov Dolomite Cave: International Congress Series, v. 1276, p. 381–382. https://doi.org/10.1016/j.ics.2004.11.114.

Thinová, L., and Burian, I., 2008, Effective dose assessment for workers in caves in the Czech Republic-experiments with passive radon detectors: Radiation Protection Dosimetry, v. 130, no. 1, p. 48–51. https://doi.org/10.1093/rpd/ncn118.

Thinová, L., Fronka, A., and Milka, D., 2005b, Personal dosimetry enhancement for underground workplaces: Acta Polytechnica, v. 45, no. 5, p. 44–47. https://doi.org/10.14311/770.

Turek, K., Stefanov, P., Svetlik, I., Orcikova, H., and Simek, P., 2015, Radon and CO_2 concentration screening in Bulgarian caves: International Journal of Geoheritage, v. 3, no. 2, p. 14–23. https://doi.org/10.17149/ijg.j.issn.2210.3382.2015.02.003.

UNSCEAR, 2000, Sources and effects of ionizing radiation – Annex B: Exposures from natural radiation sources, UNSCEAR 2000 Report Vol. I, Vienna, Austria, United Nations Scientific Committee on the Effects of Atomic Radiation, 156 p.

Wigley, T.M.L., 1967, Non-steady flow through a porous medium and cave breathing: Journal of Geophysical Research, v. 72, no. 12, p. 3199–3205. https://doi.org/10.1029/JZ072i012p03199.

Zahorowski, W., Whittlestone, S., and James, J.M., 1998, Continuous measurements of radon and radon progeny as a basis for management of radon as a hazard in a tourist cave: Journal of Radioanalytical and Nuclear Chemistry, v. 236, no. 1–2, p. 219-225. https://doi.org/10.1007/BF02386346.

Zelinka, J., 2004, Prehľad najnovších poznatkov z mikroklimatického monitoringu ochtinskej aragonitovej jaskyne (Summary of the newest knowledges of the microclimatic monitoring in the Ochtinská Aragonite Cave): Slovenský kras, v. 42, p. 109–120.

Linda Sobolewski, Christian Stenner, Charlotte Hüser, Tobias Berghaus, Eduardo Cartaya, and Andreas Pflitsch. Ongoing genesis of a novel glaciovolcanic cave system in the crater of Mount St. Helens, Washington, USA. *Journal of Cave and Karst Studies*, v. 84, no. 2, p. 51-65. DOI:10.4311/2021ES0113

ONGOING GENESIS OF A NOVEL GLACIOVOLCANIC CAVE SYSTEM IN THE CRATER OF MOUNT ST. HELENS, WASHINGTON, USA

Linda Sobolewski[1, C], Christian Stenner[2], Charlotte Hüser[1], Tobias Berghaus[1], Eduardo Cartaya[3], and Andreas Pflitsch[1]

Abstract

Mount St. Helens, one of the highest-risk volcanoes in the Cascade Volcanic Arc, hosts a novel system of glaciovolcanic caves that has formed around the 2004−2008 lava dome. From 2014 to 2021 a multidisciplinary research team systematically explored and mapped these new caves to ascertain their characteristics. Air and fumarole temperatures, volume flow rates, and wind regimes were also monitored. More than 3.0 km of cave passages have formed in a semicircular pattern in the volcanic crater and provide an opportunity to (1) observe cave development over time, (2) identify low temperature fumaroles as the main driving force for cave formation, (3) verify the impact of seasonal snow accumulation on cave climate, and (4) assess heat distribution in subglacial and subaerial portions of the new lava dome. Glaciovolcanic cave systems on Mount St. Helens are comparatively young (<10 years) and the most dynamic in the Pacific Northwest. Observed cave expansion during the study suggests ongoing genesis and future formation of interconnected systems. However, further expansion may also be limited by increasing fumarole temperatures towards the upper parts of the lava dome, cave instability due to snow overload, or variable subglacial volcanic heat output. New glaciovolcanic cave system development provides a unique barometer of volcanic activity on glacier-mantled volcanoes and to study the subglacial environment. We present the results of eight years of initial study within this dynamic cave system, and discuss a pathway towards future longitudinal analyses.

INTRODUCTION

The term glaciovolcanism describes all processes in which heat from the Earth's interior interacts with ice masses (Smellie and Edwards, 2016). Edwards et al. (2020) identified 245 Holocene volcanoes that potentially impact or can be impacted by surrounding ice. However, volcanically-influenced subglacial voids are rarely studied. Volcanoes that currently host glaciovolcanic cave systems include Mount Erebus (Antarctica) (Giggenbach, 1976; Curtis, 2016); Mutnovsky (Kamchatka Peninsula, Russia) and Hrafntinnusker and the Kverkfjöll mountain range (Iceland) (M. Szeglat, personal communication, 2021). Mount Rainier in the Cascade Volcanic Arc (USA) hosts the world's largest glaciovolcanic cave system, with more than 3.5 km of surveyed passages in the summit East Crater (Florea et al., 2021). The first mapping efforts on Mount Rainier date back to the 1970s (Kiver and Mumma, 1971) and comparison to recent studies by Florea et al. (2021) reveal that main passages have remained static for half a century.

The elements of volcano-ice interactions and their related hazards are known from literature (Curtis and Kyle, 2017 and references therein). However, glaciovolcanic caves have often been overlooked. Recent approaches to describe these systems are those of Zimbelman et al. (2000), Curtis (2016), and Pflitsch et al. (2017). These and previous studies examined preexisting glaciovolcanic cave systems, while Mount St. Helens presents an exceptional opportunity to observe system evolution and examine factors involved in the genesis of glaciovolcanic caves.

A brief summary of Mount St. Helens' recent eruptive history and environmental setting identifies exceptional conditions for glaciovolcanic cave formation. Mount St. Helens is an active andesite-dacite volcano (Anderson and Vining, 1999) located in the State of Washington near the Portland and Seattle Metropolitan areas (Fig. 1). It is part of the Cascade Range and the subduction of the oceanic Juan de Fuca Plate beneath the continental North American Plate (Miller and Cowan, 2017). During the past four decades Mount St. Helens has undergone dramatic morphological changes. The cataclysmic eruption in May 1980 mobilized a huge debris avalanche, removing ~400 m of the volcano's conical summit and leaving a horseshoe-shaped 2 × 3.5 km diameter north-facing crater. Two subsequent periods of activity from 1980−1986 and 2004−2008 generated lava domes. A new glacier formed in response to the morphological changes (Harris, 2005). Despite the relatively low elevation of the crater floor (<2,200 m), deep shade and insulating dust layers allow snow, rime, and avalanche deposits to accumulate (Schilling et al., 2004). The glacier, since 2006 officially called Crater Glacier (Scott et al., 2008), is impacted by rockfall from the surrounding crater walls and has an average rock content of 15 % (Walder et al., 2008); Schilling et al. (2004) estimated one-third of the glacier to be rock debris in some areas.

[1]Institute of Geography, Ruhr-University Bochum, Universitätsstraße 150, 44801 Bochum, Germany
[2]Alberta Speleological Society, Calgary, AB T2Z2E3, Canada
[3]Glacier Cave Explorers, Redmond, OR 97756, USA
[C]Corresponding author: linda.sobolewski@ruhr-uni-bochum.de

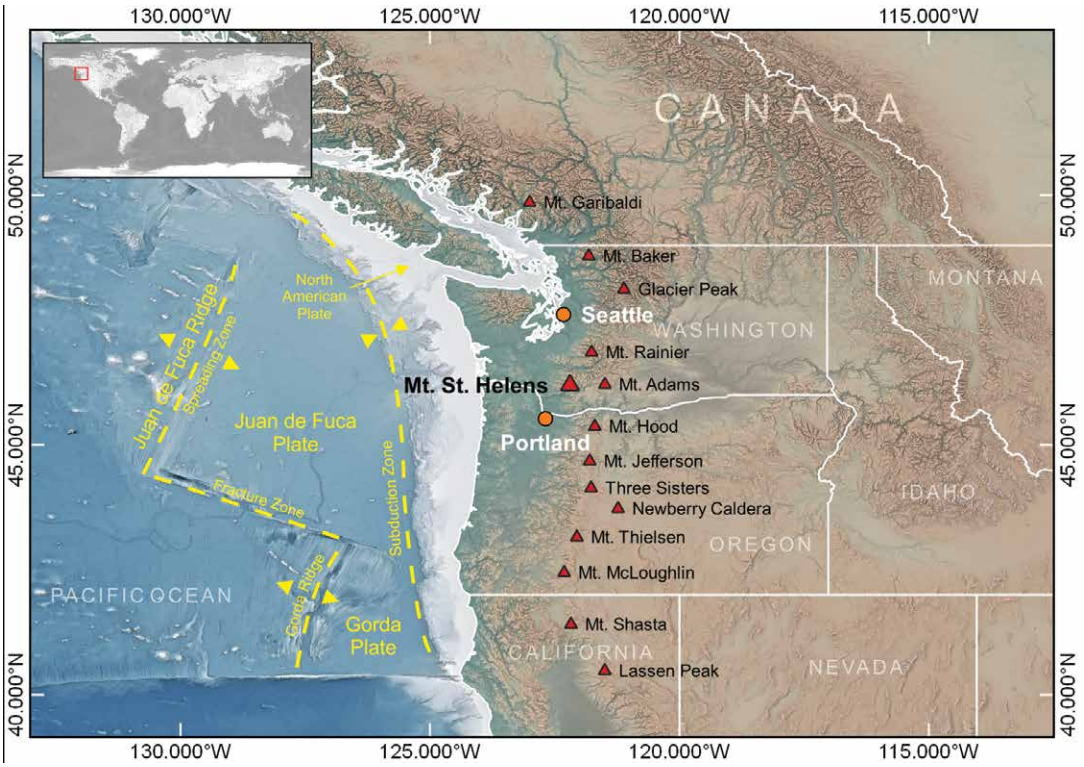


Figure 1. The Cascade Volcanic Arc with selected geological structures and major cities. Volcanism results from subduction of the oceanic Juan de Fuca Plate beneath the continental North American Plate. Basic map: General Bathymetric Chart of the Oceans (GEBCO). Inset: Natural Earth.

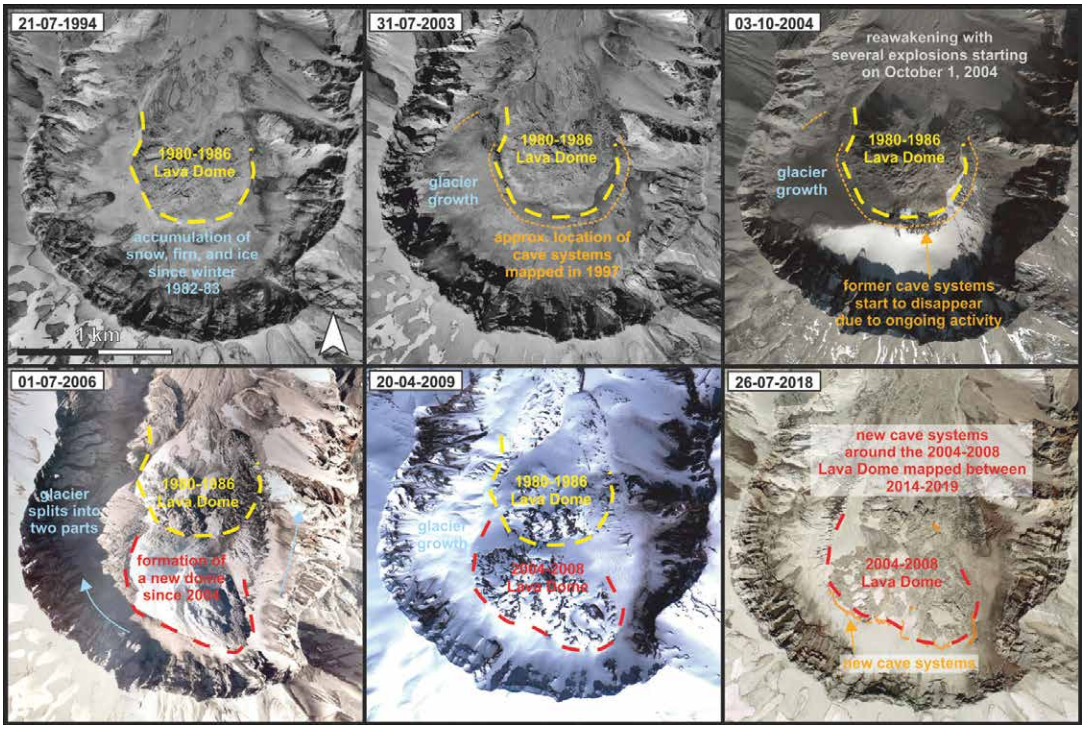


Figure 2. Development of Mount St. Helens crater and Crater Glacier. Images derived from Google Earth and document the main morphological changes from 1994 to 2018. Today, the crater is characterized by two lava domes, the 1980−1986 lava dome and the 2004−2008 lava dome; a newly formed glacier; and more than 3.0 km of glaciovolcanic cave systems which circumnavigate the new dome. Former cave systems were obliterated by renewed eruptions between 2004 and 2008. © Google Earth.

Anderson et al. (1998) described the formation of firn caves around the 1980−1986 lava dome (Fig. 2). More than 2.4 km of cave passages were mapped at that time. Volcanic activity from 2004 to 2008 and the formation of a second lava dome disrupted and obliterated these caves. In 2012, aerial observations suggested the existence of new glaciovolcanic caves, as indicated by a large chasm south of the 2004−2008 lava dome. Our study commenced with this discovery and from 2014 to 2021 we identified numerous glaciovolcanic caves which surround the new lava dome. In 2020 the crater hosted 10 individual caves with 2.3 km of mapped passages, arranged in a semicircular pattern around the 2004-2008 lava dome (Fig. 3). By June, 2021, 13 caves were described with a combined length of 3.0 km.

This paper presents a detailed description of the Mount St. Helens caves in order to illustrate different stages of glaciovolcanic cave development and their dynamics, and forecast further evolution. Climatic data include air temperatures and wind regimes and are supplemented by fumarole temperatures and flow rates. These data, supplemented by snow accumulation from nearby climate stations, help to understand season-

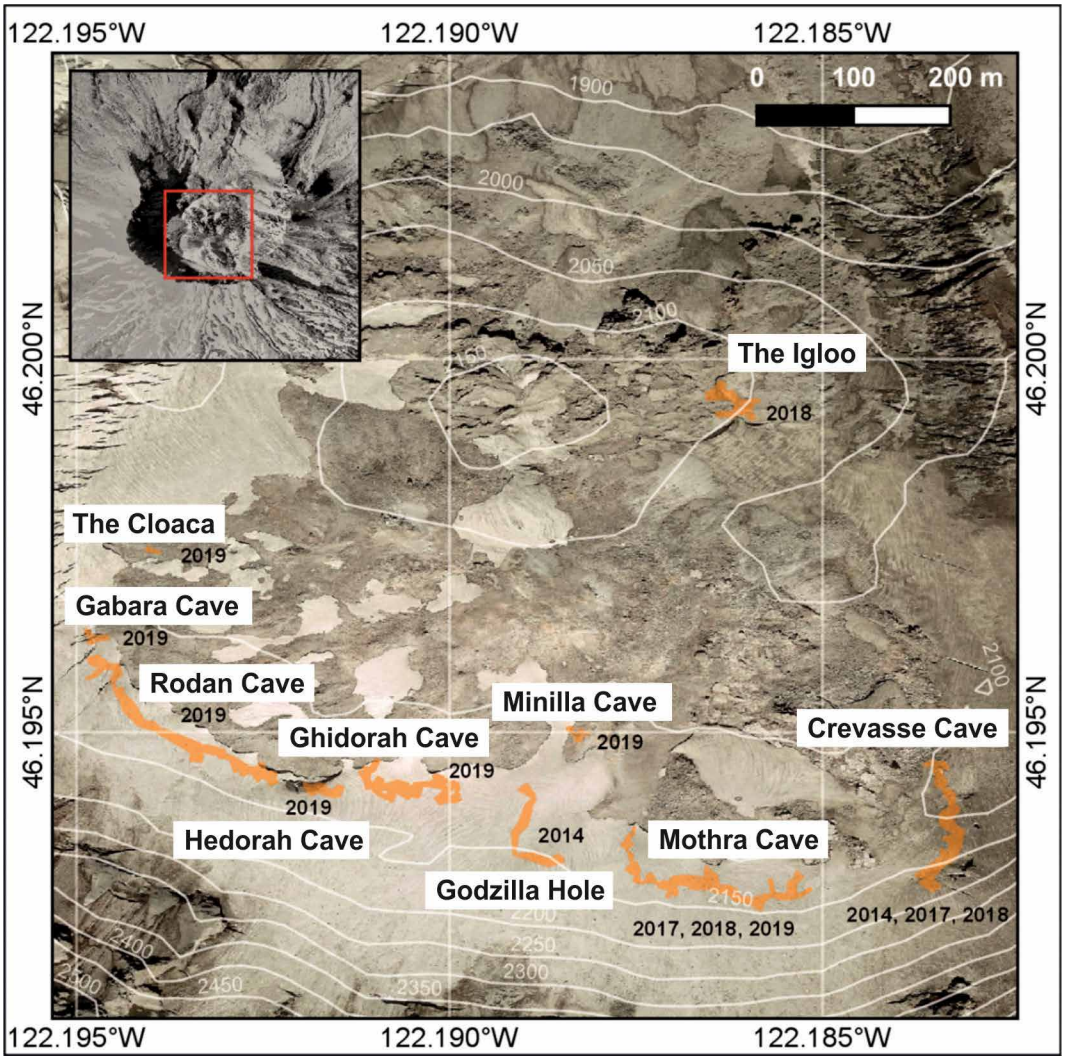


Figure 3. Location of glaciovolcanic cave systems around the 2004–2008 lava dome in the crater of Mount St. Helens (survey results to 2019 only). Black numbers indicate the year(s) the cave was surveyed. Image taken in 2018, © Google Earth (the latest available version). The Igloo, Cloaca, and Minilla caves were firn caves in 2019, although this 2018 image indicates a location on bedrock. The inset illustrates the dimensions of the crater. Image: High Resolution Orthoimagery (2006) from USGS Earth Explorer.

al changes, identify driving forces, and predict a possible transition from several individual caves to an interconnected passage system. This work focuses on this initial cave genesis and also provides a pathway towards future analyses. As this is a developing cave system requiring longitudinal study, this paper also discusses limitations and challenges.

METHODS AND DATA PROCESSING

Fieldwork in the Mount St. Helens crater was conducted from 2014 to 2021. To mitigate risks such as severe weather, rockslides, and cave collapses, most of the expeditions were confined to May and June when glacial ablation is moderate but cave entrances are no longer sealed with snow. The exploration in 2020 was limited to data logger download. Surveying efforts were conducted in 2014, 2017–2019, and 2021; long-term air and fumarole temperature data were collected from 2017–2020. Missing time series are attributable to loss of instrumentation or technical problems. Short-term studies investigated wind regimes and velocity profiles of individual fumaroles. The location of instrumentation is illustrated in Figures 4 and 5. Fumarole temperatures were recorded inside the caves and outside on various locations on the 2004–2008 lava dome.

Typical tacheometric cave survey methods were used to record cave morphology and to record the location of fumaroles and temperature loggers inside Mothra Cave and Crevasse Cave. Georeferenced stations were recorded at each cave entrance using GPS. Cave survey data were collected using calibrated DistoX and DistoX2 to generate distance, azimuth, and inclination measurements and to compute passage volumes via splay measurements at each station (Heeb, 2009). The DistoX2 communicated with a Dell Axim X51 PDA and PocketTopo cave survey software or Samsung Galaxy Note 4 or similar Android OS devices and TopoDroid software. The 2014 survey data generated with the DistoX were manually recorded, with passage cross sections hand drawn at key stations. The International Union of Speleology (UIS) grading standard was used. Precision of the majority of surveys meets standards for Grade 5 survey as per Häuselmann (2012) which gives a minimum precision for measurements of 0.05 m and a 2 % error ratio.

We dealt with several challenges during the fieldwork. The DistoX laser depends on a clear line of sight with no interference from water spray, fog, mist, or other obstructions. Conditions in the caves often include thick steam depending on location in the cave or time of day. During periods of limited visibility detailed splay measurements were not possible. In such cases, basic passage measurements were estimated in four directions from the fixed stations. Other challenges included glacier movement and rockfall which made it impossible to relocate some marked stations from previous surveys.

Table 1. Summary of glaciovolcanic caves and cave statistics. Cave statistics were generated with COMPASS and indicate the most recent survey results.

Cave (most recent survey date)	Included Length, m	Cave Depth, m	Cave Volume, m³
Rodan (2021)	775	82	43,265
Mothra (2021)	594	65	38,340
Ghidorah (2019)	434	30	21,025
Crevasse Cave (2018)	276	56	27,307
Lower Crevasse (2021)	197	30	1,859
The Igloo (2018)	191	8	4,323
Godzilla Hole (2014)	176	41	10,662
Hedorah (2019)	99	13	6,543
Dogora (2021)	71	9	1,026
Gigan (2021)	47	113	1,043
Gabara (2019)	62	119	728
Minilla (2019)	54	8	614
The Cloaca (2019)	34	10	286
Total	3010	···	157,021

Notes
Included Length: This is the included slope length of all the surveys processed. Slope length is the sum of all the tape lengths in the cave. It is the distance that you move through the cave, both horizontally and vertically.
Cave Depth: This is the absolute vertical distance between the highest and lowest points in the survey. It includes no horizontal movement.
Cave Volume: This statistic gives the volume of the cave surveys processed. It is based on the passage Left, Right, Up and Down dimensions. Surveys that are missing LRUD's for part or all of the data will give inaccurate volume calculations.

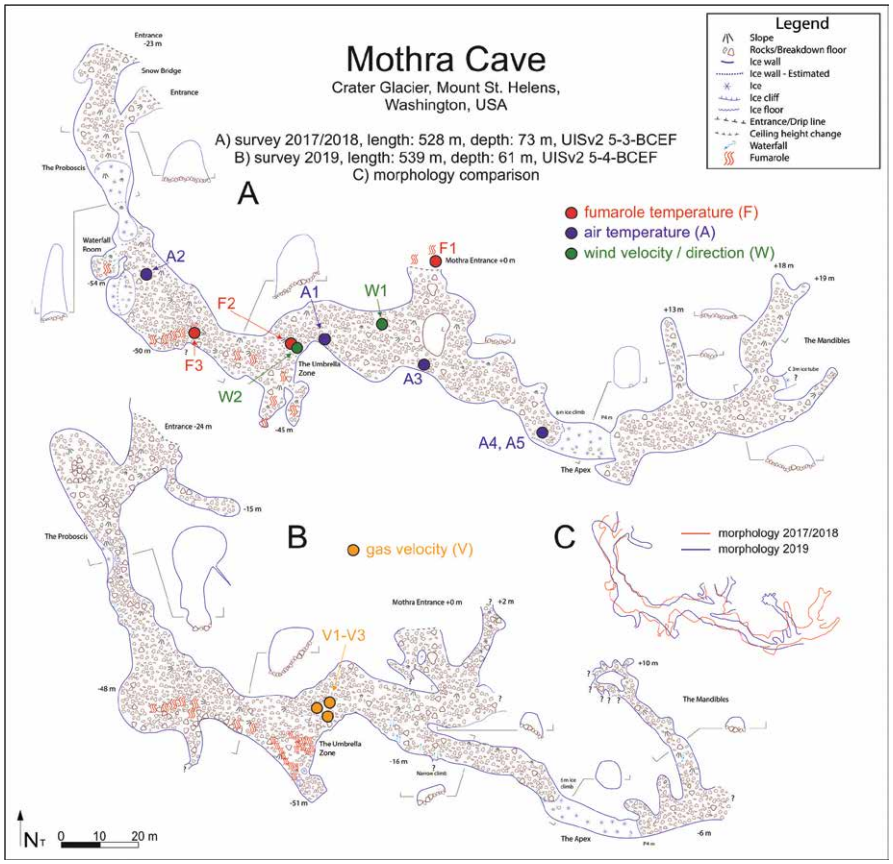


Figure 4. Map of Mothra Cave. A) Results of surveys in 2017 and 2018 and location of climatic instrumentation. Fumarole and air temperature measurements are illustrated in red and blue; wind velocity and direction measurements are shown in green. B) Results of surveys in 2019. C) Morphology changes between 2017–2019.

Post processing of survey data was conducted in COMPASS cave survey project management software. Data were corrected for annual magnetic declination. The software was used to generate statistics including length, depth, and volume (Table 1). Due to magnetic interference from volcanic rock it was expected that some survey measurements generated by DistoX2 could be erroneous. Error mitigation relied on using multiple georeferenced entrance stations and loop closure correction in the software. COMPASS makes this correction via the least square method (Schmidt and Schelleng, 1970). Final outputs included shapefiles for ArcGIS, 3D visualizations generated in CaveXO software, and the corrected line plots used in Adobe Illustrator to complete final cartographic plans of each cave.

Fumarole temperatures describe the temperature of steam or gas emitted from an opening in the ground. Four fumaroles on the crater floor of two caves were equipped with GeoPrecision M-Log5W-CABLE temperature sensors (accuracy: ±0.1 °C at 0 °C), configured for a measurement interval of 5 minutes. These were monitored between 2017

and 2020. Supplementing the fumarole temperatures are short-term gas velocity data collected from June 22−24, 2019. Single fumarole openings were equipped with a plastic tube with a given diameter of 40 mm combined with a hot-wire anemometer (Testo 425; accuracy: ±0.03 m/s) (Fig. 6L). The surrounding area was completely sealed to prevent gas escape. Gas velocity was measured every second at three different sites inside Mothra Cave and flux data were calculated afterwards. Discrete fumarole temperature measurements were also made with a thermocouple (TE Typ K; measurement range: −60 °C to +1,400 °C).

Cave air temperatures were recorded using the same instrumentation at a measurement interval of 5 minutes. Four sites inside Mothra Cave were monitored for air temperature between 2017 and 2020. Data sets from A4 and A5 represent the same site. As one of the sensors (A4) was not detectable during the expedition in 2018 and downloaded data indicated that the sensor froze, a second sensor (A5) was deployed. Freezing of sensors, and thus a probable shift of their original location, was observed at investigation sites A2 and A4, as indicated by constant temperatures of 0 °C. It is likely that sensors fell to the cave floor, where they were affected by freeze-thaw cycles. It was not possible to visually locate these sensors during freeze cycles, but wireless data download was successful.

An assessment of wind regimes inside the caves was performed for the first time using smoke tracers (Fig. 6J) to visualize major pathways and to locate appropriate sites for ultrasonic anemometers (USA-1, METEK; accuracy (max. dev.) wind speed / wind direction: 0.1 m/s or 2 % / 2° at 5 m/s). Data were collected from June 17−18 and 15−18, 2018 (Fig. 6K). Vertical and horizontal wind velocities were measured at 10 Hz at a 1 second average. Simultaneously, air temperatures were recorded. Horizontal wind velocities are supplemented by information about wind direction.

As no climate station exists in the crater of Mount St. Helens, supplementary data on air temperatures and snow depths come from nearby climate stations operated by the U.S. Department of Agriculture, National Resource Conservation Service (https://www.nrcs.usda.gov/wps/portal/nrcs/site/national/home/). Snow Telemetry (SNOTEL) sites are Sheep Canyon (~1,216 m), Swift Creek (~1,353 m), and June Lake (~1,048 m), located on the western and southern flank of the volcano at radii of 3 to 5 km. The SNOTEL snow depths are a proxy for conditions in the crater of Mount St. Helens, although absolute values differ. These surrounding climate stations also serve to reveal the onset of snowfall and the end of snow accumulation.

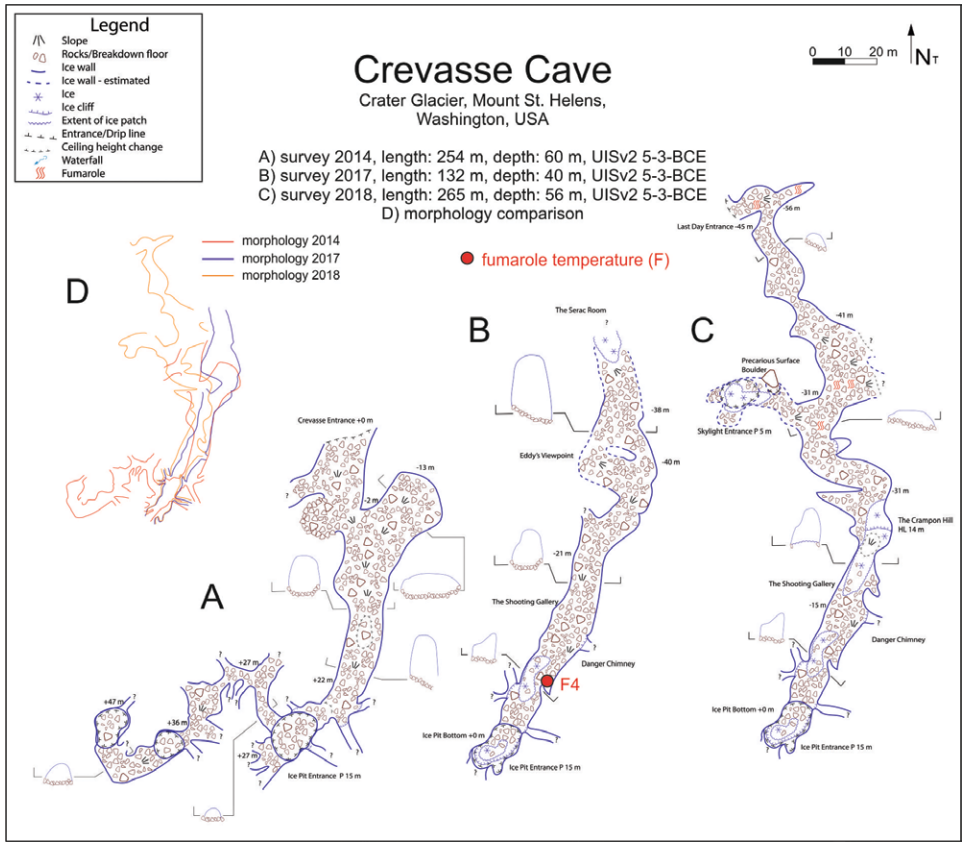


Figure 5. Map of Crevasse Cave. A) Results of survey in 2014. B) Results of survey in 2017 and location of climatic instrumentation. Fumarole temperature measurements are illustrated in red. C) Results of survey in 2018. D) Morphology changes between 2014 and 2019.

Data analysis was performed in OriginPro using the signal processing tool "smooth" after Savitzky and Golay (1964) and the fitting tool "linear fit". A simplified illustration of data sets was created using options such as multiple y-axes, line and bar diagrams, windrose graphs, and reference lines. The final editing was done with CorelDRAW.

RESULTS

Cave Survey

Between 2014 and 2021 a total of 13 newly-formed caves with a combined length of more than 3.0 km were surveyed. The longest, Rodan Cave, comprised a surveyed length of 775 m, followed by Mothra Cave with ~593 m, and Ghidorah Cave with ~433 m. The smallest cave, the Cloaca, was just over 30 m long. Cave depths ranged from less than 10 m up to ~81 m. Table 1 summarizes the main survey results and statistical analyses generated using COMPASS software. See Supplemental Figures S1−S3 for additional cave survey results.

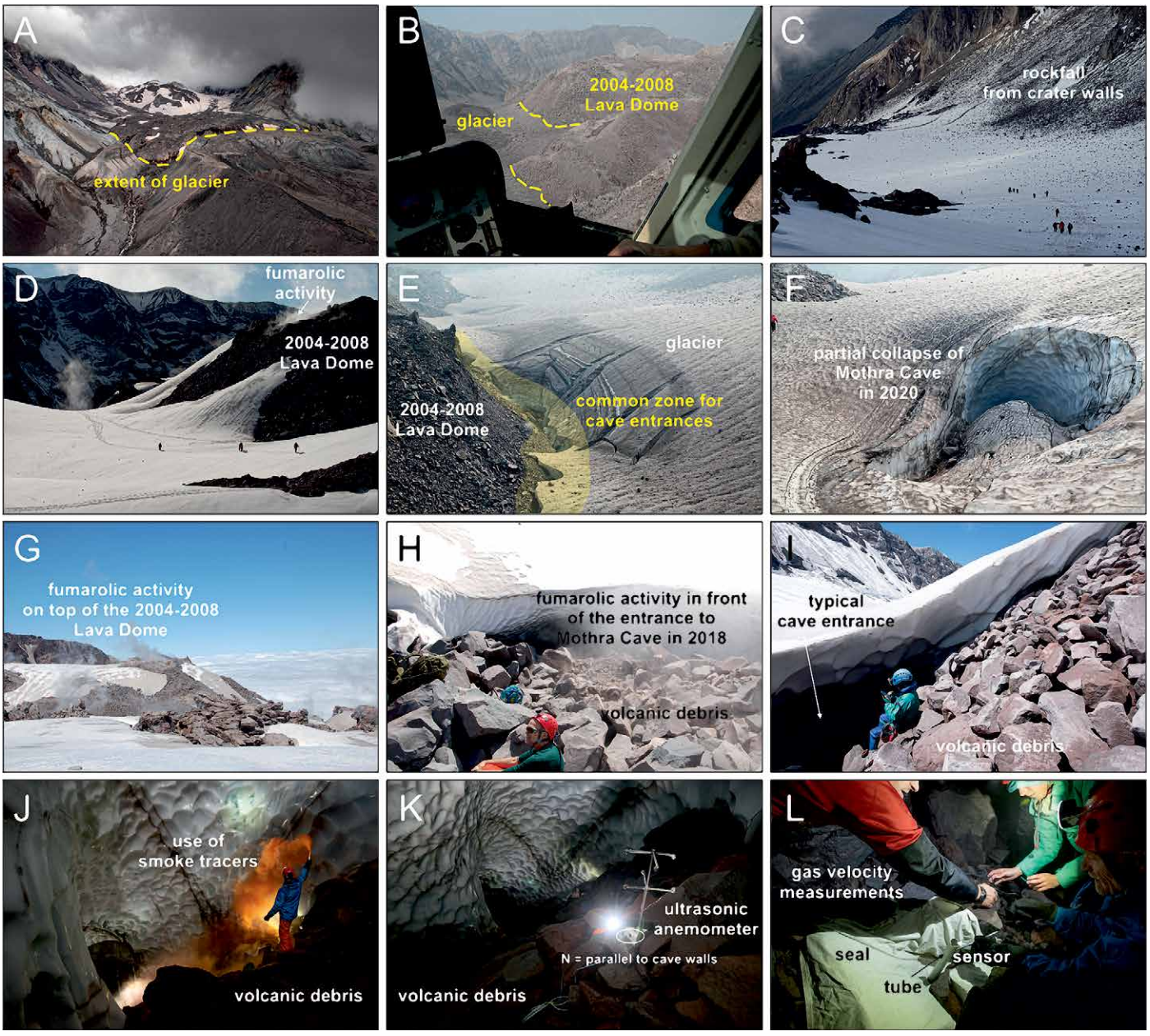


Figure 6. Mount St. Helens' crater and Crater Glacier. A) Southward view towards the crater from a helicopter. Yellow dashed line indicates the extent of Crater Glacier in 2019. B) Westward view inside the crater from the helicopter. Yellow dashed line indicates the area where the newly formed glacier (Crater Glacier) encircles the 2004−2008 lava dome. (2020). C) Rockfall in the crater which derives from the surrounding crater walls. D) 2004-2008 lava dome with fumarolic activity. E) Close-up view of where lava dome and glacier interact. Yellow area is where cave entrances form. F) Partial collapse of Mothra Cave in September 2020 and creation of a new chimney entrance. (2020). G) Fumarolic activity on the 2004-2008 lava dome. H) Entrance to Mothra Cave. Cave entrances and cave floors usually exist of volcanic debris. Fumarolic activity leads to the formation of cave systems and controls the location of entrances. I) Another typical and traversable cave entrance. (2019). J) Use of smoke traces inside Mothra Cave. K) Ultrasonic anemometers inside Mothra Cave measure wind velocity (horizontal and vertical) and indicate wind direction. The north arrow is orientated parallel to cave walls and indicates the nearest cave entrance. L) Gas velocity measurements inside Mothra Cave.

Cave systems on Mount St. Helens share many characteristics. Most have formed in proximity to the 2004−2008 lava dome with passages trending parallel to the dome perimeter. Most have developed near the lateral contact between ice and rock. Thus, they can be categorized as marginal caves. Cave passages do not extend towards the crater rim. Entrances usually occur along the interface of the ice and the lava dome with passages descending at angles of ±30−40 degrees. Vertical entrances also exist as chimneys and through moulins or crevasses. Most caves feature more than one entrance. Entrance elevations ranged from ~2,100 m (Igloo) to ~2,260 m (Mothra). Other common characteristics include vertical walls and convex ceilings, prominent scalloping, and rock debris embedded in glacial walls and ceilings. Embedded rock debris varies in size from a few centimeters to a few meters. The cave floors are subglacial portions of the lava dome,

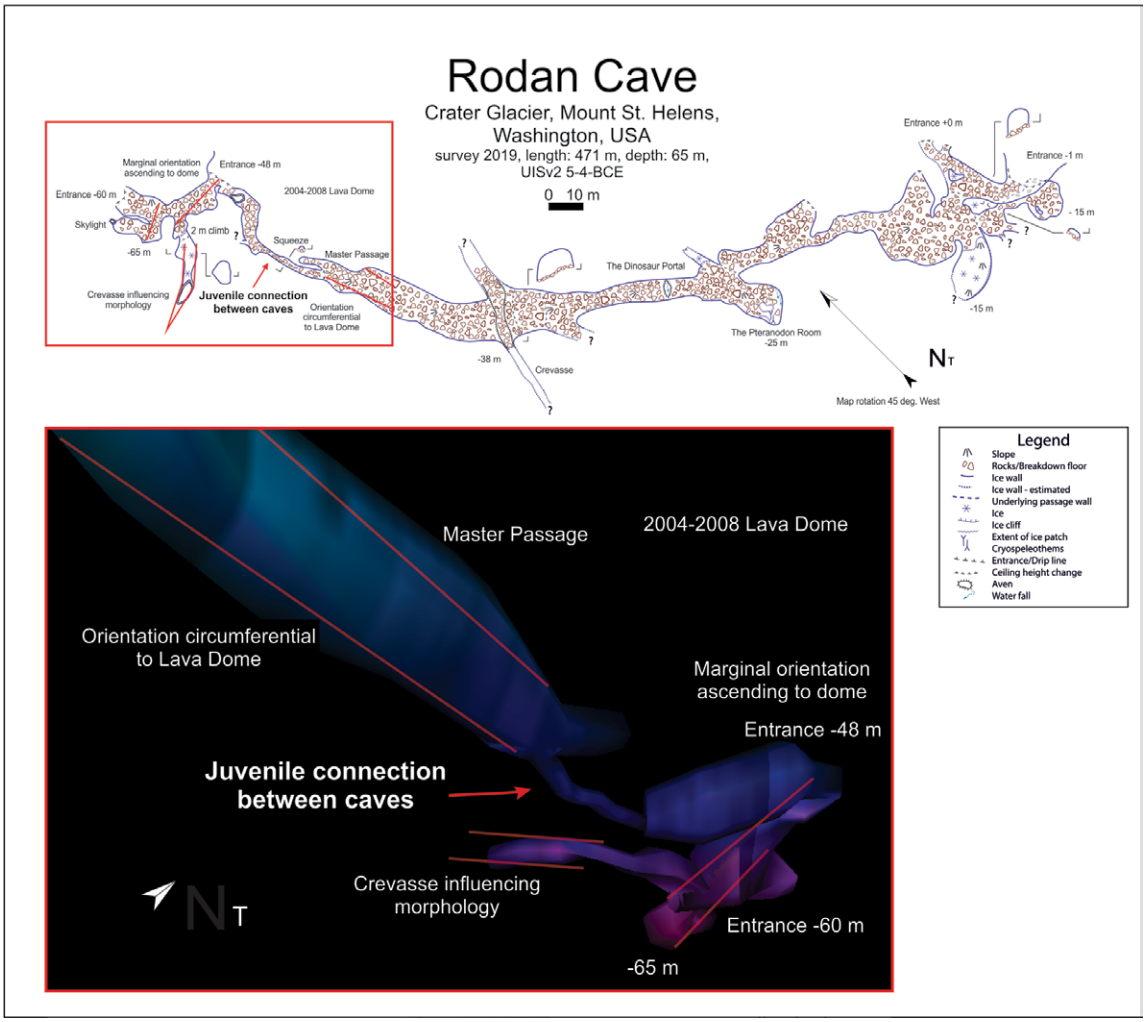


Figure 7. Map of Rodan Cave, survey 2019. Red boxes = west entrances and profile view; a laterally-orientated central passage connects a section with upward trending morphology. The west section of Rodan Cave is a juvenile cave system where formation of connecting cave passages began recently. Further expansion will likely occur.

comprising volcanic debris, tephra, and occasional sediment. Meltwater runoff from the walls and ceilings was present, however this runoff did not result in bodies of standing water as the porous debris floor does not allow water to accumulate. Within each cave occasional cryospeleothems were observed, including ice stalactites and stalagmites. Figure 6 illustrates examples of the cave environment.

There are also differences among caves. The Godzilla Hole was the first cave discovered in 2014. It was accessible by single-rope techniques through an opening in the glacial surface 10 m long × 20 m wide. The floor consisted of volcanic debris with a slope following the rock-ice interface. From 2017 to 2020 a closed depression at the former location of this entrance made further exploration impossible.

Crevasse Cave, formed beneath the east arm of Crater Glacier, was also discovered and surveyed in 2014. Resurveys in 2017 and 2018, and a brief exploration in 2019, revealed distinct morphology changes (Fig. 5). In 2014, the main chimney entrance and the southwest cave passage was explored to a dendritic series of chambers with three skylights which no longer existed in 2017. Other changes from 2014 to 2018 include expansion further north and a shift of the main passage to the west. In addition, a sloping, scalloped ice floor section had formed. Fumarole activity was not surveyed during initial explorations but is indicated in the 2018 map in the northern cave passage. In 2017, fumarole activity had been verified in the southern section.

Mothra Cave was discovered in 2017, with an initial survey in 2017−2018 and a resurvey in 2019 and 2021. Exceptional features include two large rooms (20 m × 20 m × 13m; 14 m × 21 m × 16 m) observed in 2018 and an elliptical passage in ice 6 m above the volcanic debris floor and about 15 m in length. The resurvey indicated that the main passages remained but documented small changes along the east branch and south wall. Persistent fumarolic activity was observed in the southwest section of the cave and likely formed the two largest rooms. A detailed survey of subglacial fumarole locations within Mothra Cave was conducted and is indicated on Figure 4. Isolated fumarole activity was also present (see temperature sensors). In 2020, a brief exploration without any formal survey revealed distinct morphology changes in the form of a partial collapse of the southwestern cave passage, forming a new chimney (Fig. 6F).

The Igloo was discovered in 2014 and first surveyed in 2018. This cave is contained completely in firn and has a depth of 8 m. Although its dynamic passages appear to reform every season, a distinctive and central hemispherical chamber located around a fumarole vent seems to be persistent.

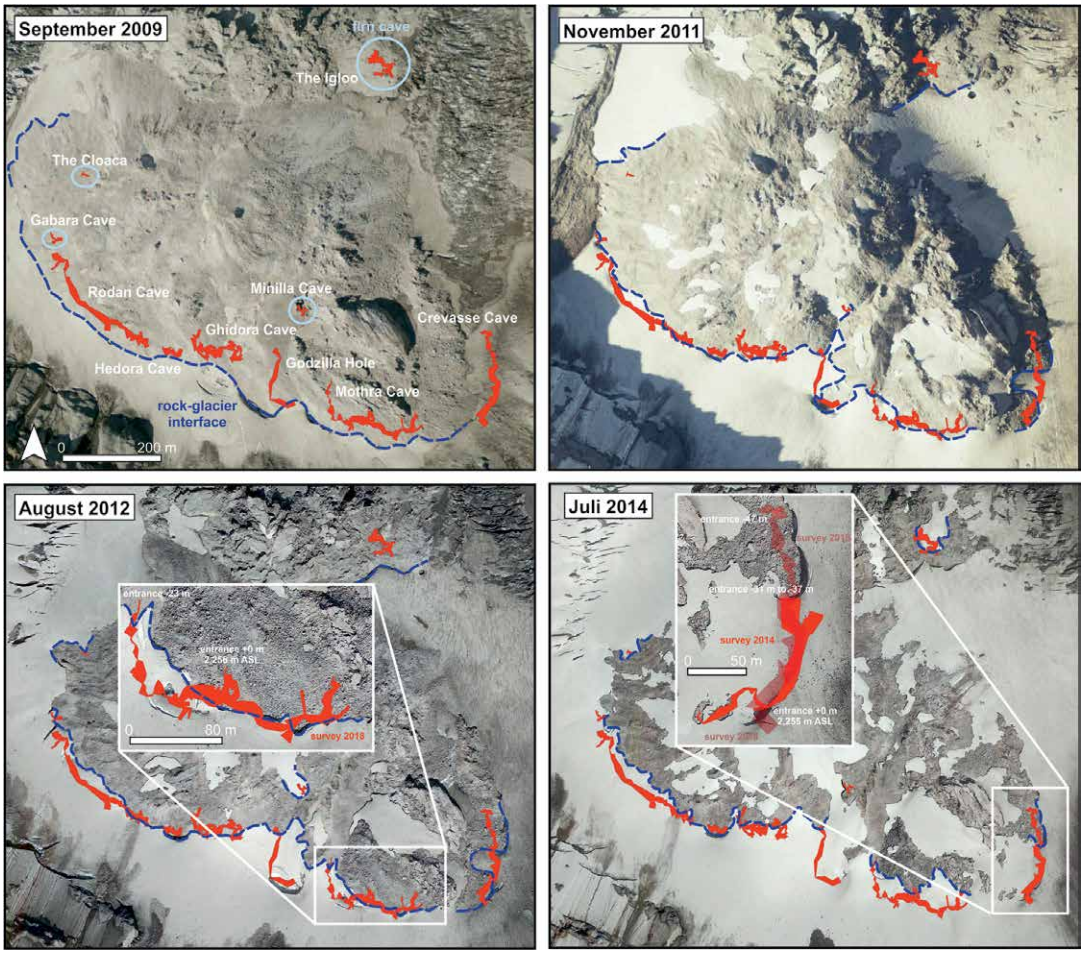


Figure 8. Glacial expansion from September 2009 to July 2014 compared to the latest known location of glaciovolcanic cave systems. Blue dashed line indicates the rock-glacier interface where relevant. Bright blue circles indicate firn caves. Detailed views of Mothra Cave in 2012 and Crevasse Cave in 2014 illustrate that passages surveyed in 2018 were bedrock in 2012 and 2014, respectively. Simplified calculations for both caves were made to estimate possible growth rates. ©Google Earth

Minilla, Ghidorah, Hedorah, Rodan, Gabara Cave, and the Cloaca were discovered and surveyed in 2019. Minilla, Gabara, and the Cloaca formed in firn, similar to the Igloo. Hedorah Cave was found near a group of fumaroles, and featured five closely-spaced entrances orientated towards the fumarole field. Ghidorah, the third largest cave in the crater, had a remarkable dendritic passage network, comparable to karstic caves. Rodan Cave is the longest and deepest of the caves. Its central passage is intersected by large crevasses and hemispherical rooms. In the western cave section the laterally orientated passage interconnects via a narrow tunnel to a zone with slope-orientated morphology (Fig. 7). Caves located and surveyed in 2021 include Dogora, Gigan, and a cave north of Crevasse Cave with passage morphology trending towards a connection with Crevasse Cave, but too tight to confirm with human exploration.

Survey results from the past years illustrate to what extent cave systems must have grown and which ones could not have existed at earlier times (Fig. 8). Images from 2009 and 2011, along with current cave survey data, indicate that most caves could not exist prior to 2011 due to absence of ice.

Cave Climatology

Fumarole temperatures fluctuate and show sudden changes (Fig. 9). The highest temperatures were observed at site F1 (60.1 °C), followed by F3 (57.4 °C), F4 (57.1 °C), and F2 (46.6 °C). Minimum temperatures were −11.7 °C (F3), −10.0 °C (F1), 0.9 °C (F4), and 1.4 °C (F2). Data smoothing indicates that some fumaroles follow similar patterns as clearly shown by F1, F3, and F4. Only F2 does not reveal the same trend. Distinct seasonality is absent. Gas velocity measurements revealed average values from 0.3 m/s to 1.3 m/s. Calculated volume flows range from about 1 m³/h to 5.5 m³/h at fumarole (gas) temperatures of up to 33 °C (Fig. 10).

Maximum air temperatures inside Mothra Cave measured 10.7 °C at A1; minimum temperatures −9.2 °C at A2. Mean air temperatures at all sites varied between 0 °C and 2.3 °C. Data smoothing clearly illustrates similarity of all five temperature profiles. All sites are subjected to seasonal air temperature changes, with the highest temperatures in spring of each year (April−May), falling temperatures during the summer months, and absolute minima in winter (November−December) (Fig. 11A). Constant temperatures around the freezing point usually indicate that the sensor has fallen to the ground and been influenced by meltwater or ice, and do not represent air temperatures.

Cave air temperatures seem to be strongly correlated to snow accumulation (Fig. 11B) and fumarole activity. Monthly mean temperatures at three different locations inside Mothra Cave reveal increasing values with the onset of snow

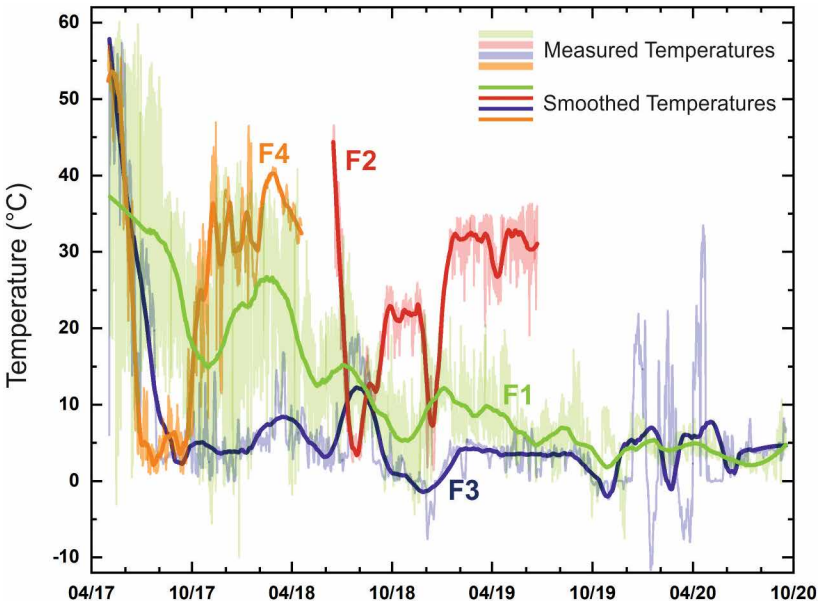


Figure 9. Fumarole temperatures (°C) at four different locations (F1−F4) inside Mothra and Crevasse Cave from April 2017 to September 2020; measurement interval 5 minutes. Transparent colors show measured temperatures. The data were smoothed for better visualization (non-transparent colors) by the method of Savitzky and Golay (1964). According to the number of measurements the Points of Window in OriginPro 2021 were set to 10 % of each individual data set.

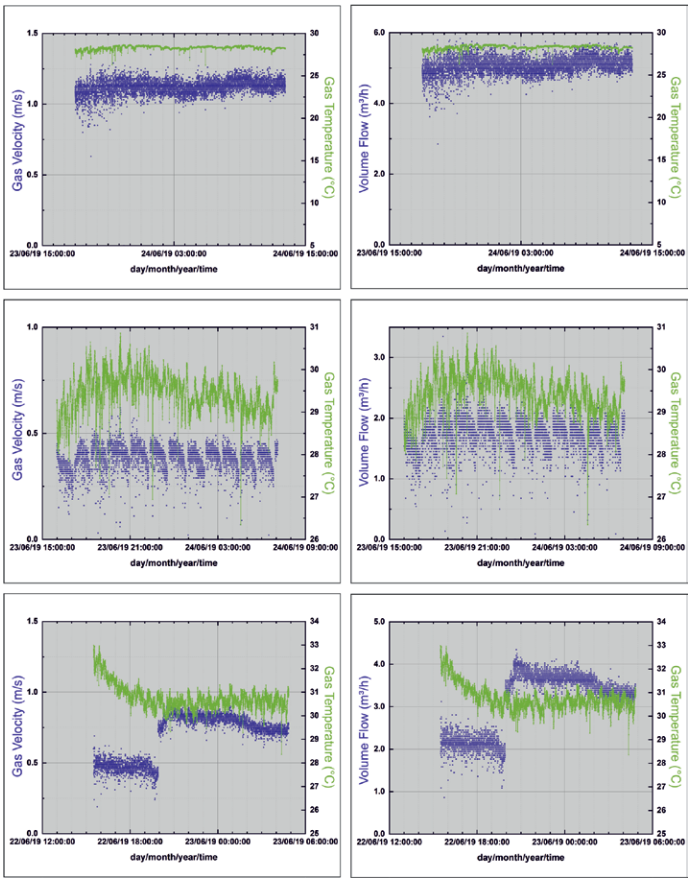


Figure 10. Gas velocity (m/s) and gas temperature measurements (°C) at three different locations (V1−V3) inside Mothra Cave from June 22−24, 2019. The term gas is used to describe the fumarolic output. Volume flow calculations (m³/h) were performed by using gas velocity values and the known diameter of a plastic tube.

accumulation. Because sensors at locations A4 and A5 were probably influenced by meltwater and internal morphology changes, only A1−A3 were chosen for further analysis. Data from these locations indicate that highest temperatures within the course of one year (June 2018−June 2019) were measured in June 2018 (A2, A3) and February 2019 (A1). Temperatures decreased from June 2018 to minima in December 2018. This period mirrors the time of missing or minor snow accumulation. Cave air temperatures and ambient air temperatures around Mount St. Helens both decrease from the middle of 2018 until November 2018 but, as soon as snow accumulation begins, cave air temperatures increase whereas outside air temperatures decrease (Fig. 11B). Correlation coefficients for snow depth and cave air temperatures approach 0.9 (Fig. 11C), whereas correlation coefficients for cave air temperatures and outside air temperatures approach −0.4 (Fig. 11D).

Smoke tracers demonstrated turbulent air flow inside the caves (Fig. 6J). This turbulence was observed during every expedition. Anemometer data verified these observations and revealed strongly varying air currents (Fig. 12). Air velocity of up 10 m/s was observed. Velocities of 1−2 m/s or more appeared infrequently and mostly on a steep slope connecting two main cave levels. Air flow was recorded parallel to cave passages and either indicated inflow of outside air or outflow of cave air. Chimney effects were identified. Data from both investigation sites illustrate that cycles of inflow and outflow are not subject to a strong diurnal rhythm.

DISCUSSION

Mount St. Helens is not the only volcanic edifice where the interaction of glaciers and volcanic activity forms subglacial cave systems, but it is unique in many ways. First, the crater is characterized by a recently formed glacier which is still advancing. Second, cave systems are comparatively young (<10 years) and rapidly evolving. Glaciovolcanic caves are dynamic systems, sensitive to climate fluctuations and changes in heat flux. However, we are not aware of any other glaciovolcanic cave system that is more dynamic at this time. On Mount Rainier, host to the largest known glaciovolcanic cave system worldwide, the caves are largely static, with apparent dynamic equilibrium having been achieved throughout the majority of passages (Florea et al., 2021).

During studies over the last eight years, a goal was to understand the evolution, formation, and dynamic nature of cave systems in the crater of Mount St. Helens. A simplified schematic (Fig. 13) illustrates the processes responsible for cave evolution and expansion. Fumaroles are the main driving force. Further evolution strongly de-

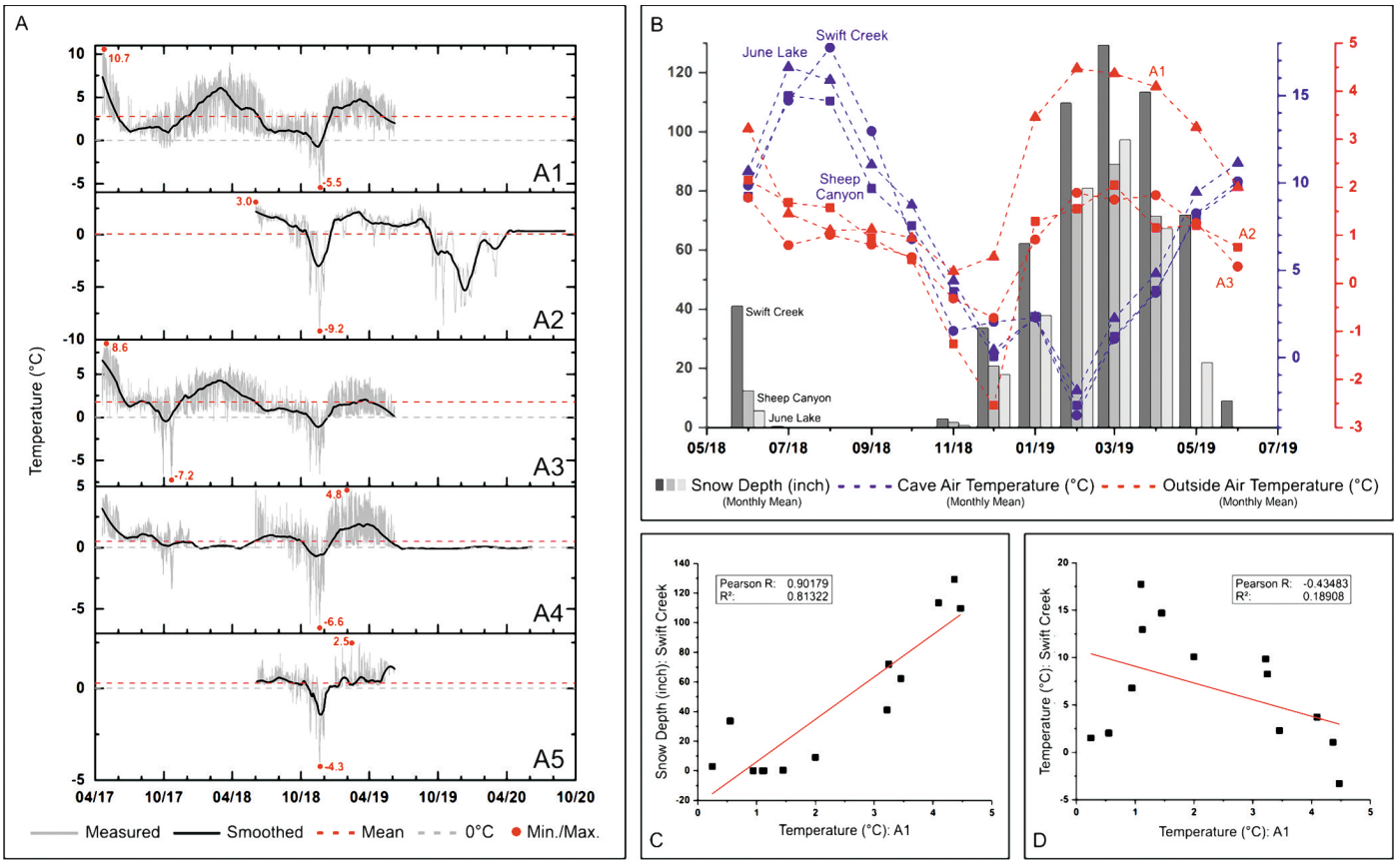


Figure 11. Comparison of cave air temperatures (°C), outside air temperatures (°C), and snow depth (inches). A) Cave air temperatures from four different locations (A1−A5) inside Mothra Cave from April 2017 to September 2020. Grey lines reveal the measured temperature; measurement interval 5 minutes. The data were smoothed for better visualization (black line) by the method of Savitzky and Golay (1964). The Points of Window in OriginPro 2021 were set to 10% of each individual data set. Red dots: maximum and minimum temperatures; red dashed line: mean; grey dashed line: 0 °C. B) Comparison between snow depths and air temperatures from three different SNOTEL sites (Sheep Canyon, Swift Creek, June Lake) and cave air temperatures at A1, A2, and A3 from Mothra Cave; May 2018 to July 2019. Data represent monthly means. Red lines: cave air temperatures; blue lines: outside air temperatures; grey bars: snow depth. C) Results of linear correlation between snow depth and cave air temperature. Snow depth at Swift Creek and cave air temperature at A1 were chosen as a representative example. D) Results of linear correlation between air temperature at Swift Creek and cave air temperature at location A1.

pends on snow and ice accumulation and the exchange of cave air and outside air. Outside air temperatures also affect the cave microclimate, but on a comparatively small scale (Fig. 11D). Glacier movement probably has an effect on caves located towards the east and west arm of the glacier, but contributes less to changes in the southern area of the crater. We assume that there is a linkage between glacier movement and distinct morphology changes (shift to the west) of Crevasse Cave from 2014 to 2018 (Fig. 5).

Cave formation can begin subsequent to snow and ice accumulation. Depending on the rate of snow accumulation in comparison to available heat flux, there are different avenues of formation. If there is enough heat flux to entirely melt accumulating snow, vertical chimneys breaching the surface form, rather than subglacial and dendritic passages (Figs. 14A−C). If the heat flux is moderate, subglacial cave systems can form and evolve (Figs. 14D−E). Unnsteinsson et al. (2021) similarly distinguished between glaciovolcanic caves and chimneys. Evolving passages are subject to seasonal meteorological changes, with snowfall as an influential parameter. Expansion occurs laterally and vertically towards higher elevations of the dome. Passages are subject to ceiling collapses induced by snow overload, ablation of the above glacial surface, or increasing heat output. Collapses can also result from sealed entrances and resultant rising cave air temperatures (Fig. 14F), as happened to the western section of Mothra Cave after winter 2019−2020, when the glacier surface was breached (Fig. 6F). Further understanding of the mechanisms of glaciovolcanic cave formation need examination. Heat flux calculations to assess cave systems were not possible in the scope of this work but would be a noteworthy tool for future assessment. Ice calorimetry may also be a useful approach in the future, once considerable data on the dynamic cave temperatures, air/gas compositions, and ventilation effects are known. Further measurements of the factors identified here as essential for cave formation and their interrelationships need to be considered.

Fumarole temperatures inside the caves did not exceed 60 °C. Thus, all of the fumaroles can be classified as low temperature. In the literature (e.g., Balić-Žunić et al., 2016; Coradossi, 1980) thresholds of ≤100−200 °C for low

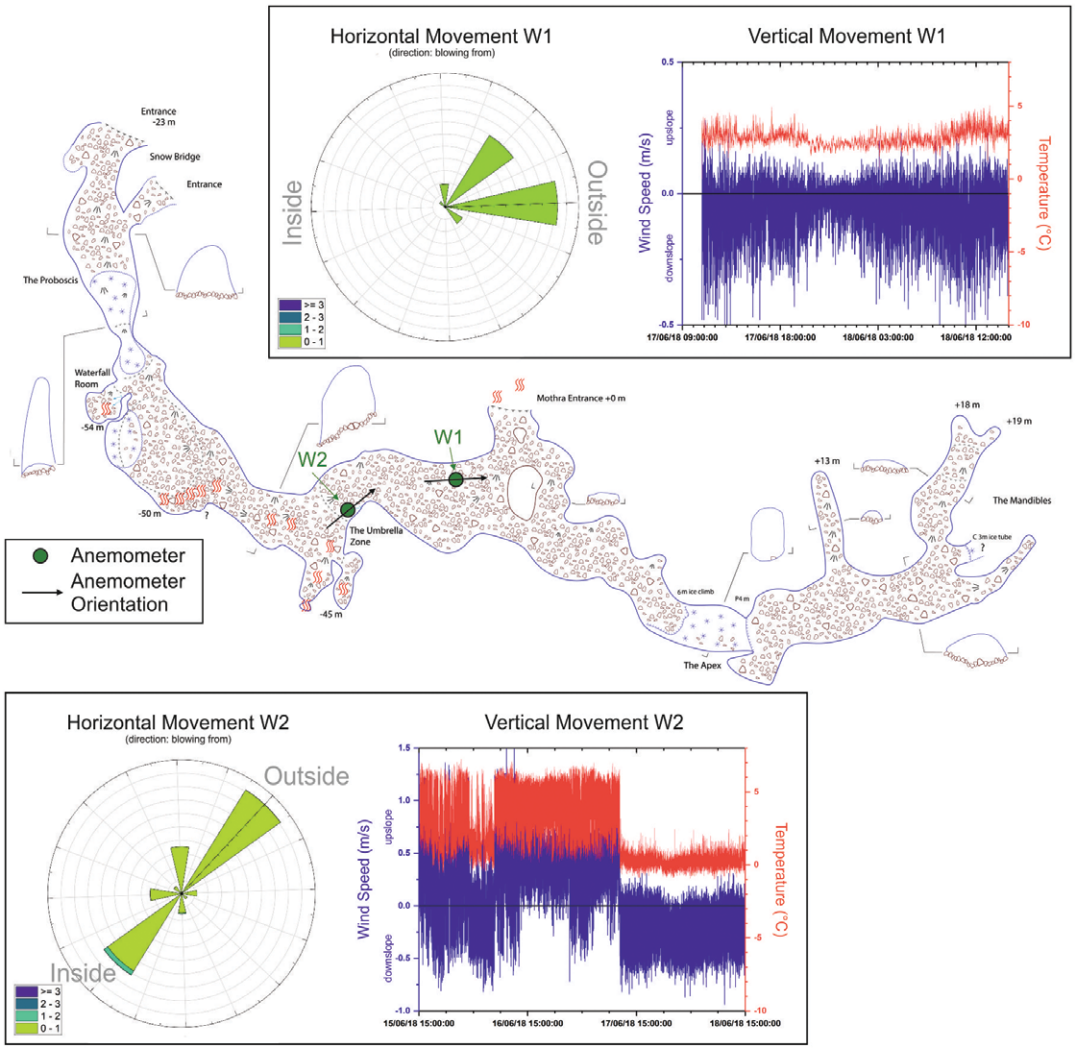


Figure 12. Ultrasonic anemometer data from two sites (W1 and W2) inside Mothra Cave. Horizontal movement (m/s) is illustrated by windrose graphs (direction: blowing from). Vertical movement (m/s) is expressed as upslope (positive) and downslope (negative) movement. Measurement interval 1 second (average; 10 Hz sampling rate). Measurements at location W1 were performed from June 17−18, 2018 and measurements at location W2 were performed from June 15−18, 2018.

temperature fumaroles can be found, although another common classification is based on the type of minerals deposited. Fumaroles in the caves around the 2004-2008 lava dome do reveal that the dome is still hot at depth. Subglacial fumarole temperatures are lower compared to subaerial counterparts on higher elevations of the dome as confirmed by a permanent monitoring station (https://www.usgs.gov/volcanoes/mount-st-helens) and recent measurements in June 2021, where maximum fumarole temperatures of 94 °C on the dome summit were recorded. Monitoring data from 2014−2015 showed temperatures of up to 380 °C (Crankshaw et al., 2018), indicating that the dome is cooling. Although summit fumaroles are usually hotter, we also located a subaerial fumarole north of Hedorah Cave of nearly 90 °C during the expedition in 2019. Similar temperatures were confirmed during recent studies in 2021 (92 °C). We assume that cave expansion towards higher elevations on the dome may be limited by higher fumarole temperatures. Future studies should include the identification of fracture zones on the dome to also explain discrete high fumarole temperatures at lower elevations.

Fumarole temperatures showed great variability and a wide range. Data smoothing (Fig. 9) shows good correlation between F1 and F3 in Mothra Cave and F4 in Crevasse Cave. The outlier is F2, located in the Umbrella Zone of Mothra Cave. Big variances are most likely linked to rain and snow melt, as is the case for fumarole areas outside the caves higher on the lava dome (P. Kelly, personal communication, 2021). Observation of the Umbrella Zone showed F2 to be greatly influenced by nearby meltwater runoff. Thus, is it not surprising that this fumarole does not present characteristics similar to F1, F3, and F4. Long-term fumarole-temperature data also exist from Mount Rainier (see Supplemental Fig. S4) where fumarole temperatures did not exceed about 60 °C and correlations in pattern trends were also present. However, strong fluctuations are apparently absent at Mount Rainier (isolated outliers). We hypothesize that the crater floor has major influence. Whereas the summit of Mount Rainier is characterized by various clays that result from strong hydrothermal alteration (Zimbelman, 1996), we observed permeable debris floors within Mount St. Helens caves and water that drains into the hydrothermal system. The way the fumaroles behave and the temperatures they show over the year is largely influenced by water and the crater floor. Future analyses need to focus on the volcano's hydrogeology. Geochemical data from fumaroles are necessary to determine the origin of gas (magmatic or recycled water) and to compare these data with hotter fumaroles higher on the dome.

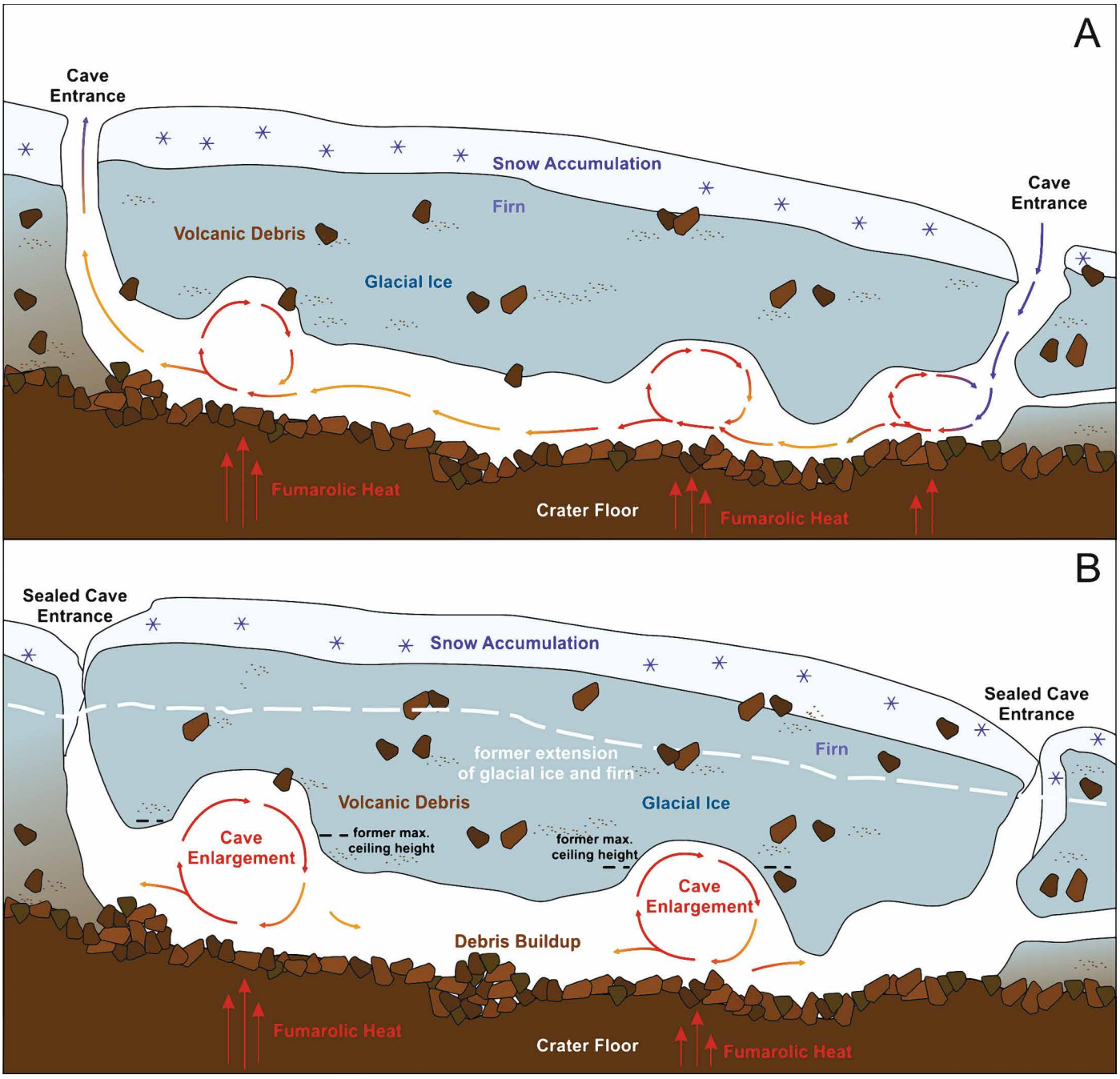


Figure 13. Transformation of cave systems over time. A) Early stage of development. Fumarolic heat from the recent lava dome interacts with the glacier and promotes formation of cave systems. Hemispherical rooms develop where fumarolic heat is concentrated. Ventilation effects occur as colder ambient air flows in and warmer cave air escapes. B) Further evolution of a cave system. Sealed cave entrances inhibit the exchange of ambient air and cave air. Cave enlargement and debris buildup take place. Continued snow accumulation leads to glacier growth above the caves. Fumarolic activity often undergoes minor changes.

Ventilation effects exist when cave entrances are not sealed with snow. Complex cave morphologies with more than one cave opening cause chimney effects and promote invasion of cold air. Use of smoke tracers inside Mothra Cave (Fig. 6J) verified these effects. Anemometer data (Fig. 12) show that there is a permanent alternation/shift from inflow to outflow. Similar observations were made on Mount Hood (Pflitsch et al., 2017) and Mount Rainier (Florea et al., 2021). Recent studies by Florea et al. (2021) also illustrated the influence of sealed entrances on cave air temperatures, indicating that it may be a common process in glaciovolcanic caves. Similar reports are known from Mount Hood (A. Pflitsch, personal communication, 2020). Velocities in the Mount St. Helens caves are moderate and comparable to those observed in the summit caves on Mount Rainier and in Hot Imagination Cave on Mount Hood. However, higher velocities are also possible (e.g., Pure Imagination Cave, Mount Hood: >6 m/s, June 23−25, 2015).

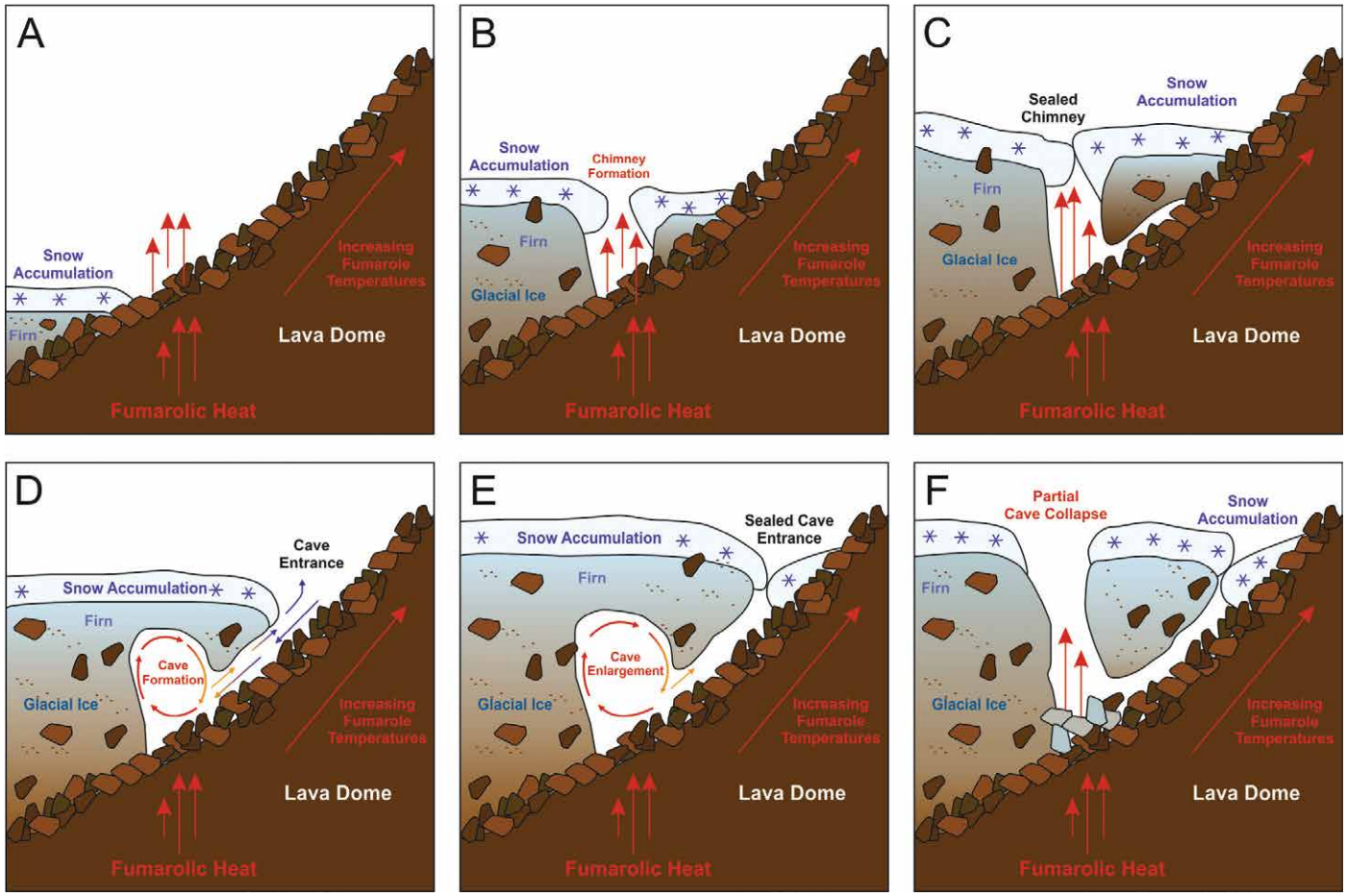


Figure 14. Transformation of cave systems over time viewed in profile. Caves are characterized by steep slopes circumnavigating the lava dome. Fumarole temperatures increase with elevation on the 2004−2008 lava dome. Glacial ice expands towards the lava dome. A) Glacial expansion begins encroaching on fumarolic areas, but is still limited to lower elevations along the lava dome and does not yet affect fumarolic activity. B) Heat output is too high to allow snow accumulation directly above fumarolic activity and leads to chimney formation. C) Where chimneys have formed, snow overload may eventually cause chimneys to seal off; then, subglacial passage volume increases and passages expand along the rock-ice interface. D) Subglacial dome shaped passages and entrance passages form along the rock-ice margin. There is interaction between outside air and cave air. New subglacial fumarolic output may cause renewed cave formation at this stage. E) Cave enlargement continues laterally (not shown in profile view) and vertically along the lava dome, with further snow accumulation and seasonal cave entrance blockages in winter. F) Snow overload, increasing heat output, or a combination thereof may lead to partial cave collapse (though this is rather uncommon). Usually, the main passages remain comparatively stable and pass through several cycles of D and E.

Gas output (Fig. 10) is much lower compared to Mount Rainier (Stenner et al., 2021). Although the Mount Rainier fumarole only presents one example of more than 100 fumaroles found in summit caves, no fumarole with a comparable flux was found in the Mount St. Helens caves. Differences in gas output and composition were also obvious during recent expeditions to both volcanoes: persistent risks in the summit of Mount Rainier due to CO_2-traps, or O_2 deficiencies often complicated research (Stenner et al., 2021). Comparable situations were not observed on Mount St. Helens. The absence of hazardous atmospheres on Mount St. Helens facilitates fieldwork to a great extent. Other advantages include the comparatively low elevation of the crater, extensive monitoring efforts by the USGS, and accessibility (e.g., in contrast to Antarctica and Kamchatka).

Cave systems on Mount St. Helens are distributed in a semicircular pattern around the 2004−2008 lava dome. In future years we expect that (i) cave systems will continue to expand vertically and laterally, (ii) the rock-ice interface will move towards higher elevations on the dome, and (iii) individual caves may merge over time and form longer central passage systems around the southern part of the dome. Resurveys have already shown growth of individual caves. Moreover, comparison of available satellite images from 2012 and 2014 with the current location of cave systems indicates a growth during the last few years and also illustrates that some caves could not have existed at earlier times due to lack of snow and ice. As most parts of Ghidorah Cave did not exist in 2012, we can estimate that the rock-ice interface moved upward ~30 m by 2019. The rock-ice interface in August 2012 and July 2014 were compared to survey results for Mothra and Crevasse Cave in order to estimate the growth of passage length and volume (Fig. 8). For

Mothra Cave an estimated increase of ~240 % in length and 530 % in volume was calculated from 2012 to 2018; for Crevasse Cave an increase of ~100 % in length and ~250 % in volume were calculated for the north extension from 2014 to 2018. The depth of individual caves can be a proxy for glacier growth. Cave mergers and formation of a longer master passage is suggested by the western part of Rodan Cave (Fig. 7), where a connection formed recently. Further expansion of Rodan will probably connect to Ghidorah and Hedorah Cave in the east and Gabara Cave in the west. A similar situation of circular cave morphology with a central passage is known from the summit East Crater of Mount Rainier (Florea et al., 2021), albeit with orientation of entrance passages towards the crater rim.

CONCLUSIONS AND FUTURE WORK

The glaciovolcanic cave systems of Mount St. Helens exhibit rapid growth within the last decade. We were able to observe the onset of cave formation and subsequent evolution. We expect that individual caves will expand in the near future and may interconnect, forming a semicircular passage around the 2004-2008 lava dome. This circular morphology exists on nearby Mount Rainer and is supported by our observations of dynamic genesis of caves in the crater of Mount St. Helens. Vertical passage extension towards higher elevations along the dome is expected but may also be limited by increasing fumarole temperatures (see Supplemental Fig. S4 for fumarole temperature data from Mount Rainer). It is not surprising that fumarolic activity turned out to be the main driving force of cave evolution and transformation. However, seasonal meteorological patterns also emerged to be a major factor, particularly snow accumulation. Variations of cave air temperatures are related to seasonally sealed entrances, and the resulting absence of ventilation.

From 2017 to 2020 we performed long-term monitoring of fumarole temperatures inside glaciovolcanic caves, supported by temporary gas velocity measurements and volume flow calculations. Similar to observations on top of the lava dome, cave fumaroles revealed a high variability that appears to be closely related to precipitation. Subglacial gas emissions were observed to be quite weak compared to fumaroles inside the Rainier caves and also much less than on upper parts of the lava dome.

This paper summarizes the results of eight years of exploration of an expanding cave system and illustrates the factors involved in cave formation. Work inside the caves was often challenging, and the continuous, ongoing evolution of the system both hinders and necessitates further analyses. However, pathways towards future studies were discussed in this paper and may lead to a detailed understanding of glaciovolcanic caves.

ACKNOWLEDGMENTS

We thank Brent McGregor, one of the expedition leaders of Glacier Cave Explorers. We also acknowledge cave surveyors Kathleen Graham, Scott Linn, Neil Marchington, Mark Dickey, Jessica Van Ord, and Barb Williams. We thank Jared Smith, Tom Wood, Tom Gall, Becca Stubbs, and Andrew Blackstock for safety & HAZMAT support; Aaron Messinger and Special Projects Operations for custom SCBA equipment; and Lynn Moorman for enabling cave reconnaissance via Virtual Reality. Thanks to Industrial Scientific and Hilleberg for equipment support. We finally acknowledge Lee J. Florea, Glyn Williams-Jones and Thor Hansteen for advice.

REFERENCES

Anderson, C.H., Behrens, C.J., Floyd, G.A., and Vining, M.R., 1998, Crater Firn Caves of Mount St. Helens, Washington: Journal of Cave and Karst Studies, v. 60, no. 1, p. 44–50.

Anderson, C.H., and Vining, M.R., 1999, Observations of glacial, geomorphic, biologic, and mineralogic developments in the Crater of Mount St. Helens, Washington: Washington Geology, v. 27, no 2/3/4.

Balić-Žunić, T., Garavelli, A., Jakobsson, S.P., Jonasson, K., Katerinopoulos, A., Kyriakopoulos, K., and Acquafredda, P., 2016, Fumarolic minerals: an overview of active European volcanoes: *in* Nemeth, K., ed., Updates in Volcanology − From Volcano Modelling to Volcano Geology, InTech. http://doi.org/10.5772/64129.

Coradossi, N., 1980, I SUBLIMATI: Società Italiana di Mineralogia e Petrologia, v. 36, no. 2, p. 573–584.

Crankshaw, I.M., Archfield, S.A., Newman, A.C., Bergfeld, D., Clor, L.E., Spicer, K.R., Kelly, P.J., Evans, W.C., and Ingebritsen, S.E., 2018, Multiyear high-frequency hydrothermal monitoring of selected high-threat Cascade Range volcanoes: Journal of Volcanology and Geothermal Research, v. 356, p. 24–35. http://doi.10.1016/j.jvolgeores.2018.02.014.

Curtis, A., 2016, Dynamics and global relevance of fumarolic ice caves on Erebus Volcano, Antarctica [Ph.D thesis]: New Mexico Institute of Mining and Technology, 154 p.

Curtis, A., and Kyle, P., 2017, Methods for mapping and monitoring global glaciovolcanism: Journal of Volcanology and Geothermal Research, 333-334, p. 134–144. http://doi.10.1016/j.jvolgeores.2017.01.017.

Edwards, B., Kochtitzky, W., and Battersby, S., 2020, Global mapping of future glaciovolcanism: Global and Planetary Change, v. 195, p. 103356. http://doi.10.1016/j.gloplacha.2020.103356.

Florea, L.J., Pflitsch, A., Cartaya, E., and Stenner, C., 2021, Microclimates in fumarole ice caves on volcanic edifices—Mount Rainier, Washington, USA: Journal of Geophysical Research: Atmospheres, v. 126, no. 4. http://doi.10.1029/2020JD033565.

Giggenbach, W.F., 1976, Geothermal ice caves on Mt Erebus, Ross Island, Antarctica: New Zealand Journal of Geology and Geophysics, v. 19, no. 3, p. 365–372. http://doi.10.1080/00288306.1976.10423566.

Harris, S.L., 2006, Fire mountains of the West: The Cascade and Mono Lake volcanoes: 3. ed., 2. pr: Missoula, Mont., Mountain Press Publishing Co, 454 p.

Häuselmann, P., 2012, UIS Mapping Grades: http://www.uisic.uis-speleo.org/UISmappingGrades.pdf (accessed April 2021).

Heeb, B., 2009, An all-in-one electronic cave surveying device: https://paperless.bheeb.ch/download/DistoX.pdf (accessed April 2021).

Kiver, E.P., and Mumma, M.D., 1971, Summit firn caves, Mount Rainier, Washington: Science (New York, N.Y.), v. 173, no. 3994, p. 320–322. http://doi.10.1126/science.173.3994.320.

Miller, M.B., and Cowan, D.S., 2017, Roadside geology of Washington, Second edition: Missoula, Montana, Mountain Press Publishing Company, Roadside geology series, 378 p.

Pflitsch, A., Cartaya, E., McGregor, B., Holmgren, D., and Steinhöfel, B., 2017, Climatologic studies inside Sandy Glacier at Mount Hood Volcano in Oregon, USA: Journal of Cave and Karst Studies, v. 79, no. 3, p. 189–206. http://doi.10.4311/2015IC0135.

Savitzky, A., and Golay, M.J.E., 1964, Smoothing and differentiation of data by Simplified Least Squares Procedures: Analytical Chemistry, v. 36, no. 8, p. 1627–1639. http://doi.10.1021/ac60214a047.

Schilling, S.P., Carrara, P.E., Thompson, R.A., and Iwatsubo, E.Y., 2004, Posteruption glacier development within the crater of Mount St. Helens, Washington, USA: Quaternary Research, v. 61, no. 3, p. 325–329. http://doi.10.1016/j.yqres.2003.11.002.

Schmidt, V.A., and Schelleng, J.H., 1970, The application of the method of least squares to the closing of multiply-connected loops in cave or geological surveys: Bulletin of the National Speleological Society, v. 32, no. 3, p. 51–58.

Scott, W.E., Sherrod, D.R., and Gardner, C.A., 2008, Overview of the 2004 to 2006, and continuing, eruption of Mount St. Helens, Washington, *in* Sherrod, D.R., Scott, W.E., and Stauffer, P.H., eds., A volcano rekindled: the renewed eruption of Mount St. Helens, 2004-2006: U.S. Geological Survey Professional Paper 1750, p. 3–23.

Smellie, J.L., and Edwards, B.R., 2016, Glaciovolcanism on Earth and Mars: Cambridge, Cambridge University Press. http://doi.org/10.1017/CBO9781139764384.

Stenner, C., Pflitsch, A., Florea, L.J., Graham, K., and Cartaya, E., 2022, The development and persistence of hazardous atmospheres within a glaciovolcanic cave system – Mt. Rainier, Washington, USA: Journal of Cave and Karst Studies (in press).

Unnsteinsson, T., Flowers, G., Williams-Jones, G., 2021, An analytical approach to understanding the morphologies of glaciovolcanic caves and chimneys: AGU Fall Meeting 2020. https://doi.org/10.1002/essoar.10505976.1.

Walder, S.J., Schilling, S.P., Vallance, J.W., and LaHusen, R.G., 2008, Effects of lava-dome growth on the Crater Glacier of Mount St. Helens, Washington: *in* Sherrod, D.R., Scott, W.E., and Stauffer, P.H., eds., A volcano rekindled: the renewed eruption of Mount St. Helens, 2004-2006: U.S. Geological Survey Professional Paper 1750, p. 257–273, https://doi.org/10.3133/pp175013.

Zimbelman, D.R., 1996, Hydrothermal alteration and its influence on volcanic hazards—Mount Rainier, Washington, a Case History [Ph.D. thesis]: University of Colorado, Boulder, unpublished.

Zimbelman, D.R., Rye, R.O., and Landis, G.P., 2000, Fumaroles in ice caves on the summit of Mount Rainier—preliminary stable isotope, gas, and geochemical studies: Journal of Volcanology and Geothermal Research, v. 97, 1-4, p. 457–473. https://10.1016/S0377-0273(99)00180-8.

Christian Stenner, Andreas Pflitsch, Lee J. Florea, Kathleen Graham, and Eduardo Cartaya. Development and persistence of hazardous atmospheres in a glaciovolcanic cave system—Mount Rainier, Washington, USA. *Journal of Cave and Karst Studies*, v. 84, no. 2, p. 66-82. DOI:10.4311/2021EX0102

DEVELOPMENT AND PERSISTENCE OF HAZARDOUS ATMOSPHERES IN A GLACIOVOLCANIC CAVE SYSTEM—MOUNT RAINIER, WASHINGTON, USA

Christian Stenner[1, C], Andreas Pflitsch[2], Lee J. Florea[3], Kathleen Graham[1], and Eduardo Cartaya[4]

Abstract

Glaciovolcanic cave systems, including fumarolic ice caves, can present variable atmospheric hazards. The twin summit craters of Mount Rainier, Washington, USA, host the largest fumarolic ice cave system in the world. The proximity of fumarole emissions in these caves to thousands of mountaineers each year can be hazardous. Herein we present the first assessment and mapping of the atmospheric hazards in the Mount Rainier caves along with a discussion on the microclimates involved in hazard formation and persistence. Our results are compared to applicable life-safety standards for gas exposure in ambient air. We also describe unique usage of Self-Contained Breathing Apparatus (SCBA) at high altitude. In both craters, subglacial CO_2 traps persist in multiple locations due to fumarole output, limited ventilation, and cave morphology. CO_2 concentrations, calculated from O_2 depletion, reached maximum values of 10.3 % and 24.8 % in the East and West Crater Caves, respectively. The subglacial CO_2 lake in West Crater Cave was persistent, with atmospheric pressure as the main factor influencing CO_2 concentrations. O_2 displacement exacerbated by low O_2 partial pressure at the high summit altitude revealed additional cave passages that can be of immediate danger to life and health (IDLH), with O_2 partial pressures as low as 68.3 mmHg. Planning for volcanic research or rescue in or around similar cave systems can be assisted by considering the implications of atmospheric hazards. These findings highlight the formation mechanisms of hazardous atmospheres, exploration challenges, the need for mountaineering and public awareness, and the broader implications to volcanic hazard assessment and research in these environments.

INTRODUCTION

Mount Rainier is an iconic landmark in the U.S. Pacific Northwest. Designated as a Decade Volcano by the International Association of Volcanology and Chemistry of the Earths' Interior (IAVCEI), the U.S. Geological Survey lists Mount Rainier as the third highest volcanic threat in the United States and a 'very high threat' category location in the National Volcanic Early Warning System (Ewert et al., 2018). A popular mountaineering objective, Mount Rainier National Park reports that approximately 10,500 people attempt to climb Mount Rainier each year (NPS, 2020). The National Research Council (1994) has identified the need for monitoring of hydrothermal activity, including fumaroles in the summit area, and changes in surface appearance, such as distribution of snow and ice cover.

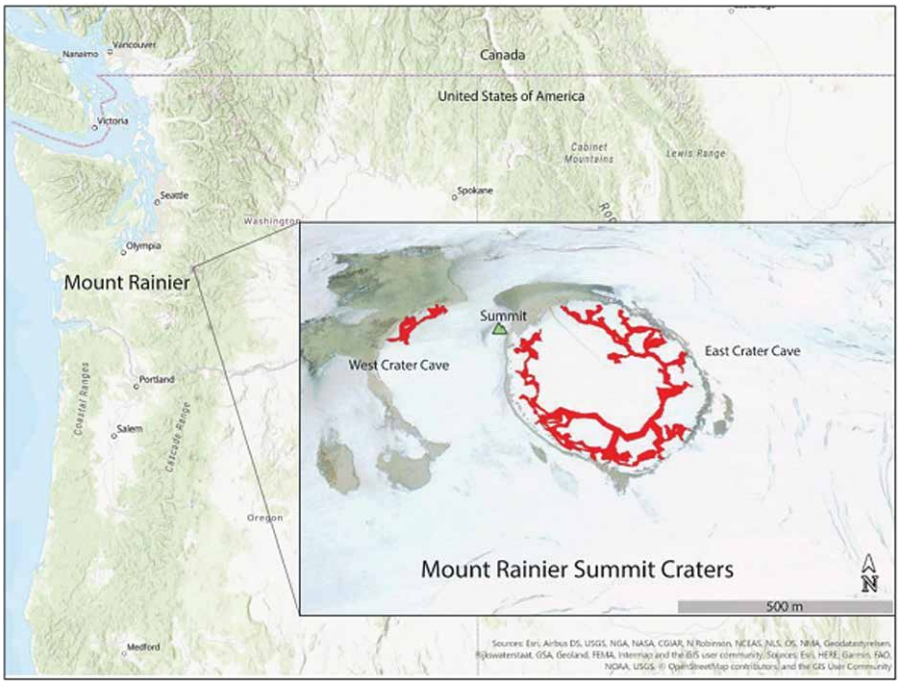


Figure 1. Base map of the Pacific Northwest, United States of America, with the location of Mount Rainier. Inset image of the surveyed extent of the East and West Crater cave system passages at the summit of Mount Rainier, marked in red and overlaid on GIS satellite.

The world's largest fumarolic ice caves exist underneath the glaciers in the summit craters (Fig. 1). They were formed by >100 fumaroles and include a network of 3.5 km of subglacial passages in the East Crater (Florea et al., 2021). A further 300 m of passages exist in the more volcanically active West Crater Cave (Fig. 1). Previous studies in the caves attempted to understand their morphology and the hydrothermal system (Kiver and Steele, 1975; Frank, 1995; Zimbelman et al., 2000). Addi-

[1] Alberta Speleological Society, Calgary, Alberta, Canada
[2] Department of Geography, Ruhr-University Bochum, Bochum, 44801, Germany
[3] Washington State Geological Survey, Department of Natural Resources, Olympia, Washington, USA
[4] Glacier Cave Explorers, Oregon High Desert Grotto of the National Speleological Society, Redmond, Oregon, USA
[C]Corresponding author: (cstenner@telus.net)

tionally, the characteristics of these unique subglacial environments are thought to mimic void spaces in ice masses in other parts of the solar system (Curtis 2016, 2020). The National Academies of Sciences, Engineering, and Medicine (2019) report on astrobiology highlighted the importance of understanding terrestrial subsurface sites as crucial to the search for life on other worlds. Fumarolic ice caves are dark, oligotrophic volcanic environments that may provide insight into microbial communities as an analog for icy conditions such as those which exist on other worlds (Tebo et al., 2015; Davis et al. 2020). As Mars' lower atmosphere consists of 95.32 % CO_2 (Owen et al., 1977), a low atmospheric air pressure and high CO_2, the glaciovolcanic cave setting could be a particularly intriguing Mars polar analog.

Volcanic areas host harmful gasses such as H_2S, SO_2, CO_2, CO, and others (e.g., Hansell and Oppenheimer, 2005; Williams-Jones and Rymer, 2014). Williams-Jones and Rymer (2014) noted the importance of monitoring of gas and public education as the most effective means of hazard reduction. CO_2 can be released by volcanic systems during noneruptive periods and is often disregarded (D'Alessandro, 2006; Williams-Jones and Rymer, 2014). On review of volcanic gas fatalities, D'Alessandro (2006) concluded that CO_2 is the most dangerous volcanic gas, responsible for 90 % of victims. CO_2 is considered to be an immediate danger to life and health (IDLH) at 40,000 ppm (4 %) and can result in unconsciousness after one minute of exposure at greater than 11 % (CDC, 1994a; Williams-Jones and Rymer, 2014). For SO_2 and H_2S, levels above 100 ppm are considered IDLH (CDC, 1994b; 1994c). H_2S exposure can result in eye, nose, throat, and lung irritation at low levels (20−50 ppm) and unconsciousness and death at 500−700 ppm (Enform, 2013). SO_2 exposure ranges from low levels causing sneezing and coughing at 10 ppm, and bronchospasm at 20 ppm, but higher or longer exposures can cause death from airway obstruction (ATSDR, n.d.). These impacts affect safety in fumarolic areas and fumarolic ice caves. On Mount Hood, a well-known fumarole cave was the subject of multiple climbing accidents when a climber slid into the cave where gasses vent (KGW Staff, 2014; Young, 2015). Mammoth Mountain Fumarole in California caused the death of three persons who may have been unaware of the dangers of fumarole gasses (Cantrell and Young, 2009). In the cases of these fatalities, two initial victims fell into the hazardous atmosphere, and two rescuers lost consciousness. Only one of those rescuers survived and multiple rescuers experienced symptoms (Cantrell and Young, 2009). These incidents demonstrate the cascading effect of a single casualty in hazardous atmospheres, whereby responders to the initial victim also succumb to the toxic atmosphere, multiplying the casualties.

O_2 displacement by other gasses has discreet hazards. For example, a climber suffocated in the O_2-poor environment of Mount Hood ice caves in 1934 (Anderson, n.d.). The report identified difficulties in the rescue/recovery whereby rescuers were overcome with fumes and a filter mask did not assist. O_2 helmets were eventually worn by rescuers to complete the recovery. As tissues fail to receive necessary O_2 in environments of 94 mmHg of partial O_2 pressure (PO_2), symptomatic response can develop rapidly (Rom, 1992) including excessive rate and depth of breathing at rest (hyperventilation), poor judgment and coordination, and tunnel vision. Heavy exertion can result in collapse and unconsciousness at <79 mmHg PO_2 (ASTM, 2019). Below 16 % O_2, there is cognitive impairment that can lead to reduced risk recognition and poor decision making that has been implicated in many deaths (Spelce et al., 2016).

Data from volcanic fumarole studies have focused on the composition of fumarole gas from direct sampling to forecast magmatically driven eruptions—as a volcanic system reactivates, the gas emissions evolve from CO_2-rich to SO_2-rich (Stix and de Moor, 2018). In open atmospheres, volcanic gas concentrations expectedly decrease with distance from fumaroles. The confined space of glaciovolcanic caves reduce the dispersion of gas emitted from subglacial fumaroles.

Accumulations of concentrated volcanic gas in the Mount Rainier fumarolic ice caves have not been reported previously. First reports of volcanic gas by Stevens (1876) noted sulfurous fumes and steam vents along the north rim of the West Crater. More expansive observations of these fumes were reported by Ingraham (1895), Coombs (1936), and Kiver and Mumma (1971). Fumarole sampling in the East Crater during 1982 revealed elevated CO_2 (1.4 % to 4.2 %) and sulfur gasses below the detection level of 0.5 ppm (Frank, 1995). Zimbelman et al. (2000) reported ambient air in most cave locations on the summit as typical; however, fumarole emissions had CO_2 enrichments of 7 times to nearly 30 times that of air, trace H_2S odors were detected in the West Crater cave, and sulfate minerals encrusting a fumarole vent indicated locally high H_2S or SO_2 in the past. Separately, Le Guern et al. (2000) reported CO_2 concentrations near 300 ppm in the East Crater Cave atmosphere, and near 3000 ppm in the West Crater Cave atmosphere with H_2S concentrations of 2 ppm to 5 ppm in the West Crater Cave, below toxic levels.

Addressing their findings, Zimbelman et al. (2000) noted the need for further study of the risk of asphyxiation and CO_2 poisoning in the Mount Rainier caves. Curtis (2016) reported that gasses in fumarolic ice caves will be well mixed due to advection and CO_2 concentration is likely higher near the cave roof than the cave floor, therefore traps of CO_2 pooled near vents should not be a hazard to humans. With the previously unreported observation of large areas of IDLH CO_2 in West Crater Cave in contradiction with this, the existence of the phenomenon in the Mount Rainier cave system revealed environmental mechanisms that required better understanding. Badino (2009) concluded that gasses can accumulate in motionless atmospheres and create CO_2 traps in caves. As SO_2, H_2S, and CO_2 are less buoyant than air, the hazard is then expected to manifest in confined, poorly-ventilated spaces or the low-lying parts of the cave system.

The public, mountaineers, researchers, mountain rescue, and Mount Rainier National Park staff enter the fumarolic ice caves, therefore an assessment of hazardous atmospheres is necessary. We conducted repeat observations and gas measurements to determine the extent and persistence of volcanic gas present in the Mount Rainier cave systems and discuss in this paper the implications from a life-safety standpoint. The use of life support equipment enabled the full exploration of the cave system. We consider for the first time the reduction in O_2 concentrations due to displacement by volcanic gasses in fumarolic ice caves, and the combined effect with high altitude. Lastly, we measured airflow, air pressure, and fumarole output to understand the climatologic mechanisms and influences on CO_2-trap formation inside this volcanic subglacial environment. Understanding the connection between glaciovolcanic cave morphology and their atmospheres has further value as research into these unique environments continues from extra-terrestrial analog or volcanic hazard monitoring.

METHODS

Cave survey methods outlined in a comparison study of the long-term morphology of the Mount Rainier cave system in Stenner et al. (in review) produced detailed plan and profile maps. Survey data was reduced in COMPASS cave survey software. Cave room volumes used in calculations were computed in COMPASS by isolating survey data for two particular rooms and generating statistical reports. The room volume measurements are considered approximate.

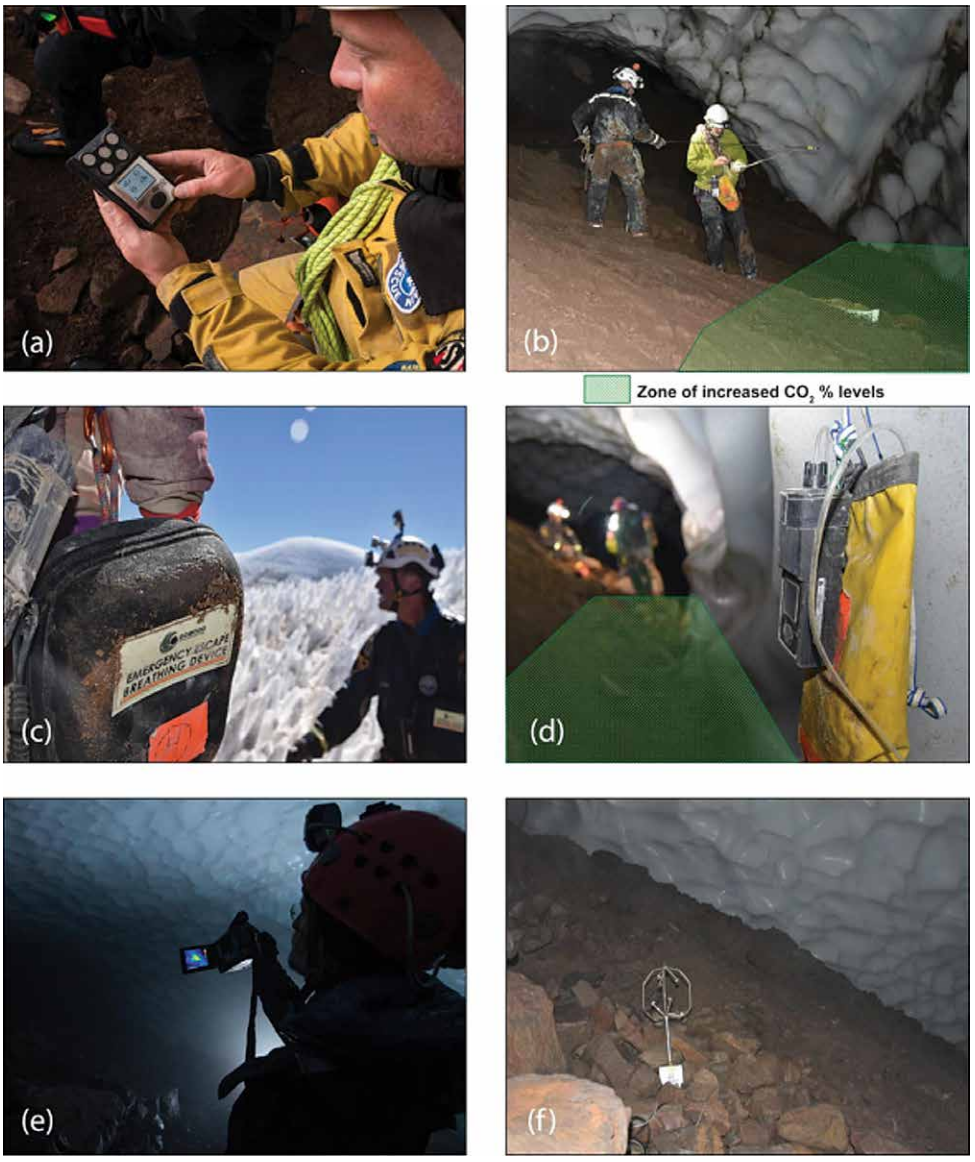


Figure 2. Methods. (a) Industrial Scientific MX6 iBrid portable gas monitor. (b) The West Crater Cave – preparing to take gas measurements using an aspirated MX6 iBrid gas monitor, hose attached to an avalanche probe above a zone of high CO_2. (c) Ocenco Self Contained Self Rescuer (SCSR) worn within the East and West Crater Caves as an emergency escape breathing device (EEBD). (d) Aspirated MX6 iBrid gas monitor mounted above a zone of high CO_2 Image: Wood, T. (e) Recording of cave floor surface temperatures using thermography. (f) Ultrasonic anemometer for detailed evaluation of air movements and flow.

Environmental measurements were made in the caves which form the framework for gas dispersion. Long-term measurements included:

- Air temperature and relative humidity using data loggers (Geoprecision).
- Air temperature and pressure measurements between August 2016 and August 2017 near Lake Adélie in East Crater Cave (In-Situ BaroTroll).

Mobile measurements during expeditions included:

- Detection of H_2S, SO_2, CO_2 and O_2 throughout all cave passages during studies from 2015-2017 using calibrated Industrial Scientific MX6 iBrid gas monitors. O_2 and CO_2 measurements were displayed as percent concentrations and H_2S/SO_2 as parts per million. An aspirated version with a 10 m hose allowed measurement at low points, prior to descending into unknown atmospheres or in fumaroles, while staying above areas with hazardous concentrations representing IDLH (Fig. 2). Sensors were limited to an upper detection range of 5 % CO_2.
- CO_2 concentration in West Crater Cave was recorded from

August 1−5, 2017 using a CO_2-Probe GMP 251, (Vaisala) with an upper detection range of 20 %, combined with a DK390 rugged data logger (Driesen and Kern) for measuring air temperature, relative humidity, and atmospheric pressure.

- Quantitative and qualitative recording of cave floor surface temperatures using thermography (VarioCam High Resolution, Jenoptik) to record and evaluate single fumaroles, as well as whole fumarole fields (Fig. 2).
- Flow measurements using ultrasonic anemometers (USA-1, METEK) for detailed evaluation of air movements and the flow in the cave system (Fig. 2).
- Selected fumarole openings were equipped with a plastic tube and a hot wire probe (Testo). Gas velocity and temperature was measured, and volume flows were calculated based on gas velocity and the known diameter of the tube. Active fumaroles were fumaroles with a visible, audible, or palpable emission of gas.
- A mobile weather station (Vaisala WXT520) recorded the weather conditions outside the cave.

Where reported CO_2 values were over range (5 %) for detection equipment, gas concentrations were extrapolated from O_2 measurements using the formula in Spelce et al. (2016) adjusted to subtract from normal tropospheric O_2 % concentration, and two O_2 values were derived similarly from CO_2 measurements

$$(20.95 - z) = \frac{x}{5}, \tag{1}$$

where

- x = contaminant gas = $\frac{y}{10^4}$ (%)
- y = contaminant gas (ppm)
- z = measured O_2 (%).

This calculation provides the maximum possible contaminant gas concentrations and is subject to error, such as a potential mix of CO_2 and other possible contaminant gases such as N_2, Ar, or H_2S.

O_2 partial pressure (PO_2) values were derived from the atmospheric pressure using the formula

$$x = \frac{y(0_2)}{100}, \tag{2}$$

where

- x = PO_2 (% mmHg)
- y = atmospheric pressure (mmHg).

To complete the exploration of hazardous atmospheres, Self-Contained Breathing Apparatus (SCBA) was worn. This exploration of a confined space in a cold, volcanic environment, with a hazardous atmosphere comprising both dangerous levels of CO_2 and deficient in O_2 by concentration and by atmospheric pressure due to high altitude, presents a unique case. Life support equipment consisted of Extreme Limited Access Breathing System (ELABS) SCBA (Special Projects Operations, Inc.). The units are a modular, compact, pressure demand SCBA for confined spaces. A single manifold connects three carbon-fiber tanks which have a combined capacity of 1791 l gas at 4500 PSI. Total weight is 10.4 kg (Special Projects Operations, 2015) (Fig. 3). This project represented the first use of this equipment model in a cold high-altitude environment. ELABS were paired with an Avon FM53 full face mask. FM53 includes positive-pressure capability, an oro-nasal cup to reduce mask dead space, and has a rebreathed CO_2 value of 0.8 % (Avon, n.d.). Positive pressure in the mask is necessary to miti-



Figure 3. (a) Product image of Extreme Limited Access Breathing System (ELABS) Self Contained Breathing Apparatus (SCBA) showing thin confined space profile. (b) ELABS three carbon-fiber tank design, regulator, and air gauge/Rapid Intervention Team (RIT) quick fill connection. (c) Preparation to enter the "CO_2 Lake of Death" while wearing ELABS SCBA as life support equipment. (d) Descending into the "CO_2 Lake of Death" using ELABS SCBA as life support equipment.

gate against leakage at the mask/facial seal. Additionally, each person wore an Ocenco Self Contained Self Rescuer (SCSR) as a backup emergency escape breathing device (EEBD) (Fig. 2). SCSR is a 1.6 kg self-contained belt-worn emergency breathing apparatus and can give a person a maximum of 15-32 minutes of breathable air to escape an area (Ocenco, n.d.). Two ELABS were worn for exploration with a third ELABS and backup air supply reservoir tank left in reserve at the base of the climb at Paradise trailhead.

Exploration of the most hazardous area was conducted using ELABS and included the following procedural methods. Exploration was on the second last day of the 2017 research deployment, which allowed four days and nights at the summit after two days of climbing to maximize acclimation and provide one additional day for contingencies. By this time research team members were partially acclimated, with blood oxygen saturation (SpO_2) levels, measured by pulse oximeter, having increased from 80−86 % to ~90 %. Acclimatization was further enhanced by prophylactic use of Acetazolamide prior to and during the ascent. Exploration was conducted with a rule of thirds protocol typical of cave diving where one third of the available breathing gas is available for penetration, leaving one third for return and one third for contingencies. Testing prior to the expedition in a cave environment at 1400 m elevation revealed a 45 minute and one-hour ELABS tank capacity for Stenner and Graham, respectively, limiting penetration time to a maximum 15 minutes for the team. At the summit, a reduction in ELABS tank pressure of 300 PSI from maximum was noted. Additional safety mitigations included each team member wearing a climbing harness, use of a PMI reflective static rope and the pre-establishment of a fumarole rescue counterweight raise system (e.g., Cartaya, 2018). This system was secured above the hazardous atmosphere chamber with redundant ice screw anchors and manned by two team members and the expedition doctor. Medical O_2 and an Automated External Defibrillator were available.

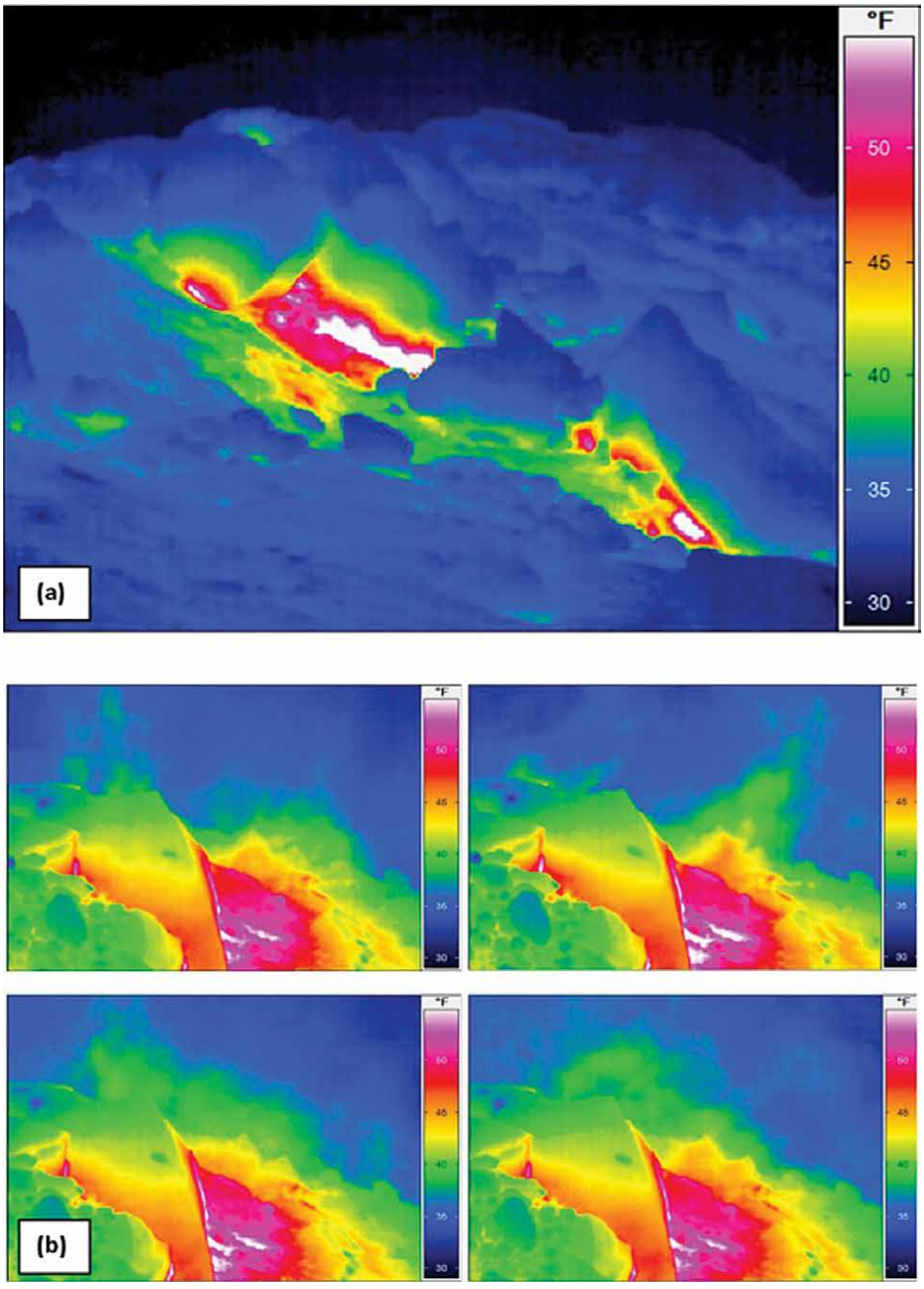


Figure 4. Thermographic images of fumarolic activity. (a) Thermographic image of a fumarole field in the main passages of the East Crater Cave system of Mt. Rainier without visible outgassing. (b) Thermographic image series showing the outgassing of water vapor above an active fumarole in the East Crater Cave system of Mt. Rainier.

RESULTS

Thermography revealed many areas on the East Crater floor with temperatures above the general surface temperature of about +2 °C to −2 °C as so-called hotspots. These ranged from small holes with temperatures of up to 59 °C to larger areas with temperatures ranging from 2 °C to 25 °C. Small but very hot spots were small fumaroles, while the larger areas were heated sediments or rock blocks. All active fumaroles were found to have vent temperatures above 40 °C and inactive fumaroles had temperatures up to 30 °C. The hottest fumarole had a degassing temperature of 59 °C. Figure 4 shows a typical fumarole

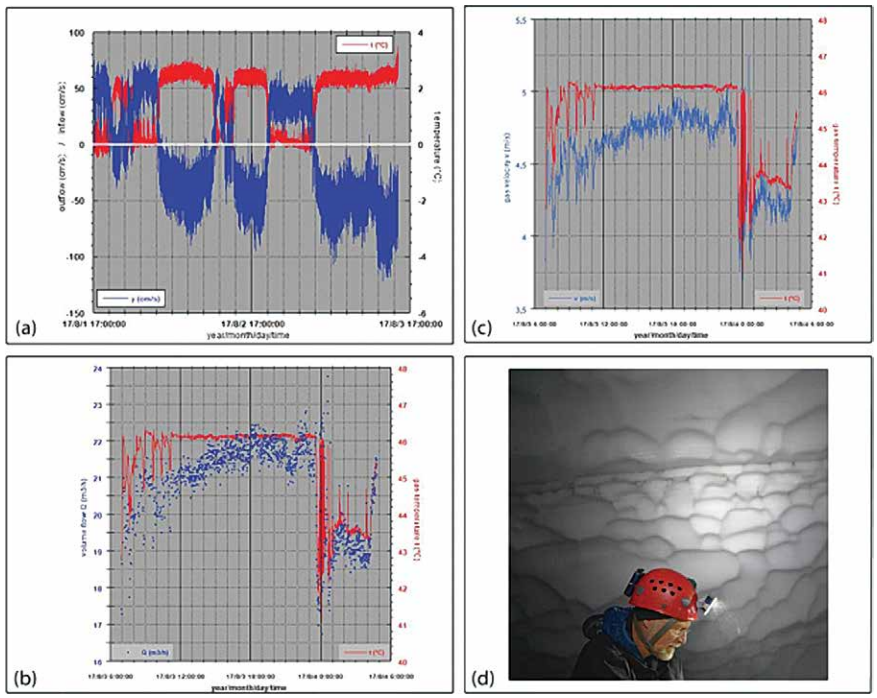


Figure 5. East Crater Cave climatologic and fumarole information. (a) Ultrasonic anemometer airflow (cm/s) and air temperature (°C) from passage junction below High Noon Entrance with alternating inflow (cold) and outflow (warm). Measurement interval: 1 sec. (b) Gas volume and temperature measurements of the fumarole near the Coliseum at survey station 1.42. (c) A possible warm air trap. The change of the scallop patterns at the transition from the side walls to the ceiling may show a change in airflow. (d) Gas velocity and temperature measurements of the fumarole near the Coliseum at Survey station 1.42.

field with small hotspots and the heated area around them. Degassing was visible at some hotspots due to water vapor condensing in the cold cave air.

Strong degassing with visible and audible steaming was uncommon, while wide fumarole fields of hotspots were more prevalent. An example of clear water vapor degassing can be seen in the thermographic Figure 4. Here, the sequential images show the movement of the water vapor, which could only be detected as hot vapors up to a maximum of 1.5 m above ground. In the East Crater cave system there are only a few fumarole sites (<10) with strong degassing. A selected fumarole displayed volume flows between August 3, 2017 and August 4, 2017, of 16.7 m^3/h to 23.8 m^3/h. The volume flow as well as the degassing temperature is shown in Figure 5.

Measurements of gases in ambient air and our calculations to derive CO_2 concentrations revealed the following. In the East Crater Cave, ambient air in the main passages typically comprised 20.95 % O_2 and <0.3 % CO_2. One reading in the main perimeter passage reached a maximum of 1.6 % CO_2 at a low point in the passage. This reading was specific to the trough formed against the ice walls, on the far side of debris ridges common in the perimeter passage noted by Kiver and Steele (1975). The zone of elevated CO_2 was approximately 40 cm in depth and confined to the trough. Two passages were noted with a maximum reading between 1.5 % to 1.6 % CO_2, the Bird Grotto and the Low Loop. Both Bird Grotto and Low Loop begin as a low crawl way branching from the main passage and descending at a slope of 35−40 degrees. There was no distinct planar boundary, with CO_2 concentrations slowly increasing as the passages descended after branching off from the main passage

The Belly of the Beast differs, as it is a large, open room with a sloping floor of 35−40 degrees, terminating in a steeper slope near its lowest point. A measurement taken 7 m above the lowest point in the chamber found an 18.9 % O_2 concentration. The displacement of O_2 here is estimated to be by 10.3 % CO_2, well above IDLH levels even at this point 7 m above the base of the chamber, which was not measured. East Crater Cave ambient air gas measurements are described in Table 1. IDLH areas are identified in Figure 6.

The Canary Room in the West Crater Cave was observed to have a persistent CO_2 trap whereby CO_2 concentrations were over detection range (over 5 %) and O_2 was under 18 %, stopping exploration in both 2015 and 2016 (Fig. 7). In the same years, measurable levels of SO_2 were observed at 0.3 %, and a trace scent of H_2S below monitor detection range. The hazard remained persistent in 2017 and exploration continued using ELABS. Using this equipment further penetration was focused on a downclimb into a dome shaped chamber with an apparent continuation, described during expeditions as the CO_2 Lake of Death (Fig. 3). Notable is the initial descent into the chamber, which was not strenuous, causing an increase in heart rate in the senior author to 178 beats per minute (BPM), in contrast to a resting heart rate of 90 BPM on the morning of the descent, both measured by wrist heart rate monitor. The chamber was explored, surveyed, and consisted of a single room with breakdown block and sediment floor. The apparent continuation became low, pinched out, and was not a viable passage. No obvious fumarole activity was noted. In 2017 the O_2 level in the CO_2 Lake of Death room was 16.0 %, and CO_2 measured over range for detection equipment. The displacement of O_2 is estimated to be by 24.8 % CO_2, the highest ambient concentration in the Mount Rainier cave system. No H_2S or SO_2 was detected in this area. The West Crater cave ambient air gas measurements are described in Table 1 and IDLH areas are identified in Figure 8.

Discussion of hazards can be furthered by accounting for displacement of O_2 by CO_2. Atmospheric air pressure recorded in the East Crater cave system during the study period reported by Florea et al. (2021) ranged from 426.7 mmHg

Table 1. Ambient air gas concentrations of areas inside the Mount Rainier Fumarolic Ice Caves, 2015−2017.

Cave	Passage Name	Date	Gas Concentrations, % CO_2	O_2	SO_2	S	PO_2[a] (mmHg)	Notes
East Crater	Main passages	08/2017	<0.3	>20.9[c]	···	···	>89.1	Obs. maximum
East Crater	Main passage	08/2015	1.6	20.6[c]	···	···	88.0	
East Crater	Bird Grotto	08/2017	1.6	20.6[c]	···	···	88.0	
East Crater	Belly of the Beast	08/2015	10.3[b]	18.9	···	···	80.6	7 m above floor
East Crater	Low Loop	08/2017	1.5	20.7[c]	···	···	88.1	
West Crater	Canary Room	08/2017	15.3[b]	17.9	···	···	76.4	
West Crater	CO_2 Lake of	08/2017	24.8[b]	16.0	···	···	68.3	
West Crater	Entrance	08/2016	···	···	0.3	···	···	
West Crater	Entrance	08/2017	···	···	0.3	···	···	
West Crater	Main passage	08/2015	···	···	···	Trace[d]	···	
West Crater	Main passage	08/2017	···	···	···	Trace[d]	···	
West Crater	High passages	08/2015	0.25	20.9[c]	···	···	89.1	

[a] Partial pressure values given for O_2 concentrations only. Values are assuming lowest recorded in cave air pressure measurement of 426.7 mmHg at O_2 20.95 %.
[b] Concentrations are extrapolated from O_2 measurements.
[c] Concentrations are extrapolated from CO_2 measurements.
[d] Scent detected but was below detection range for monitoring equipment.

to 462 mmHg. PO_2 is therefore between 89.3 mmHg and 97 mmHg assuming 20.95 % atmospheric O_2 concentration in the main passages. Accounting for the lowest observed atmospheric air pressures and the displacement of O_2 by CO_2, the lowest PO_2 in East Crater Cave was 80.6 mmHg and 68.3 mmHg in West Crater cave. These values assume that no other contaminant gasses than CO_2 are present to cause O_2 displacement and do not account for displacement by water vapor in the cave atmosphere, considered a small effect at 2 °C.

The Canary Room and CO_2 Lake of Death room in West Crater cave exhibited a distinct invisible planar boundary between safe and IDLH atmospheres. Normal ambient air gas concentrations of 20.95 % O_2 sharply degraded in the span of 0.3 m of elevation loss to 16 %, the lowest concentrations recorded. Symptoms of one support team member who briefly moved his head below the threshold unprotected described normal breathing suddenly interrupted by tunnel vision and a rapidly declining level of consciousness. The Canary Room exhibited an IDLH CO_2 trap over 3 m in depth (Fig. 7). Repeated measurements during our early expeditions showed the exact elevation of boundaries between IDLH atmospheres and breathable ambient air was variable.

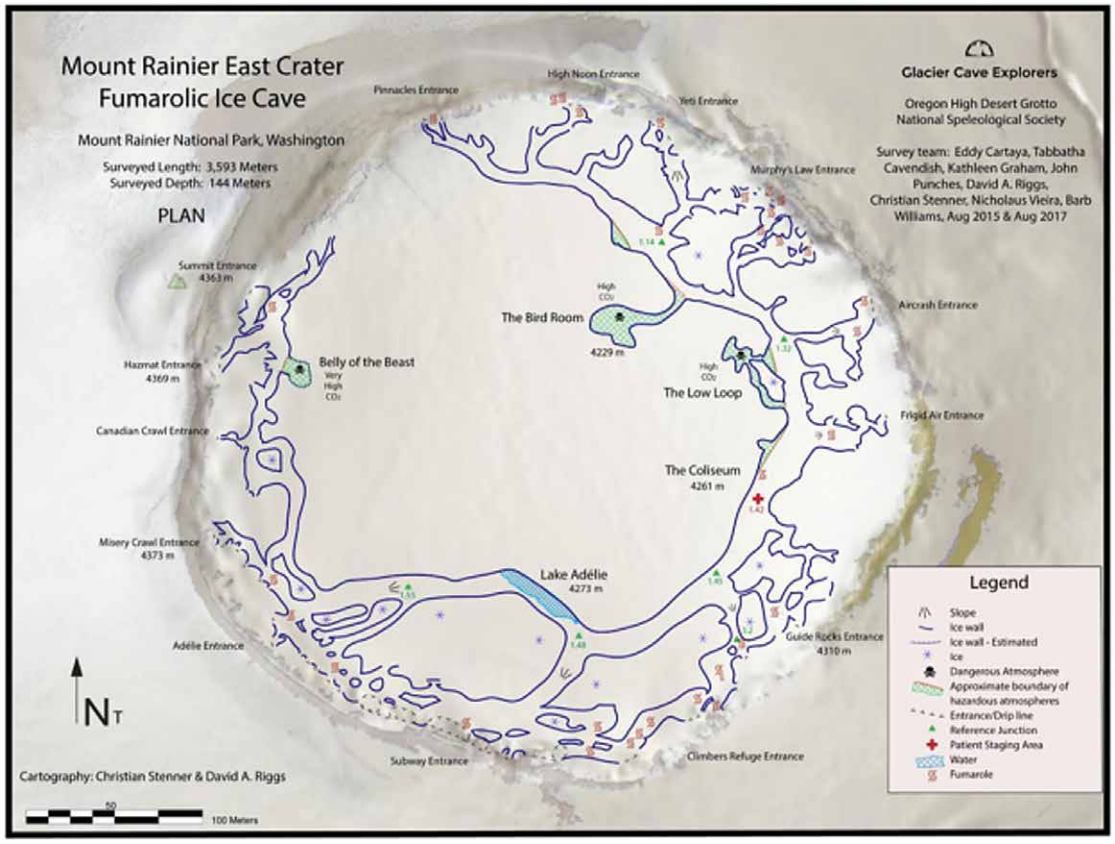


Figure 6. Survey in plan view of the East Crater Cave with zones of IDLH atmospheres identified. Map legend lists key features. Base map is a combination of digital elevation hillshade and satellite imagery.

To understand the CO_2 lakes in this

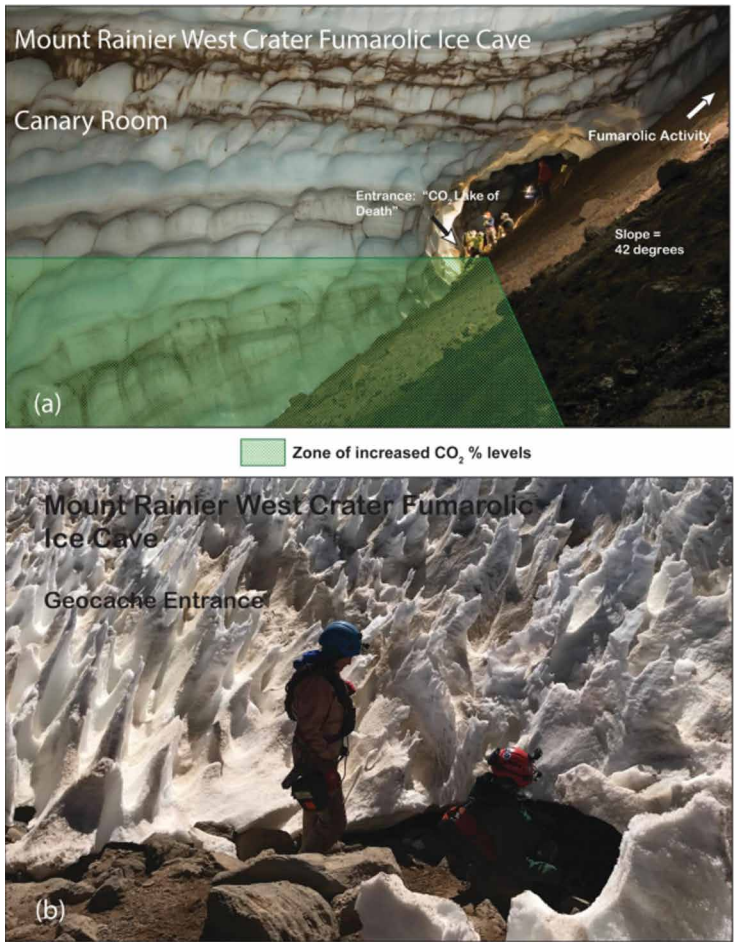


Figure 7. (a) A view across the Canary Room of the West Crater Cave, with the approximate planar boundary of IDLH CO_2 atmosphere identified. The room dimensions are 23 m × 26 m × 17 m (L × W × H) and not easily recognized as a confined space trapping CO_2. (b) The "Geocache" entrance to West Crater Cave. This entrance is typical of the West Crater Cave entrances alongside the crater rim.

region of West Crater Cave, a CO_2 sensor was installed at the approximate boundary of safe and IDLH atmosphere during the 2017 expedition, which records the CO_2 concentration (%) every second. Additionally, the air temperature, relative humidity, and the atmospheric pressure inside the cave were recorded. The measured data are summarized in Figure 9. It is noticeable that the CO_2 concentration seems to oscillate during the first half of the measurement period. Relatively long phases of higher CO_2 concentrations are repeatedly interrupted by significant drops of 2 % to 5 %. Both the relative humidity and the air pressure show a similar pattern, but with opposite tendencies, while the air temperature seems to have no influence. The CO_2 dips are accompanied by increasing air pressure and increasing humidity values.

In the second part of the measurement, there is a significant change. The air pressure drops rapidly at first, then somewhat more slowly without the previously oscillating fluctuations. The course of the CO_2 concentration responds with a noticeable increase at first, followed by sudden collapse before it stabilizes again at a high level. The decreasing concentration towards the end of the measurements is not considered further. The reason for the strong decrease of about 3.5 % is not explained by air pressure fluctuations. Rather, it coincides with a significant temperature drop of >1.5 °C, which is unique for this short measurement series.

Examining correlation calculations for the entire measurement series in Figure 9d, the best correlation by far is between CO_2 concentration and air pressure of approximately Pearson *R*: −0.70, while only Pearson *R*: −0.35 is achieved between CO_2 and relative humidity and just Pearson *R*: 0.18 in relation to temperature. Thus, air pressure can be identified as the main influencing factor on the CO_2 level. The correlations of the individual measured variables to the CO_2 concentration can be seen in Figure 9b, c and e. By calculating the cross-correlation between CO_2 concentration and air pressure, an increase of the correlation to Pearson *R* of nearly −0.80 can be achieved with a shift of 7.6 hours (Fig. 9f); there is no improvement for humidity and only an insignificant improvement for air temperature.

However, a change in the CO_2 concentration several hours before a change in air pressure makes no sense from a scientific point of view. Instead of a pressure change the change in CO_2 concentration can be explained by a drop in the air temperature as observed in the temperature collapse on August 3, 2017 at 22:15 to August 4, 2017 at 05:45, which disturbs the concentration-pressure correlation and creates the 7.6-hour shift.

In a second step, the time series was divided and only the first part, prior to the temperature drop, was examined more closely until the temperature drops (Fig. 9g). Here, Pearson *R*: values of −0.77 and *R*1 of 0.60 are obtained (Fig. 9h). The cross correlation did not yield better values when the time series were shifted (Fig. 9i).

DISCUSSION

The proximity of mountaineers to the cave system puts them in the vicinity of hazards in addition to those of regular mountaineering. As the caves have been entered by climbers for shelter in bad weather, or out of curiosity, safety information is necessary given our findings. Currently there is no public facing information by the National Park Service directed towards climbers regarding the cave system warning about hazards. Notwithstanding the fact that gas concentrations near source fumaroles are considerably higher and a known hazard, our findings indicate ambient air in the caves is a serious concern.

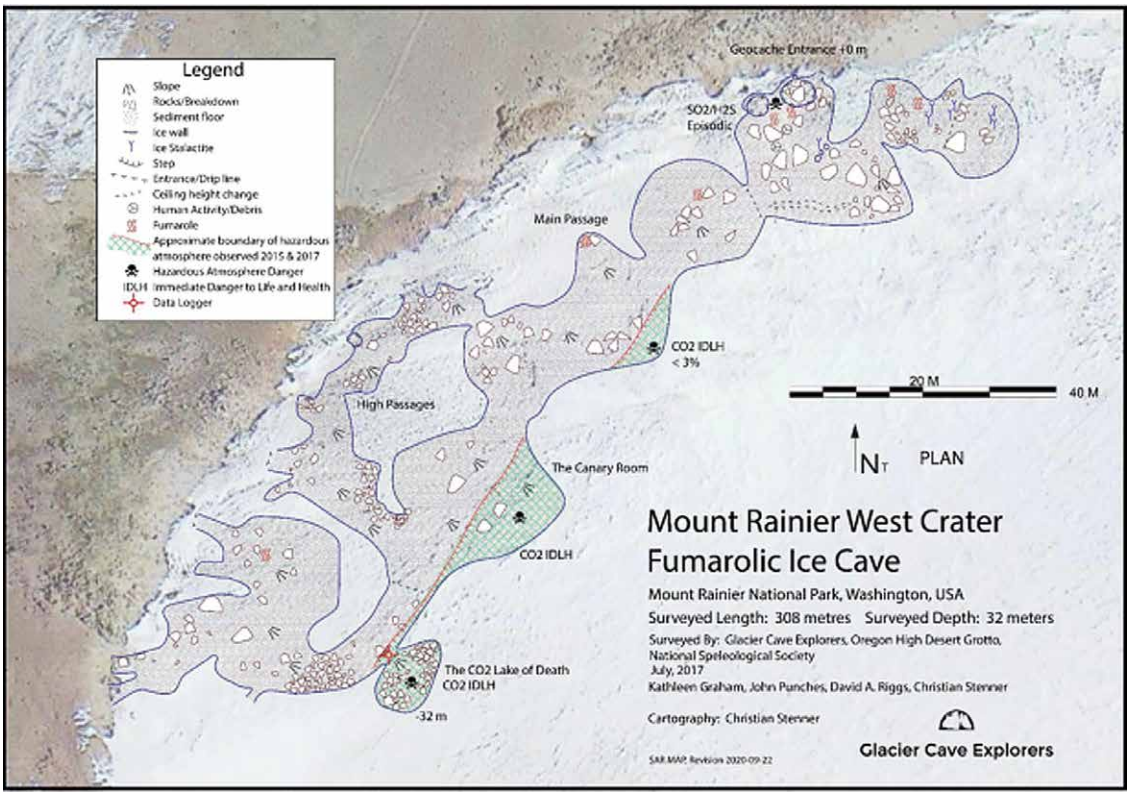


Figure 8. Survey in plan view of the West Crater Cave with zones of IDLH atmospheres identified and indicating the CO_2 data logger location. Map legend lists key features. Basemap is from satellite imagery.

Other glaciovolcanic cave systems have typically revealed low concentrations of volcanic gas in ambient air. Studies by Ilanko et al. (2019) at Mount Erebus, Antarctica, caves using various methods found vent samples over 2 % CO_2 and ranging up to 2.9 %, but ambient air concentrations of up to 0.94 % CO_2. Curtis (2016) found up to 2 % CO_2 inside Warren Cave at Mount Erebus. Studies at Sandy Glacier on Mount Hood and on Mount St. Helens reveal none or only traces of CO_2 in safe amounts and no other volcanic gasses. Measurements throughout the new Mount St. Helens fumarolic ice caves revealed a maximum of 0.3 % CO_2 (Sobolewski et al., 2020). On Mount Hood volcano a hydrothermally-influenced ice cave contained no volcanic gas (Pflitsch et al., 2017).

Contrasting these results is the well-known fumarolic pit on Mount Hood (Tomlinson, 2019). Known as Devil's Kitchen, analysis reported by Nehring et al., (1981) reported CO_2, H_2S, and O_2 measurements from fumarole sampling in the pit of up to 94.4 %, 3.9 %, and 0 %, respectively. High CO_2 concentrations also exist at Mammoth Mountain Fumarole. Direct sampling revealed CO_2 98.7 %, O_2 0.09 % H_2S, 0.02 %. After the fatalities there, ambient air measurements taken one to two hours following the incident revealed O_2, 18 %, CO_2, 10 %, CO, 4 %, and H_2S, 0.003 % (Cantrell and Young, 2009). Limited information on Mount Baker summit crater reported the presence of fumarolic ice caves and measurements from 1974−1977 of CO_2 from 14.4 % to 36 % maximum and H_2S 0.0074 % to 7.4 % maximum, levelling off at 3.8 % (Kiver, 1978). Adding to this, our data shows that CO_2 emitting fumaroles have caused CO_2 accumulations to form where they had not previously been noted in the Mount Rainier caves, suggesting the possibility of such accumulations to be dynamic due to variable ventilation and fumarole output. Also, that this phenomenon can persist in fumarolic ice caves, even those with ventilation effects such as the Mount Rainier system.

Mount Rainier cave hazardous atmospheres

The Hazmat entrance to East Crater Cave is near Columbia Crest and is an attractive curiosity easily visible to mountaineers. Within, the steep slope descends to the base of the passage at Belly of the Beast where the highest CO_2 concentrations are recorded in East Crater Cave (Fig. 10). Even the main passages, which held a trough of CO_2 adjacent to debris ridges, could be a hazard in the case of a person who slips on the steep slopes and lands with their head and airway in a hazardous atmosphere. The entrance to the Bird Grotto and Low Loop are tight and unlikely to be visited, except for persons who may want to explore the lowest point in the cave. The West Crater Cave is a significant concern due to the highest levels of CO_2 observed, an attractive curiosity (geocache) at a fumarole known to vent SO_2, and little ventilation observed during the expeditions that would assist in dispersal of fumarole gasses. Our measurements across expeditions reveal another danger in that the location of the IDLH atmosphere boundary is inconsistent and cannot be reliably defined, making communication of exact zones of IDLH atmospheres difficult. The Canary Room is a considerable hazard. Within, a person can walk across a large, open chamber on the sloping cave floor with their head, gas monitor, and airway in safe air, and their knees in IDLH atmosphere. A layperson would not recognize the vast room as a confined space and the potentially lethal consequence of walking along the bottom (Fig. 7).

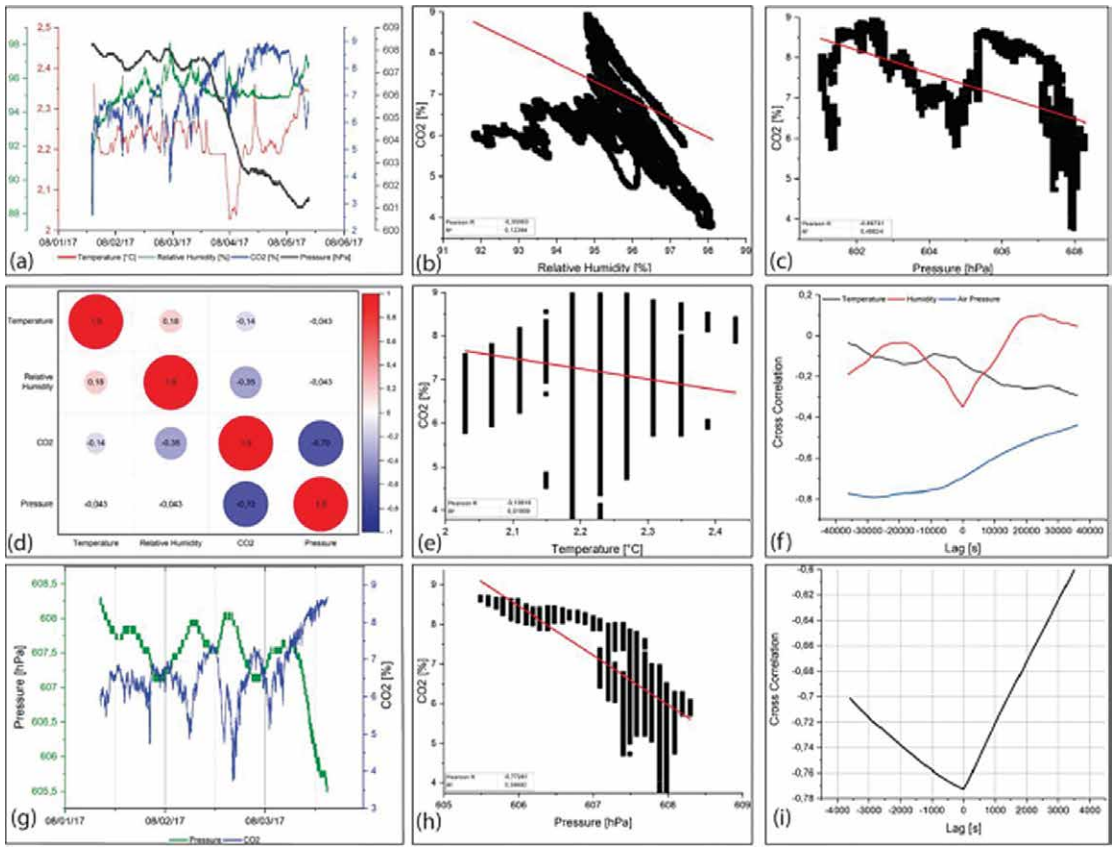


Figure 9. Graphs of measurements inside the West Crater Cave of Mt. Rainier, WA, USA. Measurement interval: 1 sec. The air temperature data were smoothed hourly for better visualization by the method of Savitzky & Golay (1964). (a) Course of the measurement parameters temperature (°C), relative humidity (%), CO_2 content (%) and atm. air pressure (hPa) during the measurement period of August 1 to August 5, 2017. (b) Results of the linear correlation between CO_2 (%) and rel. Humidity (%) during the measurement period of August 1 to August 5, 2017. (c) Results of the linear correlation between CO_2 (%) and atm. air pressure (hPa) during the measurement period of August 1 to August 5, 2017. (d) Summarized results of correlation analyses of all measured variables based on Pearson's correlation coefficient. (e) Results of the linear correlation between CO_2 (%) and air temperature (°C) during the measurement period of August 1 to August 5, 2017. (f) Results of the cross correlation between CO_2 (%) and atm. air pressure (hPa), rel. humidity (%) and air temperature (°C) during the measurement period of August 1 to August 5, 2017. (g) Course of the measurement parameters CO_2 content (%) and atm. air pressure (hPa) during the measurement period of August 1 to August 3, 2017. (h) Results of the linear correlation between CO_2 (%) and atm. air pressure (hPa) during the measurement period of August 1 to August 3, 2017 (i) Results of the cross correlation between CO_2 (%) and atm. air pressure (hPa), rel. humidity (%) and air temperature (°C) during the measurement period of August 1 to August 3, 2017.

The obvious IDLH atmospheres due to high concentrations of volcanic gasses, as per CDC or OSHA requirements, must not be considered alone. Areas of seemingly low concentrations of CO_2 such as the Bird Room and Low Loop in the caves can be IDLH when considering O_2 displacement and PO_2 due to the high altitude. Literature does not reveal information on O_2 displacement in fumarolic ice caves, probably because where volcanic gasses displace O_2 in significant amounts the hazard would likely manifest first in the displacing gasses. With increasing altitude, the atmospheric pressure decreases, and the amount of O_2 molecules available for respiration decreases as well (Spelce et al., 2017). The OSHA respirator standard defines O_2-deficient atmospheres as having an oxygen concentration below 19.5 % by volume, which it considers IDLH. However, human performance and survival at high altitudes and O_2-deficient atmospheres is more substantially affected by the amount of biologically available oxygen based on PO_2. (Spelce et al., 2016). ASTM (2019) considers this, and in this standard, IDLH atmospheres include where total atmospheric pressure is less than 584 mmHg (77.86 kPa) equivalent to 2134 m altitude or any combination of reduced percentage of oxygen and reduced pressure that leads to an oxygen partial pressure less than 122 mmHg (16.27 kPa). Atmospheres with $PO_2 \geq 122$ mmHg and less than 148 mmHg are oxygen deficient but not IDLH. (ASTM, 2019).

Air at the summit is O_2 deficient for unacclimated individuals and can be further exacerbated by reductions in O_2 concentration due to displacement by volcanic gasses in the caves. CO_2 concentrations in some areas are not considered toxic as they are below the OSHA IDLH level of 4 %, such as the Low Loop and Bird Grotto in East Crater Cave. However, considering the displacement of O_2 and reduced PO_2 at altitude these areas are considered IDLH for unacclimated persons as per the 122 mmHg level in ASTM (Table 1), which has implications for researchers or rescuers who may respond to trauma or asphyxiation underground and would require wearing SCBA for life safety.

Implications of the reduced PO_2 include the effect on SCBA users, as SCBA do not overcome O_2 deficient atmospheres very well at high altitude, and maximum in mask pressures during expiration are only 6.5 mmHg above ambient (McKay, 2020). Additionally, inside the facepiece, CO_2 can range in concentration from 2 % to 5 % (Spelce et al., 2016). As full-face mask SCBA with fills of regular O_2 concentration are not likely to elevate PO_2 higher than the IDLH level of 122mmHg in unacclimated individuals, entry into the Mount Rainier caves or others with contaminant gases at high altitudes is a fac-



Figure 10. East Crater Cave. (a) View from just below the Mt. Rainier summit (Columbia Crest) towards glacio-volcanic cave entrances. "Hazmat Entrance" of the East Crater Cave. Descending from the Hazmat entrance is steep passage terminating at the "Belly of the Beast" area of highest CO_2 concentrations recorded in the East Crater Cave system. (b) "Summit Entrance" passage connects to the "Hazmat Entrance" passages and terminate at a low point "Belly of the Beast". Both entrances are visible to the public from the East Crater side of the crater rim just below Columbia Crest. (c) Coliseum room and master passage circumnavigating the East Crater Cave. (d) Fumarolic area in cave entrances near the East Crater rim.

tor to consider. The solution is to use acclimated personnel or use O_2 enriched air fills. Complete acclimatization requires about four weeks' residence at the ambient PO_2 (Spelce et al., 2016; McKay, 2020). ASTM (2019) requires at least 23 % O_2 at 3048 m (air pressure <523 mmHg) and 27 % O_2 at 4267 m (air pressure <450 mmHg) to provide the same amount of O_2 in the tracheal region of the lungs that is available for biological processes as one would receive by breathing ambient air at sea level (Spelce et al., 2016).

Although these cave atmospheres are primarily IDLH due to CO_2, we seek to quantify the impact of reduced O_2 to those who are acclimated or only partially acclimated such as in our case. One way would be to extrapolate the low PO_2 of the O_2 deficient areas to an equivalent altitude above sea level. As SCBA will only add 6.5 mmHg above ambient pressure this assists in understanding the potential physiological effects of reduced PO_2 even when fully protected against contaminant gases. To model and compare O_2 deficient areas with atmospheres at regular tropospheric O_2 concentrations and various altitude dependent pressures we adapt the barometric formula (Berberan-Santos et al., 1997). However, using the previous ratio to calculate the equivalent atmospheric pressure of reduced cave PO_2 as if in a normal atmosphere of 20.95 % O_2 at 426.7 mmHg, substituting those values for P and solving for altitude (h)

$$P = P_b\left[\frac{T_b}{T_b + L_b(h - h_b)}\right]^{\frac{g_0 - M}{R^* L_b}}, \quad (3)$$

where

P = Equivalent air pressure (Pa)

P_b = reference pressure (Pa): 101300

T_b = reference temperature (K): 275.15

L_b = temperature lapse rate (K/m) in International Standard Atmosphere: −0.0065

h = altitude of P (m)

h_b = altitude of reference, sea level (m)

R^* = universal gas constant: 8.3144598 J/(mol·K)

g_0 = gravitational acceleration: 9.80665 m/s2

M = molar mass of Earth's air: 0.0289644 kg/mol.

The equivalent altitude of O_2 deficient cave atmospheres is calculated using the PO_2 as determined for each passage, using the low of 426.7 mmHg in cave air pressure and an average in cave temperature of 2 °C (Florea et al., 2021). Table 2 compares actual altitudes of O_2 deficient passages and their PO_2 with others and allows comparisons to be made.

Table 2. Comparison of O_2 deficient Mount Rainier Cave passages and their equivalent altitudes.

Location	Altitude (m)	Temp. (°C)	O_2 (%)	Atmospheric Pressure (mmHg)	PO_2 (mmHg)	Equivalent Atm. Pressure[a] (mmHg)	Equivalent Altitude (m)
Comparison Locations							
Sea Level	0	15[b]	20.95	760.0	160.0	760	0
Rainier Paradise Center	1646	15[b]	20.95	625.3	131.0	625.3	1646
Mount Rainier Summit	4392	0[b]	20.95	438.9	91.9	438.9	4392
Mount Everest Summit	8848	−19[b]	20.95	231.5	48.5	231.5	8848
Mount Rainier Cave Passages							
Main passage trough	4269	2	20.4	426.7	87.0	415.0	4779
Bird Grotto	4230	2	20.4	426.7	87.0	415.0	4779
Belly of the Beast	4344	2	18.9	426.7	80.6	384.7	5487
Low Loop	4260	2	20.4	426.7	87.1	415.8	4770
Canary Room	4355	2	17.9	426.7	76.4	364.7	5950
CO_2 Lake of Death	4350	2	16.0	426.7	68.3	326.0	6821

[a] Atmospheric pressure of reduced PO_2 extrapolated to a normal atmosphere of 20.95 % O_2 at 426.7 mmHg.
[b] Temperatures used as estimates to calculate air pressure and PO_2 values for comparison.

In addition to the primary hazard of contaminant gases, exposure to reduced PO_2 results in experiencing an equivalent felt altitude increase of 510 m in Low Loop, 1143 m in Belly of the Beast of East Crater Cave, and a worst-case increase of 2471 m from actual in West Crater Cave CO_2 Lake of Death. The O_2 deficiency could be a potential factor for the heart rate increase of 88 beats per minute in the senior author as only partially acclimated during the study. Were it not for the fact that O_2 deficiency in some cases is caused by IDLH levels of CO_2, regular mountaineering O_2 and masks would be sufficient protection. SCBA with positive pressure full face masks to mitigate contaminant gas leakage is necessary. Partial acclimation due to conducting the summit climb over two days, three further sleeps at the summit and use of Acetazolamide likely assisted in negating negative symptoms of O_2 deprivation. Most mountaineers are more acutely exposed to the altitude and do not benefit from the same partial acclimation, or in case of helicopter transport may receive no acclimation.

Development of hazardous atmospheres in the caves

CO_2 traps would not exist if the positive buoyancy effect of vent gas heat content overcomes the negative buoyancy effect of vent gas composition, as discussed by Curtis (2016). We explore why CO_2 traps of IDLH form and persist in the Mount Rainier system. The CO_2 accumulations of 3 m and over 7 m deep appear to be an outlier in comparison to other glaciovolcanic systems, notwithstanding high CO_2 output fumaroles in blind unventilated pits such as Mammoth Mountain Fumarole and Devil's Kitchen which may conform to the situation described by Badino (2009). Strong ventilation effects inside the Mount St. Helens caves in combination with their morphology are a possible explanation why concentrations there are relatively low (Sobolewski et al., 2020). As well, at Mount Rainier the mostly impermeable crater floor of breakdown and sediment contrasts with the Mount St. Helens cave floors which consist mostly of stacked volcanic rocks with gaps between, thus providing more possibilities for CO_2 to accumulate and become trapped at Mount Rainier.

In this context of gas buoyancy, two effects must be considered: the degassing of the fumaroles, and the airflow conditions in the cave system and at passage junctions. It should be noted that degassing fumarole openings at Mount Rainier are usually not exposed, and degassing does not occur directly into the cave atmosphere but is hindered by

boulders or smaller debris. This causes the gas flow to diffuse rapidly and mix with the ambient air, which leads to cooling and condensation of the water vapor (Fig. 4). Furthermore, the rock/debris is heated and, in return, the escaping gas is cooled quickly. Another case that should not be underestimated occurs where fumaroles are in marginal areas to the glacier ice or in narrow pockets under the ice. There, escaping gas directly encounters the glacier ice and cools down rapidly. All this leads to a significant reduction in the buoyancy of the escaping gases. In addition, most fumaroles are located in the upper sloping passages close to the crater rim (Fig. 10) so a large part of the warm air is led directly outside.

A second important point is the general air flow in the cave system, which determines the air exchange with the outside atmosphere and the mixing of the fumarole gasses with the cave air. During the expeditions in 2015 and 2016 we observed periods of little air movement in the main annular tunnel of the cave system alternating with periods of strong air movement. A good indicator for this was the formation of fog. When the air was predominantly calm, very strong fog sometimes formed over the whole system, whereas when the air was well ventilated, the area was mostly clear. It was also observed that higher flow velocities and clear visibility were always accompanied by cold air intrusion from one or more of the numerous openings. In 2017, air flows were recorded for the first time using ultrasonic anemometers. In Figure 5a we see a recording of the flow situation, as well as the air temperature, measured at the junction below High Noon Entrance over a period of almost 3 days. The location is in the influence of the openings to the High Noon and Pinnacles Entrance (Fig. 6).

The most obvious feature is the continuous change of the flow direction with respect to the main tunnel's corridor axis. The changes in direction are also visible by the significant temperature changes. The data shows the inflow of cold air from Pinnacles Entrance into the cave system and the outflow of warmer air from the cave system towards Pinnacles Entrance. The air currents are clearly pronounced at 0.5 m/s to 1 m/s. These constant changes of direction confirm our direct observations from 2015 and 2016, where we observed that the respective flow situation appears to exist over the entire vertical extent. A vertically stratified flow with outflowing warm air in the ceiling area and inflowing cold air at the bottom would be considerably more stable. Furthermore, we never observed stratified layers of fog below the ceiling and clear air. The observed flow is caused by the complex interaction of the numerous openings of the system to the outside atmosphere, which have different tunnel morphologies. Many openings have significant narrowing in the upper area, which also speak against vertical stratification.

A good example of this is the fumarole at the Coliseum room, which yields the data in Fig. 5b and 5c. This fumarole is quite active, with audible, blowing steam and located in a widened tunnel section in the lower part of the conduit, 10 m below the ceiling. We measured a volume flow of around 22.1 m^3/h over a twelve-hour period before the volume flow dropped to a lower level. Compared to the volume of the Coliseum room, which is approximately 10,500 m^3, the fumarole exhaled 0.2 % of the room volume, or 2.5 % over the twelve hours.

Summarizing the results and observations of airflow and volume flow, it can be assumed that degassing CO_2 in the main passage of the cave is diluted and removed quite quickly due to low to moderate buoyancy. This process is supported by the morphology of the cave ceilings, which are partly inclined and form guiding paths to the entrances. CO_2 can only accumulate under the ceiling where bow-like morphological structures form traps for warm air.

An identifiable instance is the hall above survey station 1.14 below the Yeti and Murphy's Law entrances, with a volume of approximately 3,100 m^3. Here the passage structure is interrupted by a dome-like deck and based on the ice structure a clear inversion limit can be determined (Fig. 5d). Especially the fumarole in the upper slope area, close to the ceiling, with a volume flow measured of about 26.5 m^3/s up to 55.3 m^3/s leading to a noticeable warm air convection.

In the lower area of the master passage; however, a small CO_2 lake was identified, which is fed by fumaroles lying deep below the boulders in the lower slope area. These CO_2 lakes are formed at the transition area to the glacier where the weak degassing cools down quickly and cold air with heavier CO_2 accumulates preferentially. The air currents passing through the ring system and the upward cave passages have no influence on these areas, so CO_2 can easily accumulate.

Figure 11a shows a situation in the main passage of the East Crater without strong compensation winds between cave and outside atmospheres. Fumarole degassing rises into the passage. Part of the gas rises to the outside in the next connecting tunnel while cooling down slowly while another part remains inside the tunnel under the ceiling and cools down as well. The cooling effects are achieved by mixing with the ambient air but also by contact with the ice surface on the walls and ceiling. The cooled air then sinks back down the walls and collects at the lowest point. Depending on the morphology of the tunnel, it can also lead to a rotational movement in the upper part. Since the buoyancy of the escaping gases is not strong enough, only part of the heavier CO_2 is carried up, while the remainder sinks down. Further CO_2 is transported by the cooled sinking air into the deeper passages and accumulates. The heavy cold air and the heavier CO_2 reinforce each other in the stabilization of the cold CO_2 lake.

Figure 11b shows the situation in the context of a massive inflow of cold air through the connecting passage to the outside. The heavy cold air flows through the entire cross-section of the corridor into the lower ring passage and mixes

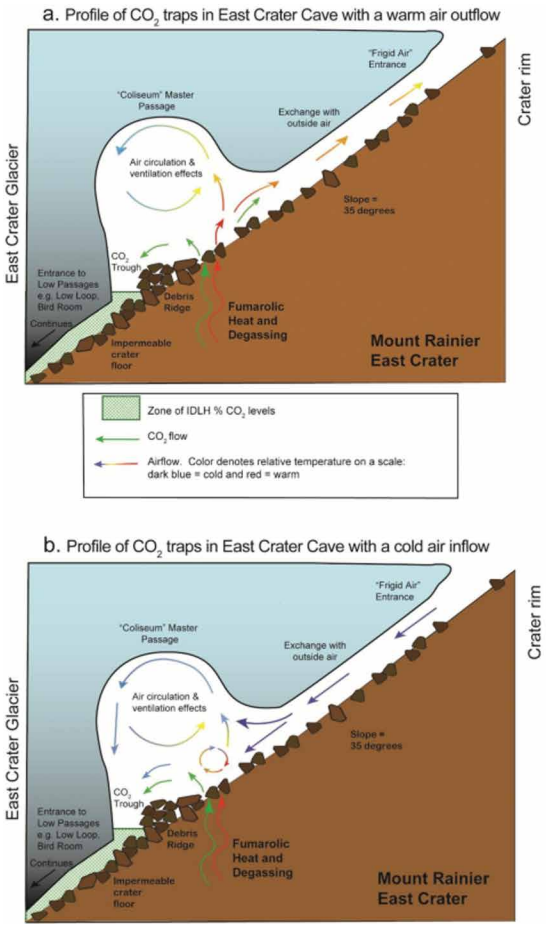


Figure 11. Cross section diagram of master passage as in the East Crater Cave coliseum passage area. The image shows the debris ridges as described by Kiver and Steele (1975) and trough of CO_2 as measured during 2015 and 2017 expeditions. (a) Shows the situation with a warm air outflow. (b) Shows the situation with a cold air inflow.

with the warm fumarole air, resulting in a temperature equalization between both flows. Since cold air also flows down to the fumarole, the cold air effect dominates, and cold air can further stabilize the CO_2 lake. The gases escaping from the fumarole cannot escape from the connecting corridor due to the massive cold air flow but are distributed in the ring passage, cooling down on walls and ceiling. The CO_2 will accumulate at low points and CO_2 lakes are likely to grow. The CO_2 lakes will dissipate only when advective currents (horizontal air flow through the tunnel) dominate and the air currents moving through the ring passage become dominant that can occur until the horizontal current can no longer reach the CO_2 lake significantly because flows are above it.

The same applies to passages below the main corridor like the Bird Room and the Low Loop. There the air exchange is considerably restricted, with the cold air remaining stable and the heavy CO_2 trapped in the whole room. Even if the cold air inflows are less frequent, the CO_2 accumulations will stabilize due to the following circumstances. The currents from the ring system do not penetrate into these lower passages and are not able to remove CO_2. Warm fumarole gases cool down relatively quickly on the surrounding walls and sink to the bottom, and only a small part of the CO_2 can escape by means of warm air, which is supported by the fact that the entire Bird Room has increased CO_2 levels and no clear layer boundary exists.

In the West Crater Cave, even though the series of measurements is short and cannot be considered representative, they provide interesting information on the climatological framework conditions and their effect on the CO_2 lake (Fig. 9).

Since the measurements were taken at the edge of the CO_2 lake, the detected concentration fluctuations are likely based on the following mechanisms. The boundary layer of the CO_2 lake may shift slightly downwards with increasing atmospheric pressure, which would be shown by an immediate decrease in concentration. Or, fumarole activity is dependent on atmospheric pressure and the volume flow from the fumaroles decreases with increasing air pressure, so that expansion of the lake is reduced by a lower recharge. In this case, the concentration changes are likely to show a time lag, which has not been observed.

The decrease in humidity will probably be caused by different moisture content of the cave atmosphere and the CO_2 lake. In the upper cave passages, the water vapor-rich fumarole gasses condense and simultaneously rise to the surface, and an accumulation of humid to even misty air masses will occur, while the CO_2 lakes will be influenced more so by the sinking, drier, and CO_2-rich air.

The marked drop in CO_2 concentration combined with a significant drop in temperature on 3 and 4 August is probably due to the intrusion of cold air masses through one of the entrances and thus a shortchange of flow. Here, short-term, inflowing, colder outside air leads to dilution of the CO_2 concentration, but at the same time to a stabilization of the CO_2 lake, because the cold air strengthens the inversion.

Our hypothesis about the environmental conditions and processes in the West Crater are shown in Figures 12 and 13. Figure 12a shows the most common situation where part of the degassing escapes directly to the outside, while the other part cools down at the ceilings and walls and sinks to the bottom. While the cooler air moves directly to the lower areas, the slightly warmer air rises to the top, cools down under the ceiling and sinks to the bottom at the ice wall at the lower end. The heavy CO_2 supports this movement. There are no buoyancy forces to start circulation. Also, the strong compensation currents between the outside atmosphere and the cave, as seen in the East Crater, seem to be missing. This is probably due to the much smaller openings to the outer atmosphere but also to the morphology of the West Crater passages that have neither the structure nor the size of the ring system of the East Crater.

Figure 12b shows the situation in the context of a less frequent cold air intrusion. Here, a large part of the fumarole output is forced downwards. While the ground-level cold air flow with part of the CO_2 is led into the cold CO_2 lake, part of the warm gas rises into the ceiling areas and cools down slowly. However, the descending air is still lighter than the

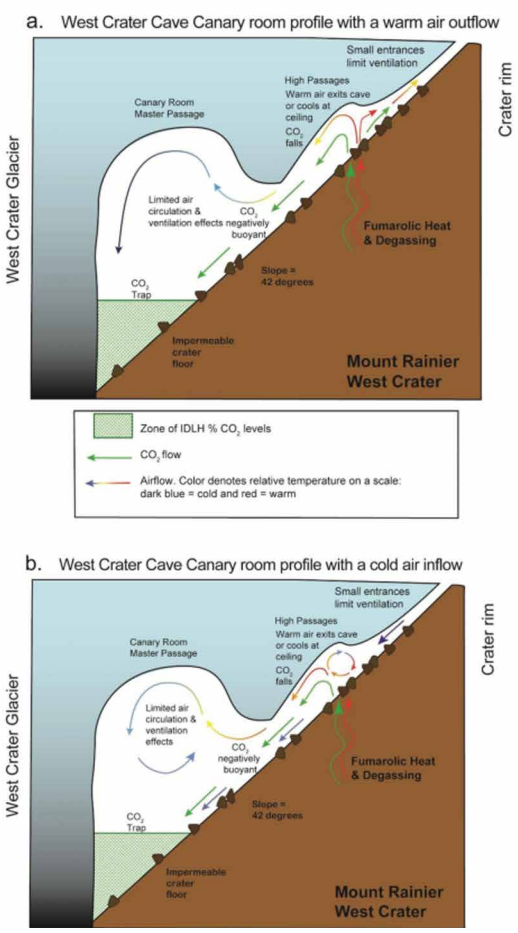


Figure 12. Cross section diagram of Canary Room as in the West Crater Cave showing conceptual CO_2 trap formation. Degassing fumaroles higher in the cave passages vent heat and CO_2 which pools due to low ventilation effects and buoyancy loss. (a) Shows the situation with a warm air outflow. (b) Shows the situation with a cold air inflow.

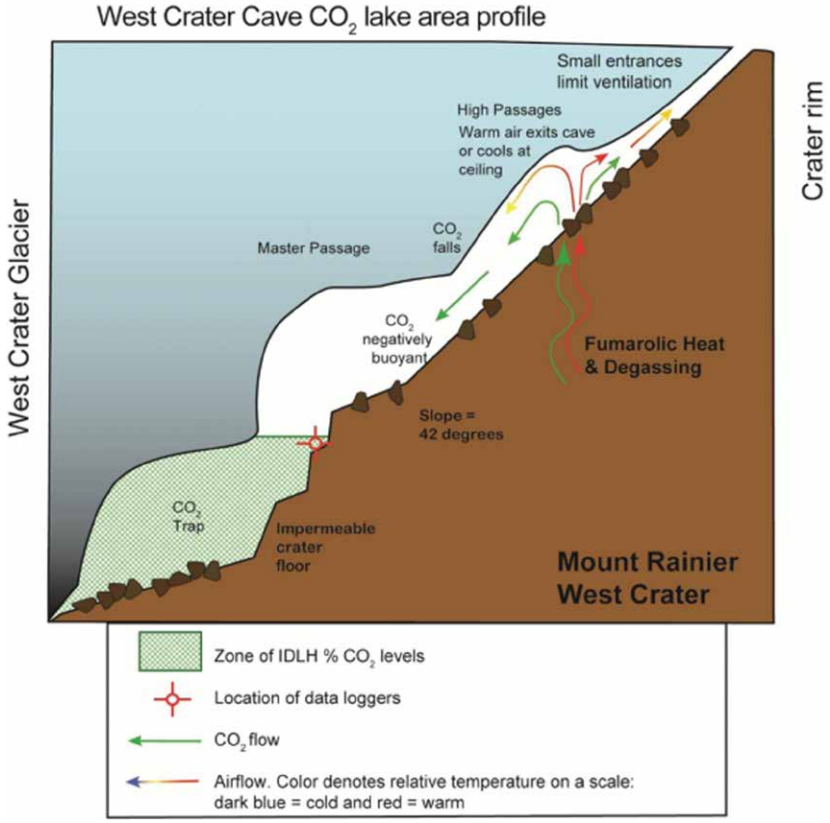


Figure 13. Cross section diagram of main passage CO_2 lake area as in the West Crater Cave showing CO_2 trap and data logger location. Degassing fumaroles higher in the West Crater Cave passages vent heat and CO_2 that pools due to low ventilation effects and buoyancy loss.

colder air of the CO_2 lake, which also has a higher CO_2 concentration, so that a rotational movement can occur when the descending air is again seized by the warmer air of the fumarole in the direction of the connecting tunnel to the outside.

The CO_2 concentration in the upper part of the CO_2 lake can be reduced. Fresh cold air flowing into the lake leads to a replenishment of the lake but also to a dilution of the CO_2 concentration. Even if the cold air carries further CO_2, its' concentration is lower than in the CO_2 lake.

It is possible that changes in fumarole output or cave morphology have caused the CO_2 traps to form in the 20−49 years since the previous studies. Even though toxic levels of volcanic gasses were not always noted in previous studies, these new measurements do not necessarily reflect a change in volcanic degassing, as our results are the first systematic recording of ambient air gas levels throughout the entire cave system. Continued study of this unique environment could include habitability for microorganisms in CO_2 rich areas, given the possible Mars analogue this dark, low nutrient, low-pressure, high CO_2 environment presents. Additional climactic measurements or modelling would help understand and validate the mechanisms of CO_2 trap formation and persistence. Public education on gas hazards could also bring beneficial information such as climbers noting sulfurous odors from East Crater, denoting a change in the magmatic system.

CONCLUSIONS

Fumarolic ice caves are not heavily studied, thus detailed studies of these cave systems must include numerous case examples. In addition to the general hazards of mountaineering, cave exploration, and the remote environment, the toxic levels of CO_2 and variability of hazardous atmospheres, outline caution required of anyone entering the Mount Rainier fumarolic ice cave system, particularly in areas where the morphology and fumarole output increases the manifestation of hazardous atmospheres. The formation and persistence of CO_2 traps result from rapidly diffusing fumarole gas mixing with the ambient air, which leads to cooling and a significant reduction in gas buoyancy. Cave morphology and fumarole location also affect CO_2 accumulation in that narrow entrances and low ceilings limit airflow and cause cooling of vented gases. Low areas of East Crater Cave, including the Hazmat entrance below Columbia Crest, and

the West Crater Cave in general include significant, large areas of IDLH atmospheres. These areas do not present a consistent planar boundary, and have an appearance of voluminous, ventilated chambers that nevertheless trap hazardous gasses. In addition to areas of high CO_2 concentrations of up to 24.8 %, O_2 displacement and low atmospheric pressure add to the hazard. Acute exposure to the high-altitude environment by humans who may not have acclimated is exacerbated in the caves by the displacement of O_2 to create IDLH atmospheres even where CO_2 concentrations are not themselves toxic. The use of SCBA is necessary to protect against volcanic gasses, however the effect of the high altitude on PO_2 and limitations of SCBA systems impact the ability to maintain PO_2 above 122 mmHg in a full-face mask SCBA system at Mount Rainier. Low PO_2 in cave passages due to O_2 displacement combined with high altitude can equate to the equivalent PO_2 of much higher altitudes, which has implications for those working in high altitude glaciovolcanic environments. Education of climbers, researchers, and the public is important to prevent accidents and to prevent the cascading effect of unprotected lay rescuers succumbing to gas exposures and amplifying the number of casualties. Studies of caves on other volcanic edifices or with potential gas hazards particularly at high altitudes would benefit from these considerations. A baseline now exists for hazardous cave atmospheres at Mount Rainier and repeat observations would be beneficial for volcano hazard monitoring.

ACKNOWLEDGEMENTS

Financial and equipment support from National Geographic Expeditions Council, the Mazamas Research Grant, the Mountain Rescue Association, Petzl, REI, Alberta Speleological Society, and National Speleological Society. Aaron Messinger and Special Projects Operations, supplier of SCBA equipment. Tom Gall, expedition HAZMAT specialist, John Punches, Tom Wood, safety officers, and Woody Peeples, Expedition Doctor. Additional cave surveyors 2015-2017, Tabbatha Cavendish, David Riggs, Nick Vieira, and Barb Williams. Cracker Jack First Response Specialists facilitated logistics for the 2015 field portion. John Meyers and Dave Clarke coordinated porter teams. Linda Sobolewski, Rick Davis, and Glyn Williams-Jones for helpful advice. The one hundred personnel who facilitated the studies by portering scientific and expedition equipment to the summit and back, supported by Corvallis Mountain Rescue (OR), Deschutes Mountain Rescue (OR), Everett Mountain Rescue (WA), Hood River Crag Rats (OR), Olympic Mountain Rescue (WA), Portland Mountain Rescue (OR), Volcano Rescue Team (WA), and the Douglas County Sheriff's Mountain Rescue Unit (OR). Research and collecting permit from the United States Department of the Interior- National Park Service – Mount Rainier. W.C. Evans and an additional reviewer provided comments which were very helpful to improving the manuscript. We thank F. De Ruydts and T. Wood for images in Figure 2; SPO, and T. Wood for images in Figure 3; A. Parness and D. Riggs for images in Figure 7; F. De Ruydts for images in Figure 10.

REFERENCES

Agency for Toxic Substances and Disease Registry, n.d., Medical Management Guidelines for Sulfur Dioxide: https://www.atsdr.cdc.gov/MMG/MMG.asp?id=249&tid=46 (Accessed August 28, 2020).

Anderson, C., n.d., Deadly Fumaroles: https://web.archive.org/web/20110717005030/http://glaciercaves.com/html/mounth_1.HTM (Accessed September 18, 2020).

ASTM International, 2019, Standard Practice for Respiratory Protection, F3387-19: ASTM International: West Conshohocken, PA, USA, 31 p.

Avon Protection, n.d., FM53 the multiple mission mask: https://www.avon-protection.com/products/fm53.htm (Accessed August 28, 2020).

Badino, G., 2009, The legend of carbon dioxide heaviness: Journal of Cave and Karst Studies, v. 71, no. 1, p. 100–107.

Berberan-Santos, M., Bodunov, E., and Pogliani, L., 1997, On the barometric formula: American Journal of Physics, v. 65, no. 5, 404 https://doi.org/10.1119/1.18555

Cantrell, L. and Young, M., 2009, Fatal fall into a volcanic fumarole: Wilderness and Environmental Medicine, v. 20, no.1, p. 77–79. https://doi.org/10.1580/08-WEME-CR-199.1

Cartaya, E., 2018, Hybrid counterweight system for glacier fumarole rescue applications [abs.]: International Technical Rescue Symposium 2018, Portland, USA, 8 p.

Centers for Disease Control and Prevention, 1994, Carbon dioxide immediately dangerous to life or halth concentrations (IDLH): https://www.cdc.gov/niosh/idlh/124389.html (Accessed August 28, 2020).

Centers for Disease Control and Prevention, 1994, Sulfur dioxide immediately Dangerous to life or health concentrations (IDLH). https://www.cdc.gov/niosh/idlh/7446095.html (Accessed August 28, 2020).

Centers for Disease Control and Prevention, 1994, Hydrogen sulfide immediately dangerous to life or health concentrations (IDLH): https://www.cdc.gov/niosh/idlh/7783064.html (Accessed August 28, 2020).

Coombs, H.A., 1936. The geology of Mount Rainier National Park: University of Washington Publications in Geology., v. 3, no. 2. University of Washington: Seattle, Washington, p. 202–203.

Curtis, A., 2016, Dynamics and global relevance of fumarolic ice caves on Erebus Volcano, Antarctica [Ph.D. thesis]: Socorro, New Mexico Institute of Mining and Technology, https://aaroncurt.is/paper/curtis2016-phd_diss.pdf (Accessed August 28, 2020).

Curtis, A., 2020, Comparison of Earth's fumarolic ice caves, with implications for icy voids on other worlds [abs.]: 3rd International Planetary Caves Conference, San Antonio, Texas. 1 p.

D'Alessandro, W., 2006, Gas hazard: An often neglected natural risk in volcanic areas: WIT Transactions on Ecology and the Environment. https://doi: 89. 10.2495/GEO060371

Davis, R., Anitori, R., Stenner, C., Smith, J., and Cartaya, E., 2020, Fumarolic glacial and firn ice caves on Mt. St. Helens may provide insight into Martian subsurface microbial communities [abs.]: Analog Field Sites Mini Symposium, Houston, Texas. The Lunar and Planetary Institute, Open University Astrobiology, andNASA Johnson Space Center.

Enform, 2013, H_2S Alive: Hydrogen Sulfide Training: 7th Ed. Enform Canada; Calgary, Canada, 121 p.

Ewert, J.W., Diefenbach, A.K., and Ramsey, D.W., 2018, 2018 update to the U.S. Geological Survey national volcanic threat assessment: U.S. Geological Survey Scientific Investigations Report 2018–5140, 40 p. https://doi.org/10.3133/sir20185140

Florea, L., Pflitsch, A., Cartaya, E., and Stenner, C., 2021, Microclimates in fumarole ice caves on volcanic edifices-Mount Rainier, Washington, USA: Journal of Geophysical Research, Atmospheres. v. 126, no. 4, p. 1−15. https://doi.org/10.1029/2020JD033565

Frank, D., 1995, Surficial extent and conceptual model of hydrothermal system at Mount Rainier: Washington. Journal of Volcanology and Geothermal Research, v. 65, no. 1, p. 51−80. https://doi.org/10.1016/0377-0273(94)00081-Q

Hansell, A, and Oppenheimer, C., 2005, Health hazards from volcanic gases: A Systematic Literature Review: Archives of Environmental Health: An International Journal. v.59., no.12, p. 628−639. https://doi.org/10.1080/00039890409602947

Ilanko, T., Fischer, T., Kyle, P., Curtis, A., Lee, H., and Sano, Y., 2019, Modification of fumarolic gases by the ice-covered edifice of Erebus volcano, Antarctica: Journal of Volcanology and Geothermal Research. v. 381, p 119−139. https://doi.org/10.1016/j.jvolgeores.2019.05.017

Ingraham, E.S., 1895. The pacific forest reserve and Mt. Rainier: The Calvert Company, Seattle, WA, p. 21−23.

KGW Staff, 2014, Tualatin man in fair condition after Mt. Hood fall: KGW. https://www.kgw.com/article/news/tualatin-man-in-fair-condition-after-mt-hood-fall/318116102 (Accessed September 14, 2020).

Kiver, E. P., 1978, Mount Baker's changing fumaroles: Ore Bin, v. 40, p. 133–145.

Kiver, E.P., and Mumma, M.D., 1971, Summit firn caves, Mount Rainier, Washington: Science, v. 173. pp. 320−322. https://doi.org/10.1126/science.173.3994.320.

Kiver, E.P., and Steele, W.K., 1975, Firn caves in the volcanic craters of Mount Rainier: The NSS Bulletin. v. 37., no. 3. p. 45−55.

Le Guern, F., Ponzevera, E., Lokey, W, and Schroedel, R.D., 2000, Mount Rainier summit caves volcanic activity: Washington Geology, v. 28, no. 1/2, p. 25.

McKay, R., 2020, Respirator use at high altitudes: The Synergist, Jan, 2020. American Industrial Hygiene Association. https://synergist.aiha.org/202001-respirator-use-at-high-altitudes (Accessed August 12, 2020).

National Academies of Sciences, Engineering, and Medicine, 2019, *An astrobiology strategy for the search for life in the universe*: Washington, DC: The National Academies Press, 188 p. https://doi.org/10.17226/25252.

National Park Service, 2020, Mount Rainier / Climbing: https://www.nps.gov/mora/planyourvisit/climbing.htm (Accessed August 18, 2020).

National Research Council. 1994. Mount Rainier: Active cascade volcano: Washington, D.C.: The National Academies Press, 128 p. https://doi.org/10.17226/4546

Nehring, N.L., Wollenberg, H.A., and Johnston, D. A., 1981, Gas analysis of fumaroles from Mt. Hood, Oregon: US Geological Survey Open File Report 81-236, 9 p.

Ocenco, n.d., M-20 SCSR: https://www.ocenco.com/ (Accessed August 16, 2020).

Owen, T., Biemann, K., Rushneck, D.R., Biller, J.E., Howarth, D.W., and Lafleur, A.L., 1977, The composition of the atmosphere at the surface of Mar:. Journal of Geophysical Research. v. 82, no. 28. P. 4635−4639. https://doi.org/10.1029/JS082i028p04635.

Pflitsch, A., Cartaya, E., McGregor, B., Holmgren, D., and Steinhöfel, B., 2017, Climatologic studies inside Sandy Glacier at Mount Hood Volcano in Oregon, USA: Journal of Cave and Karst Studies, v. 79, no. 3, p. 189−206. http://dx.doi.org/10.4311/2015IC0135.

Rom, W., 1992, Environmental and Occupational Medicine: 2nd ed; Little, Brown; Boston, 1493 p.

Savitzky, A., and Golay, M., (1964). Smoothing and differentiation of data by simplified least squares procedures: Analytical Chemistry v. 36, no.8, p. 1627−1639. doi:10.1021/ac60214a047.

Sobolewski, L., Stenner, C., Hüser, C., Berghaus, T., Cartaya, E., and Pflitsch, A., 2020. Formation and evolution of newly formed glaciovolcanic caves in the crater of Mount St. Helens, Washington, USA: The Cryosphere Discussions. https://doi.org/10.5194/tc-2020-279.

Special Projects Operations, 2015, ELABS – Extreme Limited Access Breathing Syste:. https://dwe-spo.com/shop/elabs/ (Accessed August 28, 2020).

Spelce, D.L., Mckay, R.T. Johnson, J.S., Rehak, T.R., and Metzler, R.W., 2016, Respiratory protection for oxygen deficient atmospheres: Journal of the International Society of Respiratory Protection. v. 33, no. 2, PMID: 32336876; PMCID: PMC7183576.

Spelce, D.L., Metzler, R.W., Johnson, J.S., Rehak, T.R., and Mckay, R.T., 2017, Revisiting respirators for Oxygen-deficient atmospheres: A comparison of OSHA and Z88.2 approaches to respiratory protection: The Synergist, March 2017. https://synergist.aiha.org/201703-revisiting-respirators-for-o2-deficiency (Accessed August 12, 2020).

Stevens, H., 1876. The ascent of Mount Tahoma: Atlantic Monthly. Nov., p. 511−530.

Stix, J., and de Moor, J.M., 2018, Understanding and forecasting phreatic eruptions driven by magmatic degassing: Earth Planets Space, v. 70, no. 83. https://doi.org/10.1186/s40623-018-0855-z

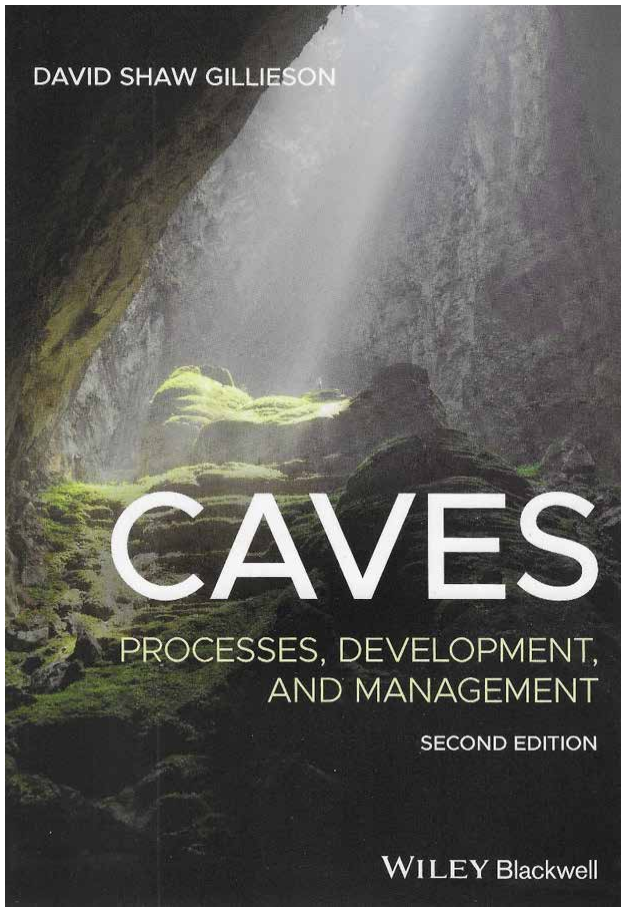
Tebo, B. M., Davis, R. E., Anitori, R. P., Connell, L. B., Schiffman, P., and Staudigel, H., 2015, Microbial communities in dark oligotrophic volcanic ice cave ecosystems of Mt. Erebus, Antarctica: Frontiers in Microbiology, v. 6, no. 179. https://doi.org/10.3389/fmicb.2015.00179.

Tomlinson, S., 2019, Mount Hood rescuers develop new protocols to save fallen climbers from toxic volcanic vents: The Oregonian. https://www.oregonlive.com/pacific-northwest-news/2015/04/fumaroles_mount_hood_rescuers.html (Accessed September 18, 2020).

Williams-Jones, G. and Rymer, H., 2015, Hazards of volcanic gases: *in* Sigurdsson, H., Houghton, B. McNutt, S., Rymer, H., Stix, J., eds., The Encyclopedia of Volcanoes. 2nd ed. Academic Press, p. 985−992, https://doi.org/10.1016/B978-0-12-385938-9.00057-2.

Young, M., 2015, Mt. Hood rescuers reach 3 climbers, including 2 who are injured, after fall: https://www.oregonlive.com/clackamascounty/2015/01/mt_hood_rescue.html (Accessed September 18, 2020).

Zimbelman, D. R., Rye, R. O., and Landis, G. P., 2000, Fumaroles in ice caves on the summit of Mount Rainier—preliminary stable isotope, gas, and geochemical studies: Journal of Volcanology and Geothermal Research, v. 97, p. 457–473, https://doi.org/10.1016/S0377-0273(99)00180-8.



Caves: Processes, Development, and Management, 2nd ed.

David S. Gillieson, 2021. Wiley, Blackwell, Hoboken, NJ; 508 p., 6.6 x 9.6 inches; ISBN 9781119455578 (paperback), ISBN 9781119455592 (adobe pdf), 9781119455622(epub). Paper $64.95 retail, USA. Kindle version $52 from Amazon.

This is a significantly updated version of the 1996 book of the same name. Since then, the science of speleology has taken on new dimensions as its relevance to such global concerns as climate change, the search for petroleum, and tourism are recognized for their importance. Caves are being taken seriously as more than a fun hobby, and there is now a vast and growing literature exploring what caves can tell us about the rest of the world. This book provides a good synthesis of this field by succinctly covering major topics, while supplying references to pertinent literature at a more advanced level, and with a broader international scope than the original edition.

The book is clearly organized and easy to follow. It begins with an explanation of karst and caves, and how they interact with their surroundings and with the hydrologic and geologic history of their surrounding area. The basic concepts of karst hydrology are covered, with the aid of simple flow equations. Methods of quantifying drainage patterns are introduced, such as dye tracing and discharge measurements, which clarify how water moves underground through soluble rock. Processes of limestone and silicate dissolution are described, along with the effects of rock structure on cave patterns. Nomenclature classifying cave systems is discussed, along with distinctions between shallow and deep cave-forming processes. Caves used as type examples include newly discovered systems in remote parts of the world. Processes of shallow vs. deep cave development are introduced, as well as caves in non-carbonate rock types such as gypsum and volcanic rock. Geologic control of cave passages is also mentioned.

The various types of cave deposits are described, including both speleothems and sediments, including ways to extract hydrologic information from them. Recent advancements in dating techniques are summarized, showing how much older many caves and karst landscapes are than previously thought. Climate studies have centered on speleothems, mainly through analysis of isotopes. The Nullarbor Plain of Australia is used as an example of how the analysis of speleothems can aid in the interpretation of environmental history.

The latter half of the book centers on the human use of caves and cave life. An overview of cave ecology is given describing cave life and their interactions, indicating how energy flows in the system. Threats to cave life are described such as White-Nose Syndrome and there is a discussion about the benefit of karst as a CO_2 sink. A chapter deals with cave archaeology detailing the prehistoric uses of caves and describing deposits of human bones. The possible migratory pathways for modern humans out of Africa are outlined, as well as the age ranges for the presence of major hominin groups such as Neandertals and modern humans. Cave deposits are discussed showing how different environments can help to preserve occupation sites. Liang Bua in Indonesia is used as an example of how cave sediment was used to date the remains of early diminutive humans. The many varied uses of caves are noted, such as mines, storage areas, religious sites, shelters, including modern homes that often make use of the cave's constant temperature and humidity. Two of the later chapters concentrate on cave management that other authors usually deal with in a separate book. Many of the concerns of how to manage a cave are addressed, citing present views that have improved past practices. Examples include cave lighting, cave tours, physical alteration of the cave, impact of visitors, and cave rescues. The management of the Gunung Mulu World Heritage site in Sarawak, Malaysia is used as an example of a thoughtfully managed commercial cave area. It is used as a model for sustainable development, balancing commercial interests with consideration for the local people, the biology and protecting the natural physical attractions. Since caves are intimately connected to the overlying karst, catchment management is also covered. Such problems as contamination, changes in drainage or soil cover are discussed. This leads to how to assess vulnerability and where to find

guidelines for cave and karst protection. The final chapter details how we document caves so that we know what we are protecting and its importance. Such innovations as 3-D laser scanning now make it possible to document a cave in blistering detail. Mapping caves and karst in the World Heritage site, Gunung Mulu National Park, is used as an example.

Diagrams are sharp and clearly designed, and many use color for greater clarity. Cave maps that are greatly reduced have fonts that are small but readable. Photos vary greatly in quality. Many, mainly the older ones, have lost their original clarity, mainly because of considerable color shift with time.

This book should appeal to students as an excellent introduction to caves and karst. It's coverage of many aspects of the field will interest cavers who want to know more about what they are crawling through. It should be valuable to anyone who is responsible for managing karst features in general, not only caves. The wide range of topics presents a broad overview without getting bogged down in detail, while still retaining the essential information.

Reviewed by Arthur N. Palmer (NSS 4059) and Margaret V, Palmer (NSS 23685), 619 Winney Hill Rd., Oneonta, NY 13820, April 30, 2022.

GUIDE TO AUTHORS

The *Journal of Cave and Karst Studies* is a multidisciplinary journal devoted to cave and karst research. The *Journal* is seeking original, unpublished manuscripts concerning the scientific study of caves or other karst features. Authors do not need to be members of the National Speleological Society, but preference is given to manuscripts of importance to North American speleology.

LANGUAGES: The *Journal of Cave and Karst Studies* uses American-style English as its standard language and spelling style, with the exception of allowing a second abstract in another language when room allows. In the case of proper names, the *Journal* tries to accommodate other spellings and punctuation styles. In cases where the Editor-in-Chief finds it appropriate to use non-English words outside of proper names (generally where no equivalent English word exist), the *Journal* italicizes them. However, the common abbreviations i.e., e.g., et al., and etc. should appear in roman text. Authors are encouraged to write for our combined professional and amateur readerships

CONTENT: Each paper will contain a title with the authors' names and addresses, an abstract, and the text of the paper, including a summary or conclusions section. Acknowledgments and references follow the text. Manuscripts should be limited to 6,000 words and no more than 10 figures and 5 tables. Larger manuscripts may be considered, but the *Journal* reserves the right to charge processing fees for larger submissions.

ABSTRACTS: An abstract stating the essential points and results must accompany all articles. An abstract is a summary, not a promise of what topics are covered in the paper.

STYLE: The *Journal* consults The Chicago Manual of Style on most general style issues.

REFERENCES: In the text, references to previously published work should be followed by the relevant author's name and date (and page number, when appropriate) in brackets. All cited references are alphabetical at the end of the manuscript with senior author's last name first, followed by date of publication, title, publisher, volume, and page numbers. Geological Society of America format should be used (see http://www.geosociety.org/documents/gsa/pubs/GSA_RefGuide_Examples.pdf). Please do not abbreviate periodical titles. Web references are acceptable when deemed appropriate. The references should follow the style of: Author (or publisher), year, Webpage title: Publisher (if a specific author is available), full URL (e.g., http://www.usgs.gov/citguide.html), and the date the website was accessed in brackets. If there are specific authors given, use their name and list the responsible organization as publisher. Because of the ephemeral nature of websites, please provide the specific date. Citations within the text should read: (Author, Year).

SUBMISSION: Manuscripts are to be submitted via the PeerTrack submission system at http://www.edmgr.com/jcks/. Instructions are provided at that address. At your first visit, you will be prompted to establish a login and password, after which you will enter information about your manuscript and upload your manuscript, tables, and figure files. Manuscript files can be uploaded as DOC, WPD, RTF, TXT, or LaTeX. Note: LaTeX files should not use any unusual style files; a LaTeX template and BiBTeX file may be obtained from the Editor-in-Chief. Table files can be uploaded as DOC, WPD, RTF, TXT, or LaTeX files and figure files can be uploaded as TIFF, AI, EPS, or CDR files. Extensive supporting data may be placed on the Journal's website as supplemental material at the discretion of the Editor-in-Chief. The data that are used within a paper must be made available upon request. Authors may be required to provide supporting data in a fundamental format, such as ASCII for text data or comma-delimited ASCII for tabular data.

DISCUSSIONS: Critical discussions of papers previously published in the *Journal* are welcome. Authors will be given an opportunity to reply. Discussions and replies must be limited to a maximum of 1000 words and discussions will be subject to review before publication. Discussions must be within 6 months after the original article appears.

MEASUREMENTS: All measurements will be in Systeme Internationale (metric) except when quoting historical references. Other units will be allowed where necessary if placed in parentheses and following the SI units.

FIGURES: Figures and lettering must be neat and legible. Figure captions should be on a separate sheet of paper and not within the figure. Figures should be numbered in sequence and referred to in the text by inserting (Fig. x). Most figures will be reduced, hence the lettering should be large. Photographs must be sharp and high contrast. Figures must have a minimum resolution of 300 dpi for acceptance. Please do not submit JPEG images.

TABLES: See http://caves.org/pub/journal/PDF/Tables.pdf to get guidelines for table layout.

COPYRIGHT AND AUTHOR'S RESPONSIBILITIES: It is the author's responsibility to clear any copyright or acknowledgement matters concerning text, tables, or figures used. Authors should also ensure adequate attention to sensitive or legal issues such as land owner and land manager concerns or policies and cave location disclosures.

PROCESS: All submitted manuscripts are sent out to at least two experts in the field. Reviewed manuscripts are then returned to the author for consideration of the referees' remarks and revision, where appropriate. Revised manuscripts are returned to the appropriate Associate Editor who then recommends acceptance or rejection. The Editor-in-Chief makes final decisions regarding publication. Upon acceptance, the senior author will be sent one set of PDF proofs for review. Examine the current issue for more information about the format used.

Journal of Cave and Karst Studies

Volume 84 Number 2 June 2022

CONTENTS

Article 41
Radon in Dead-end Caves in Europe
Miloš Briestenský, Fabrizio Ambrosino, Iveta Smetanová, Lenka Thinová, Stanka Šebela, Josef Stemberk, Lucia Pristašová, Concepción Pla, and David Benavente

Article 51
Ongoing Genesis of a Novel Glaciovolcanic Cave System in the Crater of Mount St. Helens, Washington, USA
Linda Sobolewski, Christian Stenner, Charlotte Hüser, Tobias Berghaus, Eduardo Cartaya, and Andreas Pflitsch

Article 66
Development and Persistence of Hazardous Atmospheres in a Glaciovolcanic Cave System—Mount Rainier, Washington, USA
Christian Stenner, Andreas Pflitsch, Lee J. Florea, Kathleen Graham, and Eduardo Cartaya

Book Review 83
Caves: Processes, Development, and Management, 2nd ed.
David S. Gillieson